Statistical, DFT and Continuum Electrostatics Analysis of Histidine Ligated Hemes in the Non-redundant Heme Database, in Model Complexes and in Cytochrome c Oxidase

by

Jun Zhang

A dissertation submitted to the Graduate Faculty in Physics in partial fulfillment of the requirements for the degree of Doctor of Philosophy, The City University of New York

2010

This manuscript has been read and accepted for the
Graduate Faculty in Physics in satisfaction of the
dissertation requirement of the degree of Doctor of Philosophy

12/09/2009	Marilyn Gunner
Date	Chief of Examining Committee
03/09/2010	Steven Greenbaum
Date	Executive Officer

Timothy Boyer

Mark Shattuck

Themis Lazaridis

Lynn Francesconi

Supervisory Committee

THE CITY UNIVERSITY OF NEW YORK

Abstract

Statistical, DFT and Continuum Electrostatics Analysis of Histidine Ligated Hemes in the Non-redundant Heme Database, in Model Complexes and in Cytochrome C Oxidase

by

Jun Zhang

Advisor: Professor Marilyn Gunner

Heme plays an important role in biological oxidation--reduction chemistry. Important heme structural factors of are investigated here to understand how the redox potential is shifted when bound to proteins. A statistical analysis of a non-redundant heme database shows that the redox potentials of heme are significantly correlated with heme types and heme ligand types. The patterns of histidine ligand orientation, relative histidine orientations were investigated for the proteins in the database.

The heme redox potential can be shifted by the existence of hydrogen bond partner to the axial histidine ligand of the heme. With the simplified model complex of Bis-Imidazole-Porphyrin, the redox potential shift due to the hydrogen bond was compared using DFT and Continuum electrostatics methods. Two models, with a representative hydrogen bond partner and point charges, are built for the simulation. The calculated final energy shift due to the hydrogen bond found by the two methods are within 15% of each other. Four different charge sets were compared in the electrostatics calculation. Simulation of Bis-Imidazole-Porphyrin complex using DFT method also revealed the energetic impact of relative orientation of imidazole ligands on either side of the porphryn is less than 1kcal/mol in a flat core porphyrin complex.

Cytochrome c Oxidase is one of the essential proteins in the anaerobic electron transfer chain. In the protein from *Rhodobactor sphaeroides*, S44 makes a hydrogen bond to H102, the axial ligand of Heme a, a key cofactor on the reaction pathway electron transfer chain. The electrochemical behavior of Heme a is revisited with a comparison of wild type and S44D mutant using the continuum electrostatics program MCCE. At pH7, the partially ionized Asp44 lowers the Heme redox potential by 50mV. The ΔG° between Cu_A and Heme a is more pH-dependant with Asp than Ser. Holding other cofactors oxidized, electron transfer from Cu_A to Heme a is coupled with uptake 0.6 and 1.1 protons in S44 and D44 structures respectively.

ACKNOWLEDGEMENTS

Firstly, I would like to express my gratitude to my advisor Dr. Marilyn Gunner for her invaluable guidance and support throughout the course of the study. I am grateful to Dr. Timothy Boyer, Dr. Mark Shattuck, Dr. Lynn Francesconi and Dr. Themis Lazaridis for serving as my committee member.

I am grateful to the members of my group, especailly Dr. Junjun Mao and Dr. Yifan Song for the instructions on MCCE program, and Dr. Christian Fufezan for working together with enlightening discussions on the heme statistics project. I would also like to thank the current and previous members in the group for their great teamwork, they are: Dr. Zhenyu Zhu, Dr. Xinyu Zhang, Dr. Jennifer Madeo, Zhong Zheng, Jinran Kim, Gennady Khirich, Yanjun Wang, Becier Tapia, Cat Chenal , Jianxun Lu, Xuyu Zhu, Edison Castro and Muhamed Amin.

Finally, I would like to thank my parents for their support and encouragement throughout my life. I am in gratitude to my wife Fen Ye for her love and support all the way.

TABLE OF CONTENTS

LIST OF TABLES

Table Page

LIST OF FIGURES

Figure Page

CHAPTER I

INTRODUCTION

1.1 HEME

1.1.1 Heme and its functions

Widely distributed in proteins, heme is a protein-bound organic molecule playing various vital roles in biology. One of the earliest solved X-ray crystal structures of myoglobin (*1*) is a single polypeptide chain containing a heme to selectively bind molecular oxygen (O_2). (*2*) Like the related protein Hemoglobin (*3*), myoglobin is responsible for supplying oxygen to muscle tissue in reptiles, birds and mammals. The red color associated with the oxygenated forms of the two proteins is due to the heme group. (*4*)

Heme also acts as electron transfer compound in many proteins such as cytochrome c, a small soluble protein found between the membranes of the mitochondrion. (*5*) Cytochrome c undergoes reversible oxidation and reduction of its heme, transferring one electron between cytochrome bc1 complex (complex III) and cytochrome c oxidase (complex IV). (*5*) In addition to its role in molecular transporter and electron transfer proteins, heme also plays the role of sensor in NO binding guanylate (*6*), detoxification in cytochrome P450 protein (*7*) and in controlling of gene expression

of microRNA processing. (*8*)

1.1.2 Structures of HEME

Heme consists of a tetrapyrrole ring system called protoporphyrin IX complexed with iron. (*2*) The four-pyrrole rings of this system are linked by methene bridges, so that the unsaturated porphyrin is highly conjugated and planar. The iron atom in a heme has at least four ligands with nitrogen atoms of heme porphyrin. Another one or two axial ligands can be added from the proteins and substrates. Histidine often serves as a heme ligand. The bond distance between heme Fe and histidine nitrogen axial ligand is an important parameter connecting the function of heme complex. The spin state, coordination number and oxidation state of the hemes are sensitive to the axial bond length between heme iron and the nitrogen ligand of histidine. (*9*, *10*) For electron transfer reactions, the bound iron is generally in the ferrous, or Fe^{2+}, oxidation state or ferric, or Fe^{3+}, reduction state, and the porphyrin ring always has a -2 charge. Then the overall charge of the heme is either 0 (ferrous-heme) or +1 (ferric-heme). Additionally, both of the two propionic acids attached on the edges of the porphyrin can carry 0 (neutral state) or -1 (deprotonated state) charges. The reduced heme is used in substrate transfer proteins. A Fe^{4+}=O in ferryl heme can be found when hemes play an active role in substrate redox chemistry, such as in the peroxidases and oxidases.

In 1920s, Keilin discovered that there were different cytochromes from the positions of their lowest energy absorption band in the reduced state. (*11*) Thus a-, b- and c- type hemes are named in the order of this absorption band. The most common types in

nature are b and c type hemes. The a, o, l, m, d and s are derivatives of Heme b and rare in proteins. Heme c differs from Heme b in that the two vinyl heme side chains at position 8 and 13 are covalently bound to the proteins through two cysteine residues. A typical b type ferrous-heme is shown in Figure 1.1.

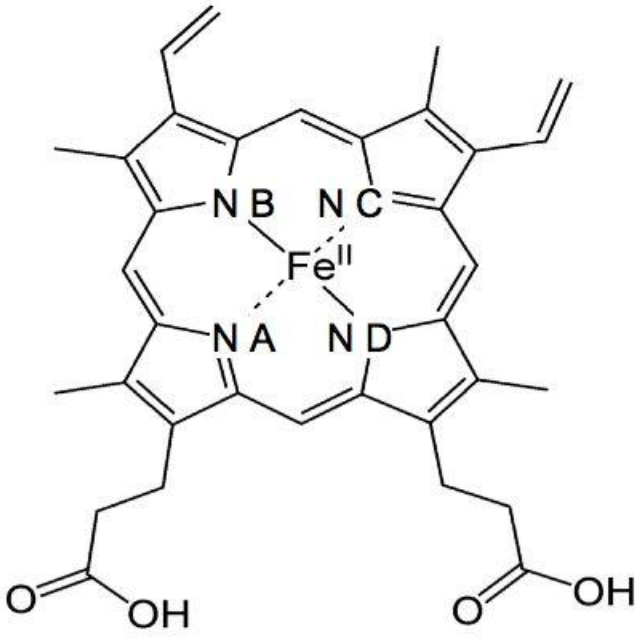

Figure 1.1 the structure of b type ferrous-heme. (*2*)

Heme has been proved an important ingredient for protein design. The heme helps to stabilize the folded protein and serves as an easily introduced active site. Designed proteins with heme porphyrin structures have been used in pioneering bionanoelectronic devices and substrate control. (*5, 12-17*) Most of the natural heme proteins are found in α-helical rather than in β sheets and mixed α/β secondary structure (*11*) and helical

bundle structures with heme cofactors have been often used in de novo protein design. (*16, 18-20*) There are geometric constraints for Histidine ligand to bind porphyrin inside helical bundle structures. (*16, 21, 22*) Koder and coworkers have determined the most common rotamers for binding by a statistical analysis of known structures and by molecular mechanism simulations. (*21*)

1.1.3 Heme redox potential

The heme redox potential is a measure of the tendency of the heme cofactor to acquire electrons and be reduced. The unit of redox potential is volts. Heme cofactors inside different proteins have their own unique reduction potential. The more positive the potential, the greater the species' affinity for electrons and tendency to be reduced. (*23*) The control of heme redox potential is important to determine the pathway and kinetics of electron transfer within and between proteins.

The measured heme redox potentials in proteins vary between -550 mV in HasA (*5*) and 450mV in cytochrome c peroxidase (*5*). Some proteins, such as cytochrome bc1 complex, have both high and low potential hemes, (*5, 12, 13*). It is a critical feature for efficient electron transfer. (*5, 13, 24*) Many experimental studies used site mutation technique to control the heme electrochemistry. (*25-30*) Computational approaches have been used to understand the sources of broad range of heme redox potential. Warshel used Protein Dipoles Langevin Dipoles (PDLD) to study the importance of protein residues and propionic acids. (*31*) Rogers and Moore calculated the pH dependent ionization of propionic acids and estimated the heme redox potential shift by solving

Poisson-Boltzmann equation of continuum electrostatics. (*32, 33*) Ullman used a hybrid statistical mechanics/Tanford−Roxby approach to calculate protonation and oxidation probabilities depending on the solution pH and heme redox potential in cytochrome c3. Multi-conformational Continuum Electrostatics (MCCE) has been used to study 141 heme proteins with heme redox potentials spanning 800mV. Hemes with arrange of different types and ligand types were investigated. (*34*) Other computational techniques, such as free energy perturbation method (*35, 36*), molecular dynamics method (*37, 38*), quantum mechanics (*39, 40*) and QM/MM methods (*41*) have been used to study different aspects of the heme ligand geometry (*39*), protein reorganization (*42, 43*) and heme-protein interactions (*44-46*).

The work presented here will describe structural features of the heme, its axial ligands and the proteins to which it is bound to better understand what controls the electrochemical property of the proteins.

1.2 Simulation Methods

1.2.1 DFT method

Widely used in computational physics and chemistry, Density Functional Theory (DFT) is a popular and powerful approach to solve the electronic structure of many-body systems, such as molecules and condensed phases using a simplified quantum mechanical analysis. (*47, 48*)

In quantum mechanics, all information is contained in the system's wave function, Ψ. With a single electron moving in a potential V, the wave function is given by

Schrödinger's equation:

$$i\hbar\frac{\partial}{\partial t}\Psi = -\frac{\hbar^2}{2m}\nabla^2\Psi + V\Psi$$

Equation 1.1

In the many-body problem with more than one electron in the system, the number of electrons determines the degrees of freedom in Schrödinger's equation. Electron-electron interactions have to be considered inside the potential function. The computational cost is expensive for traditional developed method, such as Diagrammatic Perturbation Theory based on Feynman diagrams and Green's function(*49*) or configuration interaction (CL) method (*50*).

DFT uses the electronic density as a basic quantity to simplify the many-body problem.

$$\rho(x) = \int dx_2 \ldots dx_N \left|\Psi^{(N)}(x, x_2, \ldots, x_N)\right|^2$$

Equation 1.2

Conceptually, knowledge of $\rho(x)$ implies knowledge of the wave function and potentials. The most common implementation of density functional theory is through the Kohn-Sham method. (*48*)Within the framework of Kohn-Sham DFT, the many-body problem of interacting electrons in a static external potential is simplified to an easier problem of non-interacting electrons moving in an effective potential. The effective potential includes the external potential and the effects of the Coulomb interactions between the electrons, e.g. the exchange and correlation interactions. Modeling the latter two interactions is the hardest part of KS DFT. The simplest approximation is the local-density approximation (LDA), which is based on the exact exchange energy for a uniform

electron gas, which can be obtained from the Thomas-Fermi model, and from fits to the correlation energy for a uniform electron gas. (*51*, *52*)

Compared with Hartree-Fock theory and other electronic structure theory, the way of electronic density calculated from electronic basis sets used in DFT is simpler than calculating the electronic ion wave functions needed for ab initio method of quantum mechanics. DFT is good at minimizing the total electronic energy of the system, which makes the calculations of ground states more reliable. The B3lyp method has been demonstrated to be a suitable method for computing the prospects of metal containing molecular complexes such as heme. (*53*-*57*)

Basis set, polarization and diffuse functions are important factors needed when setting up a DFT calculation. The basis set is a set of functions used to create a molecular orbital, which is modeled by a linear combination of such functions with the weights or coefficients to be determined. (Equation 1.3) (*58*) Usually these functions are atomic orbitals, in that they are centered on atoms but functions centered in bonds or lone pairs, have been used as have pairs of functions centered in the two lobes of a p orbital. For example, basis set "6-311g" includes 5 d orbital functions, while basis set "6-31g" include 6 d orbital functions.

$$\Psi = C_1\Phi_1 + C_2\Phi_2 + C_3\Phi_3 + \ldots\ldots + C_n\Phi_n \qquad \text{Equation 1.3}$$

Polarization functions add an extra electronic shell. The polarization functions are placed on all atoms except for transition metals, H and He are labeled "**". The option with "*" also include the polarization function for H and He. The diffuse function gives a more accurate description of anionic systems. This is especially useful for calculations of

van der Waals complexes or molecules that include atoms with negative charge such as ionized Asp. These functions are marked with "+".

In this research, the Jaguar (ver6.5) (*59*), a computational software specialized in simulating molecules with DFT is employed for structure optimization, single point energy calculations and to obtain atomic partial charges needed for other calculations.

1.2.2 Continuum electrostatics method

The continuum electrostatics method calculates the electrostatic potential given the distribution of charges source, dielectric medium and boundary conditions. The electric potential Φ at a distance **r** from a point charge **q** in a continuum medium of dielectric constant ε can be described by the Coulomb's equation:

$$\phi = \frac{q}{4\pi\varepsilon \bullet r} \qquad \text{Equation 1.4}$$

When the system has a non-uniform dielectric constant such as for a protein in solvent, solving Poisson-Boltzmann (PB) equation of continuum electrostatics gives the electrostatic potential. (*60, 61*) Given that PB equation cannot be solved analytically, the electrostatic potential can be calculated given the distribution of dielectric constant and atomic charges by PB solver, such as the Delphi program. Water is treated as dielectric medium with constant 80. The protein dielectric constant is generally assigned a value between 4 and 20. (*62-64*) The dielectric constant supplies the effect of the continuum medium response to a charge or polar group. A small value represents a more rigid protein environment. Methods with non-uniform dielectric constants have also

investigated allowing for the different dielectric regions in a protein. (*65*, *66*)

The Multi-conformation Continuum Electrostatics (MCCE) program combines continuum electrostatics and molecular mechanics to calculate residue pK_as or redox potentials of bonded cofactors. (*67*, *68*) The program generates multiple positions, side chain rotamers from original protein structure and protonation states of protonable group or oxidation states of redox active sites. Electrostatics and non-electrostatics energy terms, such as residue pairwise interaction and solvation energy are calculated for each conformer using the Delphi program. Monte Carlo sampling determines the conformer occupancies from Boltzmann distribution at a given pH or E_h.

The heme redox potential, E_m, is calculated as:

$$E_m = E_{m,sol} - \Delta G_{protein}/nF \qquad \text{Equation 1.5}$$

The $E_{m,sol}$ is the reference energy for an isolated heme complex in water. For the Bis-His heme complex, the $E_{m,sol}$ of -220mV of Bis-His-Heme microperoxidases in solution is used. (*69*) $\Delta G_{protein}/nF$ represent the free energy contributed from protein environment to shift E_m. "n" is the number of the charge and "F" is the Faraday constant. $\Delta G_{protein}$ can be broken down as:

$$\Delta G_{protein} = \Delta\Delta G_{rxn} + \Delta G_{pol} + \Delta G_{res} \qquad \text{Equation 1.6}$$

$\Delta\Delta G_{rxn}$ is the desolvation energy measuring the loss of favorable interactions of the heme with water when it is moved into the protein. ΔG_{pol} is the backbone dipole interaction with the heme and ΔG_{res} is the electrostatic interaction with the protein side chains.

The MCCE program has been proved to be successful in calculating the redox

potential of heme complex. A study of 141 hemes from 42 proteins with MCCE program has shown 92% calculations are within 120mV of the experimental E_m. It also revealed there is no single energy component in equation 1.1.6 that determines the heme E_m but all play a role (*34*)

1.3 Research Objectives

Heme complexes carry out many roles in nature. With its wide range of redox potentials, hemes help to control the overall biological electron transfer chain by shifting the driving force along the reaction sequence. The analysis of the structural feature of heme cofactors to be described here will help us to understand natural heme redox chemistry and design better heme containing de novo designed proteins. The interrelated factors to be stated include the type of heme ligands, the orientation of heme histidine ligand relative to the heme plane, the relative histidine orientation in Bis-His-Heme proteins, heme ruffling, the electrostatic interaction between propionic acids and histidine ligand of heme, the role of hydrophobicity of the heme environment within protein of a hydrogen bond from the protein to a heme ligated histidine. These issues have been under investigated for decades and their importance are still subject to debate. (*10, 70-74*) A statistical analysis of non-redundant heme database, a DFT analysis of heme ligand model system and an MCCE analysis of a mutation in Cytochrome c oxidase will be presented:

1) Identification of patterns of heme redox potentials and relevant structural feature in a non-redundant database of heme proteins. Case studies of hemes in important

proteins, such as cytochrome c oxidase, cytochrome bc1 complex, globins and peroxidase, are crucial to understand the links between heme structure and redox chemistry. However, general trends of structural features found by studying a broad range of proteins may reveal the general factors that control heme electrochemical properties.

Over 1000 proteins have at least one heme cofactor in the PDB database. (*11*) The abundance of heme and heme proteins can make a survey possible and reliable. Existing heme databases and other published reports have investigated the ligand orientation, binding motifs and electrochemistry. (*5*) For example, Knapp investigated the orientation of the imidazole axial ligands in a pool of 693 hemes in 432 crystal structures from Protein Data Bank. (*75, 76*). Gibney designed a heme PDB database focused on the heme redox potentials. (*11, 77*) Findlay set up a database of bioinorganic motifs including hemes named PROMISE. (*78*) Another online database, the Metalloprotein Database and Browser (MDB) offers geometrical parameters of metal-binding sites and various analytical tools. (*79*)

However, since many heme-containing proteins such as globins are easily crystallized, there are many heme protein families highly over-represented in the original PDB database. For example, there are 56 PDB structures of cytochrome b5, which differ in species, resolution, structural measurement method (X-ray or NMR), pH and presence of mutations. Thus, a nonredundant heme database is necessary to make a statistically valid statement. A nonredundant database was built picking the representative hemes using sequence and structural alignment with a reasonable resolution cutoff. (*74*) The distribution of important structural features, such as heme type, heme ligand type,

histidine orientation and relative histidine orientations were then investigated. The link between known redox potential and these factors were examined within the non-redundant heme database in Chapter 2.

2) Is there an energy difference between the relative parallel and perpendicular orientations of the two histidines in Bis-His-Heme proteins? This problem has been under investigation for decades. (*10, 54, 71, 73, 74*) The aromatic ring of histidine residue can overlap with the π orbital of heme porphyrin. Thus, particular relative orientation of two histidines in Bis-His-Heme may be energetically favorable. The tuning of parallel and perpendicular orientations could be a way to control the heme electrochemical properties in proteins.

Different experimental approaches have been used to investigate the problem. In EPR experiments, the perpendicular Bis-His-Heme in cytochrome b from Mitochondrial complex II relaxed into a parallel orientation with detergent treatment. (*73, 80*) In a signaling protein Nitrophorin 4 (PDB ID 1IKE), the ligands are in a parallel orientation and one of the heme histidine ligands is only loosely bound, suggesting this is the energetic minimum for the relative orientation uncontrolled by the protein. EPR and Mossbauer data for Bis-imidazole and Bis-pyridine coordinated OETPP-, OMTPP- and TMPFe(III) complex suggested the g_{zz} value, and hyperfine coupling constant A_{zz} are highly correlated with the relative angles between the imidazoles. (*81 2006, 82*) Therefore, Ann Walker proposes that the parallel orientation is favored in the low spin heme. (*10, 73, 81, 83-85*) However, there is evidence that the perpendicular orientation

is stabilized in TMPFe(III) structure at low temperature. (*73*) Scheidt suggested energy difference between parallel and perpendicular orientations is from 1-3kcal/mol in the TMPFe complex. (*83, 86*)

The energy stabilization of different histidine orientations is also affected by the ruffling of the heme porphyrin. (*10, 72*) For example, in TMPFE the heme plane is more ruffled than the heme in proteins because of the introduced meso-carbon groups in TMPFE model complex. (*73*) Scheidt estimated the energy impact of ruffling core can shift the energy preference between parallel and perpendicular ligand orientation by 3-5Kcal/mol. (*85*) In a model complex with no ruffling of the heme core, Straatsma calculated the perpendicular arrangement is energetically preferred by 0.3kcal/mol, a negligible amount, in ferrous heme complex using the DFT method. (*54, 84*)

In the research presented here the general tendency of the relative Histidine orientation is studied using the non-redundant heme database in Chapter 2. A DFT simulation with a simplified Bis-Imidazole-Porphyrin model complex is conducted to understand the energy preference in Chapter 3. The effect of ruffling is discussed with some calculation results from the model complex.

3) How does the hydrogen bond to the axial histidine ligand affect the heme redox potential?

The non-ligated nitrogen atom, other than the axial ligand nitrogen in the imidazole ring of a histidine ligand can be a hydrogen bond acceptor or donor, depending on the histidine protonation state. The nitrogen atom of ND1 is often found to be a

hydrogen bond donor in heme proteins. Aspartic acid is the conserved hydrogen bond partner in heme peroxidases (*5*) and oxygenases (*87*). These residues have been assigned important roles in these enzymes. (*57*) The carbonyl group of the protein backbone, another common hydrogen bond partner of histidine ligand of heme, is found in globins, cytochrome c oxidase and cyclooxygenase.

Kahn pointed out the changes in hydrogen bond geometry between the imidazole and planar formamide is coupled with the changes in oxidation state of heme. (*88*) Using B3lyp method of DFT simulation in a five-coordinate histidine containing heme complex, Jensen and Ryde found some geometric features of histidine ligand hydrogen bond related with heme electrochemistry. For example, histidine hydrogen bonds to carbonyl groups have a small influence on the heme site. However, a hydrogen bond to a carboxyl group will shorten the axial Fe-N bond length by 0.05Å. This can change the inner-sphere reorganization energy of the Fe^{2+} to Fe^{3+} transition in the five-coordinate heme complex by as much as 30kJ/mol. (*89*) Site-mutation studies in peroxidase (*90*) and cytochrome c (*91*) suggested the heme electronic configurations are affected by the hydrogen bond to the axial ligand. However, how much the heme redox potential is shifted due to the axial histidine hydrogen bond is not clear.

The DFT method and continuum electrostatics method are employed to study the problem. Two model complexes, Bis-imidazole-porphyrin and Imidazole-water-porphyrin structures were built. Representative hydrogen bond partners were selected from the statistical survey results of non-redundant heme database. The DFT method is good at calculating bonded compounds with complex electronic orbital while the

continuum electrostatics method is good at analyzing non-bonded systems with relatively litter computational cost. The results of the two simulation methods will be compared to investigate the heme redox potential shift due to the histidine hydrogen bond in Chapter 3.

4) The influences of a modified hydrogen bond on the redox potential: the MCCE study of S44D mutation in Cytochrome c oxidase.

Cytochrome c oxidase is the terminal protein of the aerobic respiratory chain located in mitochondrion or bacterial membrane. (*92*, *93*) The large transmembrane protein builds a transmembrane electrochemical gradient using chemical energy from the reduction of O_2 to H_2O. (*94*, *95*) During the process, four electrons are sequentially transferred from soluble protein cytochrome c to the oxidase Cu_A, Heme a and to the binuclear center consists of Cu_B and Heme a_3. In binuclear center, the four electrons and four uptake protons reduce a bound O_2 molecular into water. Another four protons are transferred through the membrane during the process:

$$4e^- + 8H_n^+ + O_2 \rightarrow 2H_2O + 4H_p^+$$

H_n are protons taken up from the high pH 'n' side of the membrane while H_p are protons released to the low pH 'p' side.

Heme a, an a-type low-spin Bis-His-Heme, is a key cofactor on the electron transfer chain. The electron transfer rate from Cu_A to Heme a is measured to be $2\times10^4 s^{-1}$ in the wild type *Rh. Sphaeroides* protein. (*96-98*) One residue, Ser 44, makes a hydrogen bond to His 102, the axial ligand of Heme a. Site-mutation studies of S44D were carried on to understand the effect of electron transfer rate change due to the axial ligand

hydrogen bond. (*99*) The introduction of Asp at the site can shift the redox potential of heme and change electron transfer rate between Cu_A and Heme a, especially if the Asp is deprotonated. The electrochemical behavior of Heme a is revisited with a comparison of wild type and S44D mutant using the continuum electrostatics program MCCE in Chapter 4.

References

1. Antonin, E., and Brunori, M. (1971) *Hemoglobin and Myoglobin in their Reactions with Ligands*, North-Holland: Amsterdam.

2. Berg, J. (2002) *Biochemistry*, 5th ed., W. H. Freeman and Company.

3. Pennock, B. D., and Schwan, H. P. (1969) Further observations of the electrical properties of hemoglobin-bound water, *J. Phys. Chem. 73*, 2600-2610.

4. Horton, H. R., Moran, L. A., Ochs, R. S., Rawn, J. D., Scrimgeour, K. G., and , r. E. U. S. R., NJ: Prentice Hall, 2002 (2002) *Principles of Biochemistry*, 3rd ed., Prentice Hall, Upper Saddle River, NJ.

5. Kurreck, J., Refifarth, F., Karge, M., and Renger, G. (1995) Reconstitution of the endogenous plastoquinone pool in photosystem II (PS II) membrane fragments, inside-out-vesicles, and PS II core complexes from spinach, *Biochemistry 34*, 15721-15731.

6. Rodgers, K. R. (1999) Heme-based sensors in biological systems, *Curr. Opin. Chem. Biol. 3*, 158-167.

7. Guallar, V., Baik, M. H., Lippard, S. J., and Friesner, R. A. (2003) Peripheral heme substituents control the hydrogen-atom abstraction chemistry in cytochromes P450, *Proc. Natl. Acad. Sci. USA 100*, 6998-7002.

8. Faller M, M. M., Yin S, Loo JA, Guo F. . (2007) Heme is involved in microRNA processing, *Nat Struct Mol Biol 14*, 23-29.

9. Scheidt, W. R., and Reed, C. A. (1981) Spin-state/stereochemical relationships in iron porphyrins: Implications for the hemoproteins, *Chem. Rev. 81*, 543-555.

10. Scheidt W, L. Y. (1987) Recent advances in the stereochemistry of metal-lotetrapyrroles., Springer.

11. Reedy, C. J., and Gibney, B. R. (2004) Heme protein assemblies, *Chem. Rev. 104*, 617-649.

12. Trumpower, B. L. (1990) Cytochrome bc_1 complexes of microorganisms, *Microbiol Rev 54*, 101-129.

13. Osyczka, A., Moser, C. C., Daldal, F., and Dutton, P. L. (2004) Reversible redox energy coupling in electron transfer chains, *Nature 427*, 607-612.

14. Discher, B. M., Koder, R. L., Moser, C. C., and Dutton, P. L. (2003) Hydrophilic to amphiphilic design in redox protein maquettes, *Curr Opin Chem Biol 7*, 741-748.

15. Khandogin, J., and Brooks, C. L., 3rd. (2006) Toward the accurate first-principles prediction of ionization equilibria in proteins, *Biochemistry 45*, 9363-9373.

16. Koder, R. L., and Dutton, P. L. (2006) Intelligent design: the de novo engineering of proteins with specified functions, *Dalton Trans*, 3045-3051.

17. Noy, D., Moser, C. C., and Dutton, P. L. (2006) Design and engineering of photosynthetic light-harvesting and electron transfer using length, time, and energy scales, *Biochim Biophys Acta 1757*, 90-105.

18. Gimpelev, M., Forrest, L. R., Murray, D., and Honig, B. (2004) Helical packing patterns in membrane and soluble proteins, *Biophys J 87*, 4075-4086.

19. Gibney, B. R., Isogai, Y., Rabanal, F., Reddy, K., Grosset, A., Moser, C., and Dutton, P. (2000) Self-assembly of heme a and heme b in a designed four helix bundle implications for a cytochrome c oxidase maquette., *J. Am. Chem. Soc. 39*, 11041-11049.

20. Shifman, J. M., Gibney, B. R., Sharp, R. E., and Dutton, P. L. (2000) Heme redox potential control in de novo designed four-alpha-helix bundle proteins, *Biochemistry 39*, 14818-14821.

21. Negron, C., Fufezan, C., and Koder, R. L. (2009) Geometric constraints for porphyrin binding in helical protein binding sites, *Proteins 74*, 400-416.

22. Kennedy, M. L., Silchenki, S., Houndonougbo, N., Gibney, B. R., Dutton, P. L., Rodgers, K. R., and Benson, D. R. (2001) Model hemoprotein reduction potentials: the effects of histidine-to-iron coordination equilibrium, *J. Am. Chem. Soc. 123*, 4635-4636.

23. Voet, D., and Voet, J. (1990) *Biochemistry*, Wiley, New York.

24. Crofts, A. R. (2004) The cytochrome bc1 complex: function in the context of structure, *Annu Rev Physiol 66*, 689-733.

25. Mauk, A. G., and Moore, G. R. (1997) Control of metalloprotein redox potentials: what does site-directed mutagenesis of hemoproteins tell us?, *J. Biol. Inorg. Chem. 2*, 119-125.

26. Springs, S. L., Bass, S.E., McLendon, G.L. (2000) Cytochrome b562 variants: a library for examing redox potential evolution, *Biochemistry 39*, 6075-6082.

27. Springs, S. L., Bass, S. E., Bowman, G., Nodelman, I., Schutt, C. E., and McLendon, G. L. (2002) A multigeneration analysis of cytochrome b_{562} redox variants: evolutionary strategies for modulating redox potential revealed using a library approach, *Biochemistry 41*, 4321-4328.

28. Bertini, I., Gori-Savellini, G., and Luchinat, C. (1997) Are net charges always negligible?, *J.B.I.C.*, commentary this issue.

29. Battistuzzi, G., Borsari, M., and Sola, M. (2001) Redox properties of cytochrome c, *Antioxid redox signal 3*, 279-291.

30. Battistuzzi, G., Borsari, M., Cowan, J. A., Ranieri, A., and Sola, M. (2002) Control of cytochrome c redox potential: axial ligation and protein environment effects, *J. Am. Chem. Soc. 124*, 5315-5324.

31. Warshel, A., and Churg, A. K. (1983) Converting structural changes upon oxidation of cytochrome c to electrostatic reorganization energy, *J. Mol. Biol 168*, 687-694.

32. Rogers, N. K., Moore, G. R., and Sternberg, M. J. E. (1985) Electrostatic interactions in globular proteins: Calculation of the pH dependence of the redox potential of cytochrome c_{551}, *J. Mol. Biol. 182*, 613-616.

33. Rogers, N. K., and Moore, G. R. (1988) On the energetics of conformational changes and pH dependent redox behaviour of electron transfer proteins, *FEBS Lett. 228*, 69-73.

34. Zheng, Z., and Gunner, M. R. (2009) Analysis of the electrochemistry of hemes with E_ms spanning 800 mV, *Proteins 75*, 719-734.

35. Cutler, R. L., Davies, A. M., Creighton, S., Warshel, A., Moore, G. R., Smith, M., and Mauk, A. G. (1989) Role of arginine-38 in regulation of the cytochrome c oxidation-reduction equilibrium, *Biochemistry 28*, 3188-3197.

36. Sham, Y. Y., Chu, Z. T., Tao, H., and Warshel, A. (2000) Examining methods for calculations of binding free energies: LRA, LIE, PDLD-LRA, and PDLD/S-LRA calculations of ligands binding to an HIV protease, *Proteins: Struct. Funct. Genet.*

39, 393-407.

37. Simonson, T. (1998) Dielectric constant of cytochrome c from simulations in a water droplet including all electrostatic interactions, *J. Am. Chem. Soc. 120*, 4873-4878.

38. Soares, C. M., Martel, P. J., Mendes, J., and Carrondo, M. A. (1998) Molecular dynamics simulation of cytochrome c_3: studying the reduction processes using free energy calculations, *Biophys. J. 74*, 1708-1721.

39. Ullmann, G. M., Noodleman, L., and Case, D. A. (2002) Density functional calculation of pK_a values and redox potentials in the bovine Rieske iron-sulfur protein, *J. Biol. Inorg. Chem. 7*, 632-639.

40. Olsson, M. H., Hong, G., and Warshel, A. (2003) Frozen density functional free energy simulations of redox proteins: computational studies of the reduction potential of plastocyanin and rusticyanin, *J Am Chem Soc 125*, 5025-5039.

41. Friesner, R. A., and Dunietz, B. D. (2001) Large-scale ab initio quantum chemical calculations on biological systems, *Acc. Chem. Res 34*, 351-358.

42. Muegge, I., Qi, P. X., Wand, A. J. W., Chu, Z. T., and Warshel, A. (1997) The reorganization energy of cytochrome *c* revisted, *J. Phys. Chem. 101*, 825-836.

43. Simonson, T., Archontis, G., and Karplus, M. (2002) Free energy simulations come of age: protein-ligand recognition, *Acc Chem Res 35*, 430-437.

44. Georgescu, R. E., Alexov, E. G., and Gunner, M. R. (2002) Combining conformational flexibility and continuum electrostatics for calculating pK_as in proteins, *Biophys. J. 83*, 1731-1748.

45. Stephens, P. J., Jollie, D. R., and Warshel, A. (1996) Protein control of redox potentials of iron-sulfur proteins, *Chem. Rev. 96*, 2491-2513.

46. Eidsness, M. K., Burden, A. E., Richie, K. A., Kurtz, D. M., Jr., Scott, R. A. S., E. T., Ichiye, T., Beard, B., Min, T., and Kang, C. (1999) Modulation of the redox potential of the [Fe(SCys)4] site in rubredoxin by the orientation of a peptide dipole, *Biochemistry 38*, 14803-14809.

47. Kohn, P (1964) Inhomogeneous Electron Gas, *Phys. Rev. 136*, B864-B871.

48. Sham, (1965) Self-Consistent Equations Including Exchange and Correlation Effects, *Phys. Rev. 140*, A1133-A1138.

49. Kaiser, D. (2005) Drawing Theories Apart: The Dispersion of Feynman Diagrams in Postwar Physics, University of Chicago Press.

50. Cramer, C. J. (2002) *Essentials of Computational Chemistry*, John Wiley & Sons, Ltd.

51. Yang, R. G. P. a. W. (1989) *Density-Functional Theory of Atoms and Molecules* Oxford University Press.

52. Dirac, P. A. M. (1930) Note on exchange phenomena in the Thomas-Fermi atom, *Proc. Cambridge Phil. Roy. Soc. 26*, 376–385.

53. ROBERT J. DEETH, N. F. (2004) The Performance of Nonhybrid Density Functionals for Calculating the Structures and Spin States of Fe(II) and Fe(III) Complexes *J Comput Chem 25*, 1840-1848.

54. Dayle M. A. Smith, M. D., Erich R. Vorpagel, and T. P. Straatsma. (2003) Characterization of Electronic Structure and Properties of a Bis(histidine) Heme Model Complex, *J Am Chem Soc 125*, 2711-2717.

55. Chermette, H. (1998) Density functional theory: A powerful tool for theoretical studies in coordination chemistry *Coordination Chemistry Reviews* 699-721.

56. Martin, A. D. B. a. J. M. L. (2003) The role of the basis set: Assessing density functional theory *JOURNAL OF CHEMICAL PHYSICS 119*, 68.

57. Ghosh, A. (2006) Transition metal spin state energetics and noninnocent systems: challenges for DFT in the bioinorganic arena, *J.Biol.Inorg. Chem. 11*, 712-724.

58. Jensen, F. (1999) *Introduction to Computational Chemistry*, John Wiley and Sons. .

59. Jaguar 6.5, J. (2005) Schrodinger, LLC: Porland, OR.

60. Warwicker, J., and Watson, H. C. (1982) Calculation of the electric potential in the active site cleft due to a a-helix dipoles, *J. Mol. Biol. 157*, 671-679.

61. Gilson, M. K., Rashin, A., Fine, R., and Honig, B. (1985) On the calculation of electrostatic interactions in proteins., *J. Mol. Biol. 183*, 503-516.

62. Takashima, S., and Schwan, H. P. (1965) Delectric dispersion of crystaline powders of amino acids, peptides, and proteins, *J. Phys. Chem. 69*, 4176-4182.

63. Antosiewicz, J., McCammon, J. A., and Gilson, M. K. (1994) Prediction of pH-

dependent properties in proteins, *J. Mol. Biol. 238*, 415-436.

64. Demchuk, E., and Wade, R. C. (1996) Improving the continuum dielectric approach to calculating pK_as of ionizable groups in protein, *J. Phys. Chem. 100*, 17373-17387.

65. Mehler, E. L., and Guarnieri, F. (1999) A self-consistent, microenvironment modulated screened coulomb potential approximation to calculate pH-dependent electrostatic effects in proteins, *Biophys J 77*, 3-22.

66. Sharp, K., Jean-Charles, A., and Honig, B. (1992) A local dielectric constant model for solvation free energies which accounts for solute polarizability, *J. Phys. Chem. 96*, 3822-3828.

67. Song, Y., Mao, J., and Gunner, M. R. (2009) MCCE2: Improving Protein pKa Calculations with Extensive Side Chain Rotamer Sampling, *J. Comp. Chem. epub Mar 9*.

68. Alexov, E. G., and Gunner, M. R. (1999) Calculated protein and proton motions coupled to electron transfer: electron transfer from Q_A^- to Q_B in bacterial photosynthetic reaction centers, *Biochemistry 38*, 8253-8270.

69. Wilson, G. S. (1974) Electrochemical studies of porphyrin redox reactions as cytochromes models, *Bioelectrochem. and Bioenerg. 1*, 172-179.

70. D. M. Collins, R. C., and J. L. Hoard. (1972) Stereochemistry of Low-Spin Iron Porphyrins. I. Bis (imidazole) -a@, y,G-tetraphenylporphinatoiron (111) Chloride, *Journal of the American Chemical Society 94*, 2066-2072.

71. Martin K. Safo, W. R. S., *J and Govind P. Gupta. (1990) Axial Ligand Orientation in Iron(11) Porphyrinates. Preparation and Characterization of Low-Spin Bis(imidazole) (tetraphenylporphyrinato)iron(11) Complexes, *Inorg. Chem. 29*, 626-633.

72. Ghosh, A. (2006) Transition metal spin state energetics and noninnocent systems: challenges for DFT in the bioinorganic arena , *J Biol Inorg Chem 11*, 712-724.

73. Walker, F. A. (2004) Models of the Bis-Histidine-Ligated Electron-Transferring Cytochromes. Comparative Geometric and Electronic Structure of Low-Spin Ferro- and Ferrihemes, *Chemical Reviews 104*, 589-615.

74. Fufezan, C., Zhang, J., and Gunner, M. R. (2008) Ligand preference and orientation in b- and c-type heme-binding proteins, *Proteins 73*, 690-704.

75. Zaric, S. D., Popovic, D. M., and Knapp, E. W. (2001) Factors determining the orientation of axially coordinated imidazoles in heme proteins, *Biochemistry 40*, 7914-7928.

76. H. M. Berman, J. W., Z. Feng, G. Gilliland, T. N. Bhat, H. Weissig, I. N. Shindyalov, P. E. Bourne. (2000) The Protein Data Bank, *Nucleic Acids Research 28*, 235-242.

77. Reedy CJ, E. M., Gibney BR. . (2008) Development of a heme protein structure electrochemical function database. Nucleic Acids Res, *Nucleic Acids Res 36*, D307-D313.

78. Degtyarenko KN, N. A., Findlay JB. . (1999) PROMISE: a database of bioinorganic motifs., *Nucleic Acids Res 27*, 233-236.

79. Castagnetto JM, H. S., Roberts VA, Getzoff ED, Tainer JA, Pique ME. . (2002) MDB: the metalloprotein database and browser at the scripps research institute., *Nucleic Acids Res 30*, 379-382.

80. Walker, K. I. M. a. F. A. (1997) Investigations of Rotation of Axial Ligands in Six-Coordinate Low-Spin Iron(III) Tetraphenylporphyrinates: Measurement of Rate Constants from Saturation Transfer Experiments and Comparison to Molecular Mechanics Calculations, *J.Phys.Chem. A 101*, 2787-2795.

81. Walker FA, B. H. H., Scheidt WR, Osvath SR. (1986) Models of the cytochromes b. Effect of axial ligand plane orientation on the EPR and Moessbauer spectra of low-spin ferrihemes, *J Am Chem Soc 108*, 5288-5297.

82. Walker, F. A. (2006) The heme environment of mouse neuroglobin: histidine imidazole plane orientations obtained from solution NMR and EPR spectroscopy as compared with X-ray crystallography, *J Biol Inorg Chem 11*, 391-397.

83. Munro OQ, S.-G. J., Turowska-Tyrk I, Mohanrao K, Shokhireva TK, Walker FA, Debrunner PG, Scheidt WR. (1999) Two crystalline forms of low-spin [Fe(TMP)(5-MeHIm)2]ClO4. Relative parallel and perpendicular axial ligand orientations, *J Am Chem Soc* 11144-11155.

84. Smith DM, R. K., Dupuis M, Valiev M, Straatsma TP. (2006) Electronic coupling between heme electron-transfer centers and its decay with distance depends strongly on relative orientation, *J Phys Chem B Condens Matter Mater Surf Interfaces Biophys 110*, 15582-15588.

85. Scheidt WR, C. D. (1986) Preferred orientation of imidazole ligands in metalloporphyrins, *J Am Chem Soc 108*, 1163-1167.

86. Berry EA, W. F. (2008) Bis-histidine-coordinated hemes in four-helix bundles: how the geometry of the bundle controls the axial imidazole plane orientations in transmembrane cytochromes of mitochondrial complexes II and III and related proteins., *J Biol Inorg Chem. 13*, 481-498.

87. Schlichting, I., Berendzen, J., Chu, K., Stock, A. M., Maves, S. A., Benson, D. E., Sweet, R. M., Ringe, D., Petsko, G. A., and Sligar, S. G. (2000) The catalytic pathway of cytochrome p450cam at atomic resolution, *Science 287*, 1615-1622.

88. Valentine JS, S. R., Allen LC, Kahn PC. . (1979) Coupling between oxidation state and hydrogen bond conformation in heme proteins., *Proc Natl Acad Sci 76*, 1009-1013.

89. Molina, P. A., Li, H., and Jensen, J. H. (2003) Intraprotein electrostatics derived from first principles: divide-and-conquer approaches for QM/MM calculations, *J Comput Chem 24*, 1971-1979.

90. Sinclair R, H. S., Chen M, . (1996) Active site structure in cytochrome c peroxidase and myoglobin mutants: Effects of altered hydrogen bonding to the proximal histidine, *BIOCHEMISTRY 35*, 15120-15128.

91. Usov OM, C. P., Shapleigh JP, Scholes CP. (2005) ENDOR investigation of the liganding environment of mixed-spin ferric cytochrome c', *JOURNAL OF THE AMERICAN CHEMICAL SOCIETY 127*, 9485-9494.

92. Babcock, G. T., and Wikström, M. (1992) Oxygen activation and the conservation of energy in cell respirations, *Nature 356*, 301-308.

93. Ferguson-Miller, S., and Babcock, G. T. (1996) Heme/copper terminal oxidases, *Chem. Rev. 96*, 2889-2907.

94. Brzezinski, P., and Larsson, G. (2003) Redox-driven proton pumping by heme-copper oxidases, *Biochim. Biophys. Acta 1605*, 1-13.

95. Wikstrom, M. (2004) Cytochrome c oxidase: 25 years of the elusive proton pump, *Biochim. Biophys. Acta 1655*, 241-247.

96. Winkler, J. R., Malmstrom, B. G., and Gray, H. B. (1995) Rapid electron injection into multisite metalloproteins: intramolecular electron transfer in cytochrome oxidase, *Biophysical Chemistry 54*, 199-209.

97. Ji, H., Yeh, S. R., and Rousseau, D. L. (2004) Modulation of the electron redistribution in mixed valence cytochrome C oxidase by protein conformational changes, *J Biol Chem 279*, 9392-9399.

98. Farver, O., Grell, E., Ludwig, B., Michel, H., and Pecht, I. (2006) Rates and Equilibrium of CuA to heme *a* Electron Transfer in *Paracoccus denitrificans* Cytochrome *c* Oxidase, *Biophysical Journal 90*, 2131-2137.

99. Mills, D. A., Xu, S., Geren, L., Hiser, C., Qin, L., Sharpe, M. A., McCracken, J., Durham, B., Millett, F., and S., F.-M. (2008) Proton-dependent electron transfer from CuA to Heme a and altered EPR spectra in mutants close to heme a of cytochrome oxidase, *Biochemistry 47*, 11499-11509.

CHAPTER II

Statistical study of non-redundant Heme database

2.1 General information of non-redundant heme database

There were 1503 heme proteins with resolution better than 2.5Å in the RCSB PDB protein database as of March 2007. (*1*) They can be grouped into 89 protein families using the Dunbrack PISCES web server (*2*) with cutoff parameters of 25% identity, R-factor bigger than 0.3, resolution better than 2.5Å and at least 30% of the amino acids in the protein within a 10Å sphere of the heme iron. PISCES compares both sequence identity and structural similarity to define protein families. A generated nonredundant heme database, with the total of 132 b and c type hemes in 87 heme protein families, were used in the statistical study. About half of proteins have more than one heme. Two a-type and one o-type heme-binding site found in the two protein families (1V54, 1XME) have been excluded, because there are too few of these types of heme for a valid statistical survey. The ligands of the hemes are identified by having nitrogen, oxygen, or sulfur within 2.5Å of the heme iron. The python script to generate the survey report from the original PDB structures was written by Christian Fufezan in the Gunner lab. (*3*) A summary is shown in Table 2.1.

Sixty-nine out of the one hundred and thirty-two hemes in the non-redundant

database have reported redox potentials. (*4-28*) The distribution of them is shown in figure 2.1. While there is a wide range of the heme redox potential from -550mV (1DKO) to 450mV (1IQC), 75% of the E_ms are between 0 to 400mV. The average and median values are 114mV and 130mV respectively.

Table 2.1 Distribution of ligands to b- and c-type hemes in the nonredundant heme database.

	b-Type Heme		c-type Heme		Sum	
	Occurrence	Percentage	Occurrence	Percentage	Occurrence	Percentage
His-His	17	23.9%	42	68.9%	59	44.7%
His-Met	1	1.4%	10	16.4%	11	8.3%
His-Xaa[a]	2	2.8%	2	3.3%	4	3.0%
His-Ex[b]	31	43.7%	4	6.6%	35	26.5%
Xaa-Xaa	1	1.4%	0	0.0%	1	0.8%
Xaa-Ex	17	23.9%	2	3.3%	19	14.4%
Other	2	2.8%	1	1.6%	3	2.3%
Total	71		61		132	

a). Xaa: amino acids other than His and Met. These include Asn, Asp, Cys, Tyr, Glu, and Lys. b). Ex: denotes hemes without a 6th ligand or an exchangeable, non-amino acid ligand (such as O_2 & H_2O). His-Ex is counted as mono-His in the study. (*3*)

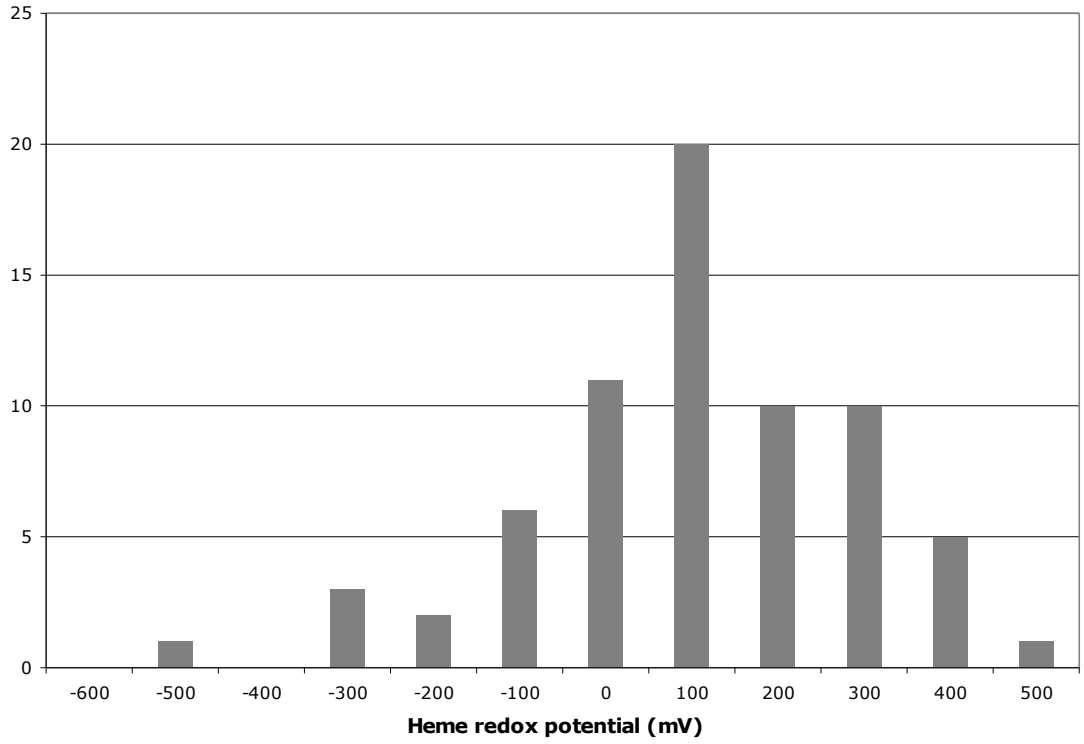

Figure 2.1 The distribution of the known heme redox potentials in the nonredundant heme database.

2.2 Factors determining the heme redox potentials

2.2.1 Heme type

There are 71 Heme b (54%) and 61 Heme c (46%) in the nonredundant heme database. (Table 2.1.1) The histogram of redox potentials for Heme b and c is shown in figure 2.1.2. Heme c is mostly found at the high redox potentials while Heme b is widely distributed from -550mV(1DK0) to 290mV(1V54). The average and median value of redox potentials of b type hemes is 12 and 68mV, while it is 180 and 250mV for c type hemes. The difference of about 170mV between b and c type heme is close to the

standard deviations of E_m's (200mV and 183mV for Heme b and c).

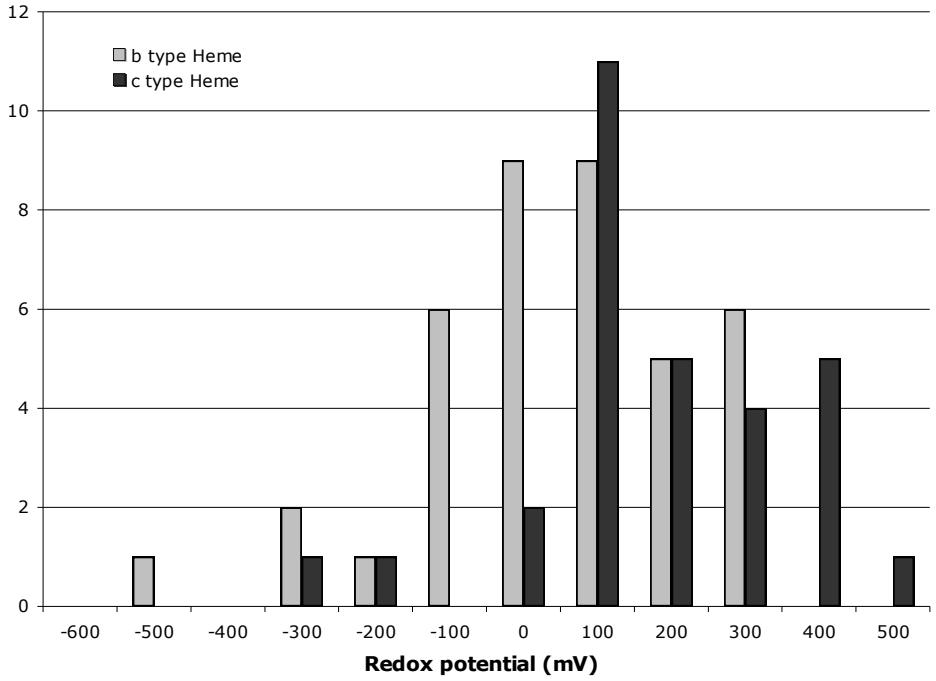

Figure 2.2 The distribution of redox potentials of b- and c- type hemes in non-redundant heme database.

2.2.2 Heme ligand type

Iron in the heme can be in a five- or six-coordinate structure by bonding one or two axial ligands. The table 2.1.1 shows the typical ligand types and their percentages in non-redundant database. The histidine side chain is the most common amino acid to serve as a heme ligand. More than 80% of the hemes have at lease one histidine as axial ligand. Bis-His ligands are 44.7% of the total. They represent 68.9% of the c type hemes but they are only 23.9% of the b type hemes. The His-Met ligand is found in 8.3% and Mono-His ligand is in 26.5% of the structures. The mono-His-Heme is more common for b type

than c type hemes. Amino acids other than histidine and methionine are found rarely.

The distribution of redox potentials in the non-redundant heme database for the different types of heme ligand is shown in figure 2.1.3. Non-histidine ligated hemes are not plotted because too few of them have reported known redox potentials.

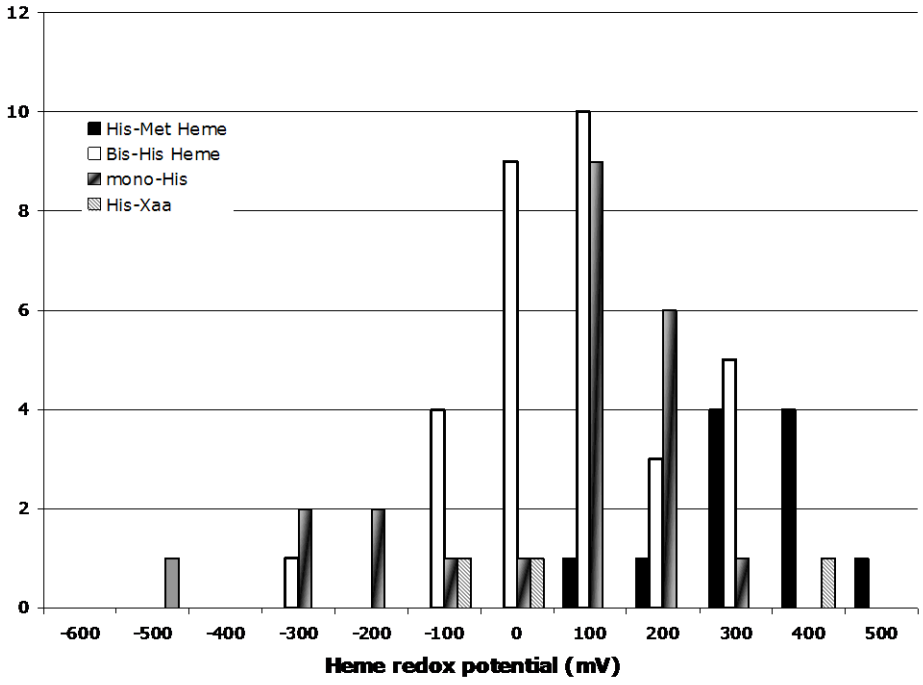

Figure 2.3 The redox potential of hemes in the non-redundant database grouped by the heme axial ligand.

His-Met type hemes are generally found to have high redox potentials. The average value in this category, 256±120mV, is significantly different from the 5±160mV, the average for Bis-His-Heme and 45±170mV, the average for mono-His-Heme. While there is no significant difference between the average of Bis-His-Heme and mono-His-Heme. Bis-His hemes are generally found between -100 to 100mV and mono-His from 0 to 200mV.

The redox potentials are separated by heme type and heme ligand type in Figure 2.1.4. There are five components: b type Bis-His, b type mono-His, c type His-Met, c type mono-His and others. Over 85% of the His-Met ligated hemes are c type. Their redox potential is generally above 250mV. The Fe-S bond between ferrous-iron and Met stabilize the electrons on the heme, favoring the reduced state. (*29*, *30*) The reason that there are much more c type than b type hemes with His-Met ligand is not clear. Many c type His-Met hemes are used in electron transfer proteins such as cytochrome c, c2 and c554.

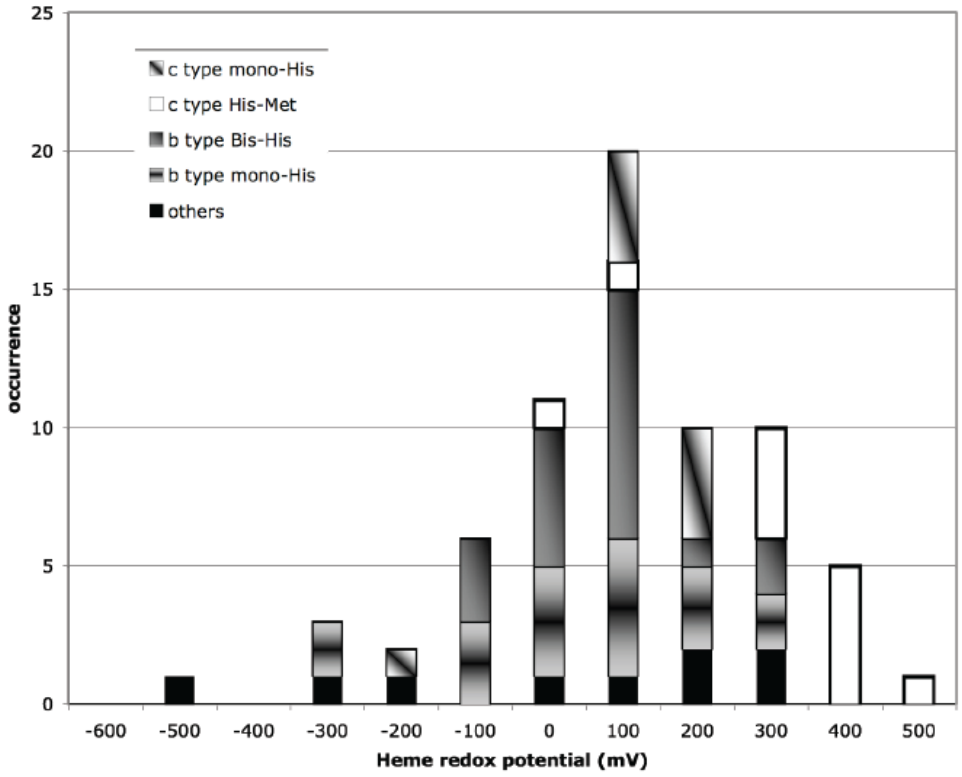

Figure 2.4 The redox potential of hemes in the non-redundant Heme database grouped by Heme type and Heme ligand types.

There are various proteins containing mono-His-Heme, such as Hemoglobin, peroxidases, Heme oxygenases and sensor proteins. The sixth ligand position is open to bind small molecules such as water molecular, dioxygen molecular and hydroxyl. Thus, these Hemes can be functional in molecular transporters or as active site to carry out chemistry as in the binuclear center of cytochrome c oxidase or in P450 protein (*31*). The redox potential distribution of c type mono-His Hemes are different from b type mono-His Hemes. The E_m values of the c type mono-His of Hemes are in the range from 0 to 200mV, compared to that of -300 to 400mV of c type mono-His-Heme.

In summary, the distribution of heme redox potentials can be classified by heme type and heme ligand type. In general, the c type His-Met-Hemes generally has high redox potential and clustered around an average value of 250mV in the nonredundant heme database. The higher potential is caused by the stable Fe-S bond interaction between ferrous-iron and axial methionine ligand according to the HSAB (Hard and Soft Acids and Base) theory. (*29*) The redox potential of Bis-His and mono-His hemes are widely distributed from -300 to 400mV. Their average values are 5 and 45mV, about 200mV lower than c type His-Met hemes. The trend is found consistently in other heme statistical surveys and databases. (*11, 32, 33*)

2.3 Structural features of His-containing hemes in the non-redundant database

Histidine ligated hemes make up 85% of the non-redundant heme database and Bis-His-Heme are 44.7% of the total. These hemes have a wide range of redox potentials. Many of them are used for electron transfer process in proteins such as cytochrome c,

cytochrome bc1 complex and cytochrome c oxidase. (*34-37*) The structural features that modify their redox potentials have been under investigation for decades. (*3, 34*) The distribution of the histidine orientation relative to the heme plane, the relative orientation of the two histidine ligands and the presence of a hydrogen bond to the histidine ligand are evaluated in the non-redundant data sets.

2.3.1 Histidine ligand orientation relative to the heme plane

The histidine ring of heme axial ligand is perpendicular to the porphyrin plane. The orientation of the ligand on the heme plane is defined by the angle alpha between the histidine CG-ND vector and the heme FE-CHA vector (Figure 2.1.5). (*3*)

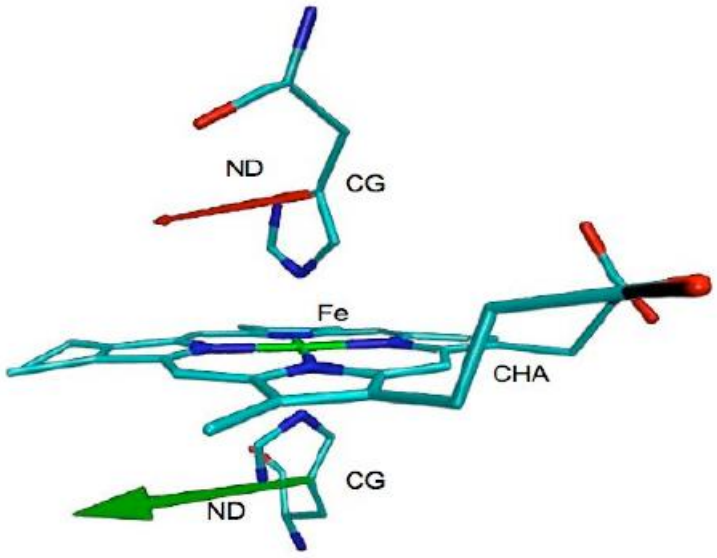

a)

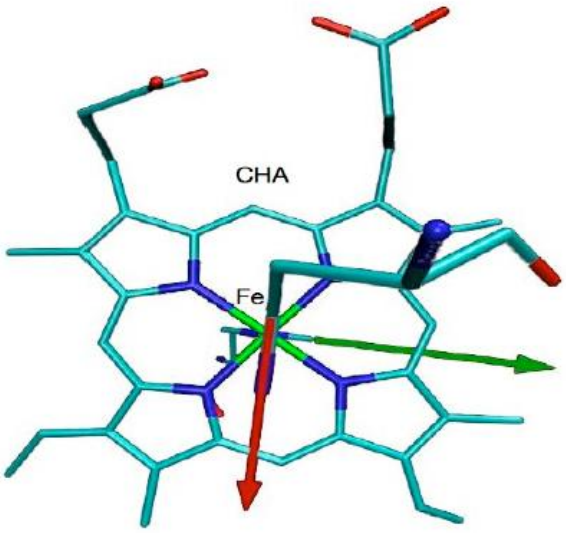

b)

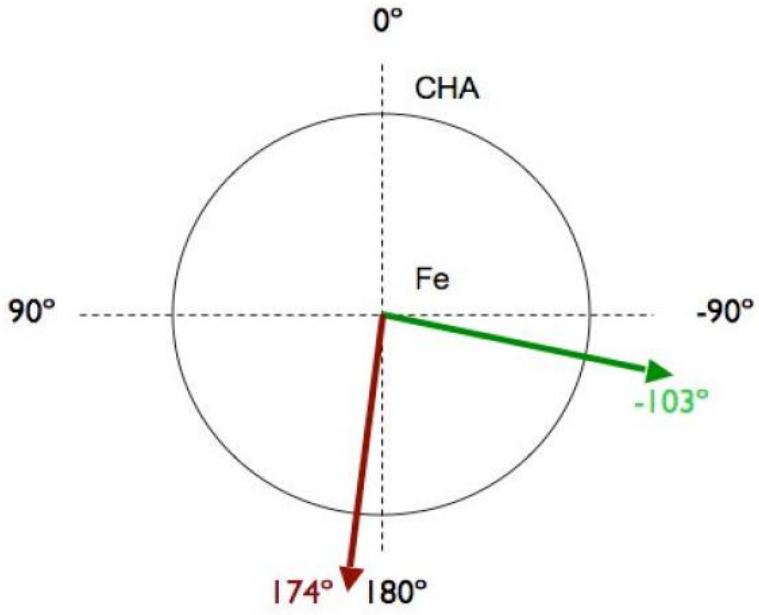

c)

Figure 2.5 The histidine ligand orientations defined by alpha angle.
a) The orientations of two histidines relative to the heme plane. CG-ND vectors are labeled in different colors for the two histidines. b) Top view of the same Bis-His-Heme, the two vectors are projected to the porphyrin plane. c) The alpha angles expressed on a circle. The structures are drawn by VMD.

In the c type histidine ligated hemes, there is a unique Cys-Xaa-Xaa-Cys-His (CXXCH) motif structure. The two cystidines ligated at position 8 and 13 of the porphyrin are in a loop that includes the axial histidine ligand. Thus, the histidine orientation relative to the heme plane is constrained by the CXXCH motif. It has been shown by a molecular mechanics calculation in c type Bis-His-Heme model complex that his keeps big positive high barrier for alpha angles around -90˚. (*3*) The energy barrier constraining the histidine disappeared when the CXXCH motif is detached from heme. (*3*) The phenomenon is also seen in the non-redundant heme database. The histogram of heme histidine ligand orientation in figure 2.1.6 showed the histidine orientation is favored at 0˚ in the CXXCH motif of c type Bis-His-Heme and it is never found around -90˚, which is the orientation with the energy peak in the molecular mechanism simulation. (*3*) By comparison, the histidine ligands without the influence of CXXCH motif in b and c types heme are generally distributed at all angles.

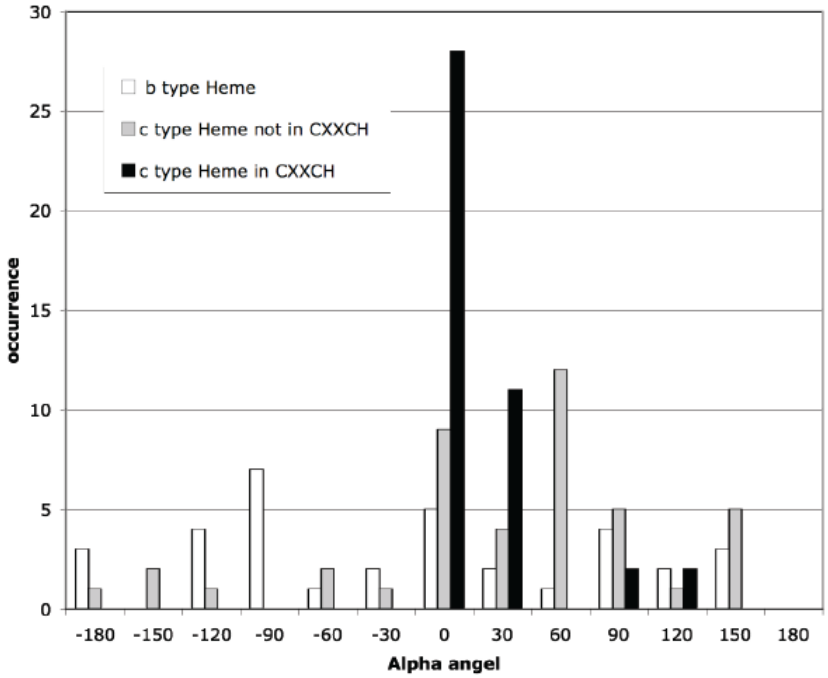

Figure 2.6 The distribution of heme histidine ligand orientation in b and c type heme.

The distribution of alpha angles for histidines not in the CXXCH motif does not have a strong angular preference. (Figure 2.1.6) However, they are more likely to be 45˚, 135˚, -45˚and -135˚ than around 0˚, 90˚, -90˚, and -180˚. The phenomenon is explained by the Van der Waals interaction between the imidazoles and the heme plane. (*34*) When the imidazole plane is rotated into the position on top of any nitrogen atom of the heme plane, the Van der Waals interaction between imidazole and the heme is more unfavorable than when the imidazole plane points between the neighboring nitrogen atoms. In addition there is an electrostatic interaction between the His and the heme propionic acids that affects the imidazole orientation preference. Assuming both propionic acids are neutral, the dipole-dipole interaction between histidine and the propionic acids is 1kcal/mol favorable in when the alpha is 0˚ than 90˚ in the

electrostatics calculation with a uniform dielectric constant 6. If the propionic acids are both ionized, the energy difference can be as big as 4kcal/mol.

2.3.2 Relative histidine ligand orientations in Bis-His-Hemes

The relative angle between the two histidine planes on either side of Bis-His-Heme in the non-redundant heme database (Figure 2.1.7) shows the different preference in b and c type hemes. The perpendicular orientation with a relative angle around 90˚ is favored in the b type Bis-His-Heme. There is no clear preference for a particular relative histidine orientation in c type Bis-His-Heme. Whether the relative histidine orientation is influenced by the CXXCH motif is unclear. DFT method was employed to study the energy preference of the different relative Imidazole orientation in Bis-His-Heme complexes in Chapter 3.

There are some patterns in the relative orientations that depend on the nature of the protein structure. Classifying the relative histidine orientations by protein families in the non-redundant dataset, there are 3 times as many perpendicular structures as parallel structures in b type Bis-His-Hemes. Cytochromes b_2, b_5 and Cytochrome c Oxidase have parallel Bis-His ligand orientations. The E_m of Cytochromes b_2 and b_5 are around 0 mV and that of Heme b of quinol oxidase are around 300mV. (*11*) The families with perpendicular ligand orientations include Globins, (*38-41*) NO_3 reductase, DHG, DHG succinate (*42, 43*) and BC1 complex (*36, 44*). Their redox potentials are distributed from -300 to 200 mV. Thus there does not seem to be a correlation of the redox potential with ligand orientation.

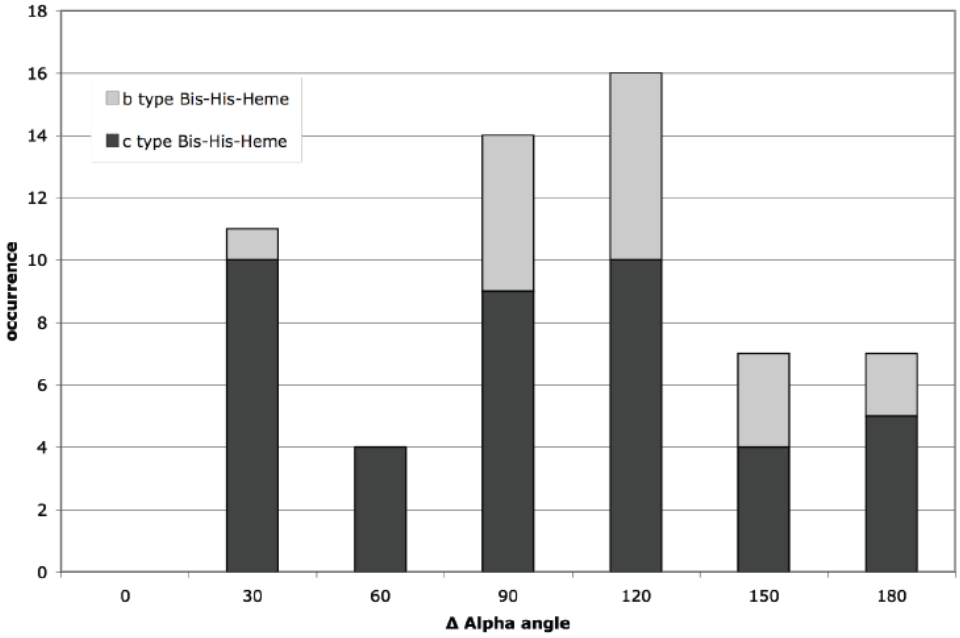

Figure 2.7 The comparison of relative histidine orientation in Bis-His-Heme. B and c type Heme.

2.3.3 The Hydrogen bond of heme histidine ligand

75% of histidine ligands can be found to make a hydrogen bond with an amino acid or crystallographic water to the 63 heme histidine ligands in the non-redundant heme database (Table 2.1). The distribution of the types of hydrogen bond partners to the histidine ligand in b type histidine ligated hemes in the non-redundant heme database is shown in Table 2.2. A hydrogen bond can shift the redox potential of heme complex down. Simulations with DFT and Continuum Electrostatics methods in Chapter 3 present a more detailed analysis of the effects of the hydrogen bond in the redox chemistry. The S44D mutation of Cytochrome c Oxidase presented in Chapter 4 gives an example of the

impact of a hydrogen bond to the heme histidine ligand on the electrochemistry of a protein.

Table 2.2 The distribution of the types of hydrogen bond partners to the histidine ligand in b type histidine ligated heme in the non-redundant heme database.

Hydrogen bond partner	Occurrence	Percentage (%)
H_2O	6	9.5%
No partner	16	25.4%
Amino Acids total	41	65.1%
Amino Acids backbone	25	39.7%
Amino Acids side chain	16	25.4%
ASP	6	9.5%
GLU	2	3.2%
SER	2	3.2%
Total	63	100.0%

2.3.4 Fe-N distance between heme iron and axial histidine ligand

The axial bond length between heme iron and the nitrogen ligand is sensitive to the spin state, coordination number and oxidation state. (*45*, *46*) The Fe-N distances in the non-redundant heme database range from 1.9Å to 2.9Å, with the peak at 2.05Å. There is no significant correlation between heme redox potential and crystal structure Fe-N distance. The lack of correlation may be due to the importance of the spin state,

coordination number and oxidation state that are not accounted for the non-redundant heme database. The other reason is the scale of Fe-N distance shift (such as 0.1Å shift from Jahn-Teller effect (*47*)) is below the resolution in the current X-ray structures with resolution of 1.2 - 2.5Å.

In summary, a non-redundant heme database was built to study the patterns of heme structural features and their linkage with heme redox potentials. The database consists of 132 representative hemes identified by sequence and structural alignments with a 2.5Å resolution cutoff using the Dunbrack webserver. The distributions of heme type, heme ligand type, histidine ligand orientation, relative orientation of histidines in Bis-His-Heme and the distance between heme iron and axial histidine nitrogen were investigated.

The average redox potentials of c type His-Met hemes are 200mV higher than the value of b or c type Bis-His heme and mono-His heme. The database also showed that the orientation of the histidine ligand in CXXCH motif of c type hemes is clustered on the alpha angle of 0˚, which is energetically consistent with the molecular mechanics calculation of the His in the CXXCH motive in a heme model complex. (*3*) In b type Bis-His-Heme, the number of the histidine ligands perpendicular to each other is three times bigger than the number with parallel orientations. These features observed in the non-redundant heme database can be used to help protein design with bonded hemes and desired heme electrochemistry. For example, knowledge of the geometric constrains of the histidine ligand orientation is useful in designing the heme cofactors in helical bundle structures. (*41, 48, 49*) Mutating the heme ligand residue can tune the redox potential of

heme. (*50-53*) The non-redundant heme database was also used to determine the protein secondary structure binding the heme and the occurrences of different amino acids in the heme binding sequences. The results have aided de novo protein design. (*48*)

A hydrogen bond to the axial histidine ligand of heme can shift the redox potential. The non-redundant heme database shows the distribution of the hydrogen bond acceptors. Computational research based on simplified model complexes was carried on to understand the redox potential shift due to the existence of an axial histidine hydrogen bond in Chapter 3. An important study of S44D mutation in *Rb. sphaeroides* Cytochrome c oxidase gives a detailed analysis of the effect of this hydrogen bond in the protein environment in Chapter 4.

References

1. Berman HM, H. K., Nakamura H. (2003) Announcing the worldwide protein data bank. , *Nat Struct Biol 10*, 980.

2. Wang G, D. R., Jr. (2005) PISCES: recent improvements to a PDB sequence culling server. , *Nucleic Acids Res 33*, W94-W98.

3. Fufezan, C., Zhang, J., and Gunner, M. R. (2008) Ligand preference and orientation in b- and c-type heme-binding proteins, *Proteins 73*, 690-704.

4. Wirtz, M., Oganesyan, V., Zhang, X., Studer, J., and Rivera, M. (2000) Modulation of redox potential in electron transfer proteins: effects of complex formation on the active site microenvironment of cytochrome b5, *Faraday Discuss 116*, 221-234.

5. Northup, S. H. (1996) Computer modelling of protein-protein interactions, in *Protein Electron Transfer* (Bendall, D. S., Ed.), pp 69-98, Bios, Cambridge.

6. Meyer, T. E., Watkins, J. A., Przysiecki, C. T., Tollin, G., and Cusanovich, M. A. (1984) Electron-transfer reactions of photoreduced flavin analogues with c-type cytochromes: quantitation of steric and electrostatic factors, *Biochemistry 23*, 4761-4767.

7. Samyn B, F. J., Meyer TE, Cusanovich MA, Van Beeumen JJ. (1998) Purification and primary structure analysis of two cytochrome c2 isozymes from the purple phototrophic bacterium Rhodospirillum centenum. , *Biochim Biophys Acta 1384*, 345-355.

8. Pettigrew, G. W., Bartsch, R. G., Meyer, T. E., and Kamen, M. D. (1978) Redox potential of the photosynthetic bacterial cytochromes c2 and the structural bases for variability., *Biochim. Biophys, Acta 503*, 509-523.

9. Meyer, T. E., and Kamen, M. D. (1982) *Adv. Prot. Chem. 35*, 105-212.

10. Louro RO, C. T., Turner DL, Picarra-Pereira MA, Pacheco I, LeGall J, Xavier AV. (1998) Functional and mechanistic studies of cytochrome c3 from Desulfovibrio gigas: thermodynamics of a ‘‘proton thruster.’’ *Biochemistry 37*, 15808-15815.

11. Reedy, C. J., and Gibney, B. R. (2004) Heme protein assemblies, *Chem. Rev. 104*, 617-649.

12. Fan, K., Akutsu, H., Kyogoku, Y., and Niki, K. (1990) Estimation of microscopic redox potentials of a tetraheme protein, cytochrome c_3 of *Desulfovibrio vulgaris*, Miyazaki F, and partial assignments of heme groups, *Biochemistry 29*, 2257-2263.

13. Turner, D. L., Salgeiro, C. A., Catarino, T., Legall, J., and Xavier, V. (1996) NMR studies of cooperativity int he teprahaem cytochrome c3 from Desulfovibrio vulgaris, *Eur. J. Bjiochem. 241*, 723-731.

14. Pieulle L, H. J., Bonicel J, Hatchikian EC. (1996) Biochemical studies of the c-type cytochromes of the sulfate reducer Desulfovibrio africanus. Characterization of two tetraheme cytochromes c3 with different specificity., *Biochim Biophys Acta 1273*, 51-61.

15. Leitch FA, B. K., Pettigrew GW. (1985) Complexity in the redox titration of the dihaem cytochrome c4, *Biochim Biophys Acta 808*, 213-218.

16. Navarro JA, H. M., De la Cerda B, De la Rosa MA. (1995) Purification and physicochemical properties of the low-potential cytochrome C549 from the cyanobacterium Synechocystis sp. PCC 6803, *Arch Biochem Biophys 318*, 46-52.

17. Holton RW, M. J. (1967) Water-soluble cytochromes from a blue-gree alga. II. Physicochemical properties and quantitative relationships of cytochromes C (549, 552, and 554 Anacystis nidulans). *4Biochim Biophys Acta 131*, 375-384.

18. Lommen A, R. A., Bijlsma N, Canters GW, van Wielink JE, Frank J, van Beeumen J. (1990) Isolation and characterization of cytochrome c550 from the methylamine-oxidizing electron-transport chain of Thiobacillus versutus. , *Eur J Biochem 192*, 653-661.

19. Saraiva LM, F. G., Besson S, Moura I. (1994) Physico-chemical and spectroscopic properties of the monohemic cytochrome C552 from Pseudomonas nautica 617. , *Eur J Biochem 224*, 1011-1017.

20. Terui, N., Tachiiri, N., Matsuo, H., Hasegawa, J., Uchiyama, S., Kobayashi, Y., Igarashi, Y., Sambongi, Y., and Yamamoto, Y. (2003) Relationship between redox function and protein stability of cytochromes c, *J. Am. Chem. Soc. 125*, 13650-13651.

21. Campos AP, A. A., Hervas M, Regalla M, Navarro JA, Ortega JM, Xavier AV, De La Rosa MA, Teixeira M. (1993) Cytochrome c6 from Monoraphidium braunii. A cytochrome with an unusual heme axial coordination. , *Eur J Biochem*

216, 329-341.

22. Gorman DS, L. R. (1966) Photosynthetic electron transport chain of Chlamydomonas reinhardi. V. Purification and properties of cytochrome 553 and ferredoxin., *Plant Physiol 41*, 1643-1647.

23. Cho YS, W. Q., Krogmann D, Whitmarsh J. (1999) Extinction coefficients and midpoint potentials of cytochrome c6 from the cyanobacteria Arthrospira maxima. Microcystis aeruginosa, and Synechocystis 6803. , *Biochim Biophys Acta 1413*, 92-97.

24. Dikiy A, C. W., Vandenberghe I, Borsari M, Safarov N, Dikaya E, Van Beeumen J, Ciurli S. (2002) Structural basis for the molecular properties of cytochrome c6., *Biochemistry 41*, 14689-14699.

25. Correia IJ, P. C., Louro RO, Catarino T, Turner DL, Xavier AV. . (2002) Thermodynamic and kinetic characterization of trihaem cytochrome c3 from Desulfuromonas acetoxidans. , *Eur J Biochem 269*, 5722-5730.

26. Fulop V, R. C., Greenwood C, Hajdu J. . (1995) Crystal structure of the di-haem cytochrome c peroxidase from Pseudomonas aeruginosa. , *Structure 3*, 1225-1233.

27. Santos H, T. D. (1989) Characterization and NMR studies of a novel cytochrome c isolated from Methylophilus methylotrophus which shows a redox-linked change of spin state. , *Biochim Biophys Acta 954*, 277-286.

28. Engel WD, S. H., von Jagow G. . (1980) Ubiquinol-cytochrome c reductase (EC 1.10.2.2). Isolation in triton X-100 by hydroxyapatite and gel chromatography. Structural and functional properties. , *Biochim Biophys Acta 592*, 211-222.

29. Pearson, R. G. (1963) Hard and Soft Acids and Bases, *J. Am. Chem. Soc. 85*, 3533–3539.

30. Ghosh, A. (2006) Transition metal spin state energetics and noninnocent systems: challenges for DFT in the bioinorganic arena, *J.Biol.Inorg. Chem. 11*, 712-724.

31. Musser, S. M., and Chan, S. I. (1998) Evolution of the cytochrome c oxidase proton pump, *J Mol Evol 46*, 508-520.

32. Zaric, S. D., Popovic, D. M., and Knapp, E. W. (2001) Factors determining the orientation of axially coordinated imidazoles in heme proteins, *Biochemistry 40*, 7914-7928.

33. Zheng, Z., and Gunner, M. R. (2009) Analysis of the electrochemistry of hemes

with E_ms spanning 800 mV, *Proteins 75*, 719-734.

34. Kurreck, J., Refifarth, F., Karge, M., and Renger, G. (1995) Reconstitution of the endogenous plastoquinone pool in photosystem II (PS II) membrane fragments, inside-out-vesicles, and PS II core complexes from spinach, *Biochemistry 34*, 15721-15731.

35. Trumpower, B. L. (1990) Cytochrome bc_1 complexes of microorganisms, *Microbiol Rev 54*, 101-129.

36. Crofts, A. R. (2004) The cytochrome bc1 complex: function in the context of structure, *Annu Rev Physiol 66*, 689-733.

37. Brzezinski, P. (2004) Redox-driven membrane-bound proton pumps, *Trends Biochem. Sci. 29*, 380-387.

38. Taylor, J. F. (1981) Measurement of the oxidation-reduction equilibria of hemoglobin and myoglobin, *Meth. Enz. 76*, 577-582.

39. Gibney, B. R., Isogai, Y., Rabanal, F., Reddy, K., Grosset, A., Moser, C., and Dutton, P. (2000) Self-assembly of heme a and heme b in a designed four helix bundle implications for a cytochrome c oxidase maquette., *J. Am. Chem. Soc. 39*, 11041-11049.

40. Koder, R. L., Valentine, K. G., Cerda, J., Noy, D., Smith, K. M., Wand, A. J., and Dutton, P. L. (2006) Nativelike Structure in Designed Four alpha-Helix Bundles Driven by Buried Polar Interactions, *J Am Chem Soc 128*, 14450-14451.

41. Koder, R. L., and Dutton, P. L. (2006) Intelligent design: the de novo engineering of proteins with specified functions, *Dalton Trans*, 3045-3051.

42. Lancaster, C. R., Herzog, E., Juhnke, H. D., Madej, M. G., Muller, F. G., Paul, R., and Schleidt, P. G. (2008) Electroneutral and electrogenic catalysis by dihaem-containing succinate:quinone oxidoreductases, *Biochem Soc Trans 36*, 996-1000.

43. Lancaster, C. R., and Kroger, A. (2000) Succinate: quinone oxidoreductases: new insights from X-ray crystal structures, *Biochim Biophys Acta 1459*, 422-431.

44. Trumpower, B. L. (1991) The three-subunit cytochrome bc_1 complex of *Paracoccus denitrificans*. Its physiological function, structure, and mechanism of electron transfer and energy transduction, *J Bioenerg Biomembr 23*, 241-255.

45. Scheidt, W. R., and Reed, C. A. (1981) Spin-state/stereochemical relationships in iron porphyrins: Implications for the hemoproteins, *Chem. Rev. 81*, 543-555.

46. Scheidt W, L. Y. (1987) Recent advances in the stereochemistry of metal-lotetrapyrroles., Springer.

47. Hajime Hirao, S. S., and Pawel M. Kozlowski. (2006) Theoretical Analysis of the Structural and Electronic Properties of Metalloporphyrin π-Cation Radicals *J. Phys. Chem. A 110*, 6091-6099.

48. Negron, C., Fufezan, C., and Koder, R. L. (2009) Geometric constraints for porphyrin binding in helical protein binding sites, *Proteins 74*, 400-416.

49. Kennedy, M. L., Silchenki, S., Houndonougbo, N., Gibney, B. R., Dutton, P. L., Rodgers, K. R., and Benson, D. R. (2001) Model hemoprotein reduction potentials: the effects of histidine-to-iron coordination equilibrium, *J. Am. Chem. Soc. 123*, 4635-4636.

50. Chen, Z. C., Ost, T. W. B., and Schelvis, J. P. M. (2004) Phe393 mutants of cytochrome P450BM3 with modified heme redox potentials have altered heme vinyl and propionate conformations, *Biochemistry 43*, 1798-1808.

51. Ishikita, H., Morra, G., and Knapp, E. W. (2003) Redox potential of quinones in photosynthetic reaction centers from *Rhodobacter sphaeroides*: dependence on protonation of Glu-L212 and Asp-L213, *Biochemistry 42*, 3882-3892.

52. Osyczka, A., Dutton, P. L., Moser, C. C., Darrouzet, E., and Daldal, F. (2001) Controlling the functionality of cytochrome c_1 redox potentials in the *Rhodobacter capsulatus* bc_1 complex through disulfide anchoring of a loop and a beta-branched amino acid near the heme-ligating methionine, *Biochemistry 40*, 14547-14556.

53. Kay, C. J., and Lippay, E. W. (1992) Mutation of the Heme-Binding Cervice of Flavocytochrome b2 form Saccharomyces cerevisae: Altered Heme Potential and Absence of Redox Cooperativity between Heme and FMN Centers, *Biochemistry 31*, 11376-11382.

CHAPTER III

A DFT and Continuum Electrostatics study of redox potentials and energy preference in Imidazole-Porphyrin model complexes

3.1 Introduction

Previous statistical surveys of a non-redundant heme database have suggested that the heme and ligand type are important factors that help to control the redox potential of a heme. (Figure 2.4) Histidine is most common ligand to heme cofactors in proteins. (Table 2.1) In Bis-His-Heme proteins, the relative orientation of two histidine ligands is not significantly correlated with redox potential in the survey of non-redundant database. However, b type Bis-His-Hemes in the database have their histidine in a perpendicular orientation 3 times more frequently than in a parallel orientation. EPR and Mossbauer studies of TMPFe model complex suggested the parallel orientation could be energetically favorable. (*1-3*) In this research, DFT simulations were used to investigate the energy preference of the relative orientation of imidazole rings of Bis-imidazole-porphyrin complex. The effect of a ruffled porphyrin is tested and discussed.

The redox potential of a heme site is sensitive to the nature of the axial ligands and to the environment around the site. (*4*, *5*) There are often abundant hydrogen bonds found between the distal histidine ligand of heme and the protein. Thus, it is interesting to

study how the heme redox potential is shifted by the hydrogen bond. The understanding of the tuning of heme redox potentials can be key to the analysis of heme containing proteins such as cytochrome c oxidase (*6-8*), peroxidase (*9-11*), hemoglobin (*12-14*) and other proteins. DFT and Continuum Electrostatics simulations based on simplified model complex of Bis-Imidazole-Porphyrin and its derivative structures were employed and compared.

3.2 DFT simulation of parallel vs. perpendicular orientation of Bis-imidazole-porphyrin

The relative orientation of the two imidazole rings of the heme ligands has been suspected an important structural factor influencing the energy in both ferric- and ferrous-Bis-His-Hemes,. (*4, 15, 16*) The dihedral angles between the two imidazole planes define the relative orientation angle. (*17, 18*) Thus the complex with a histidine at the angle of 0° or 180° are in the parallel orientation, while one at 90° and 270° are in the perpendicular orientation.

In the non-redundant survey of the b type Bis-His-Hemes discussed in Chapter 2 (see Figure 2.1.4), 85% of the histidine alpha angles are within 30° of either a parallel or perpendicular orientation, higher than the ratio of 67% if the relative orientation was uniformly distributed. The number in a perpendicular structure is about three times of the parallel structure. By contrast, in c type Bis-His-Hemes where one of the histidines is constrained by the CXXCH motif (*19*), the number in the perpendicular structure is about the same in the parallel structure.

Experiments on model hemes support a lower energy for a parallel orientation contradicting to the results of the statistical survey in the non-redundant heme database. EPR and Mossbauer data for Bis-imidazole and Bis-pyridine coordinated OETPP-, OMTPP- and TMPFe(III) complexes suggested the g_{zz} value, and hyperfine coupling constant A_{zz} are highly correlated with the relative angles between imidazoles. (*1 2006, 3*) Therefore, Walker proposed that the parallel orientation is favored for a low spin heme. (*1, 4, 5, 20-22*) There is also evidence that the perpendicular orientation is stabilized in the TMPFe(III) structure at low temperature. (*5*) However, Scheidt suggested energy difference between parallel and perpendicular orientations is less than 3kcal/mol in the TMPFe complex. (*4*)

The ruffling of the heme plane may be the reason for the conflicting results. Heme planes in most of the model systems are very ruffled because of the introduced meso-carbon groups in TMPFE model complex. (*3*) The ruffling may change the energy preference between relative parallel and perpendicular orientation (*22*).

3.2.1 Model complex

A simulation study was carried out with a Bis-Imidazole-porphyrin complex with perfect flat heme plane without ruffling. The system energy dependence on the relative orientations of imidazole rings was calculated by DFT simulation.

A simplified Bis-Imidazole-Porphyrin model was built to study the problem. Imidazole planes on the both sides are perpendicular to the heme plane. Their aromatic rings are close to the π orbital of the heme ring. In the model, the propionic acids, vinyl

and methyl groups of the heme plane are replaced by hydrogen atoms. The histidines are reduced to imidazole rings. Thus, the complex is a porphyrin ligated with two imidazoles. (See Fig3.1.1)

As the heme core has a D_{4h} symmetry, two imidazoles are placed between the neighboring porphyrin nitrogen atoms. Now the normal line of each imidazole is parallel to the perpendicular bisector of the neighboring nitrogen atoms in the porphyrin. The relative angle between the imidazole normals identifies whether the imidazoles are parallel or perpendicular to each other. The ionization state of the iron atom inside the porphyrin is either Fe^{2+} or Fe^{3+}. With the -2 charge distributed in porphyrin ring, the total charge of the complex is 0 for ferrous-porphyrin and +1 for ferric-porphyrin. There are four combinations of imidazole orientations and ionization states. Their system energies were calculated by the DFT method within the Jaguar program. (*23*)

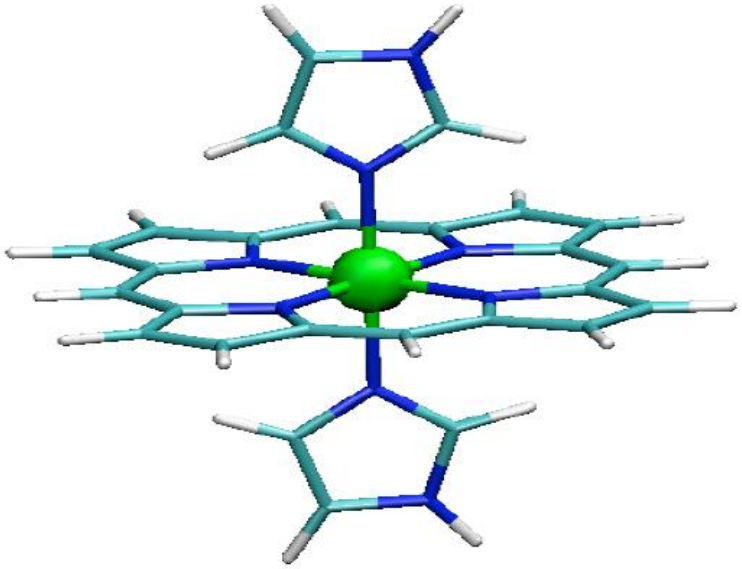

a)

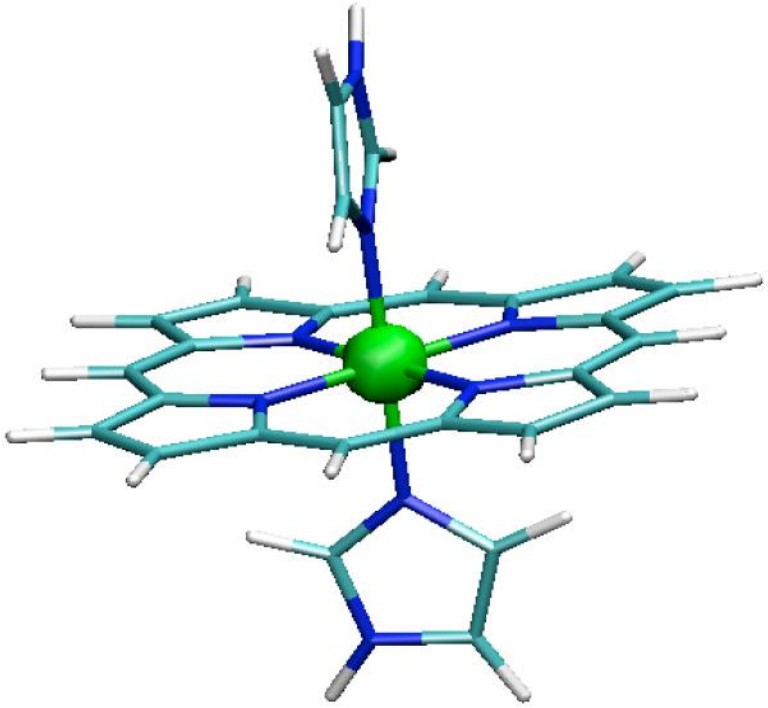

b)

Figure 3.1 Bis-Imidazole-porphyrin complex with (a) parallel orientation and (b) perpendicular orientation.

3.2.2 The simulation methods

The total system energy of a complex is calculated from a single point energy calculation based on the geometrical optimized complex. B3LYP is used as the method, based on the successful studies on heme complexes in literature (*16, 24, 25*) Two basis sets were set up for the optimization of complex: LACV3P* for Fe atom and 6-311G* for the other atoms. In the single point calculation, bases set were set up as: LACV3P* for Fe atom, 6-311G** for ligated nitrogen atoms and 6-311G**+ for the other atoms.

The formal charges of the Fe and the ligated nitrogen atoms are set given the ionization states of the complex. The iron multiplicity was in the low spin state. The dielectric constant is 6 in the Jaguar calculation. A quick geometric refinement based on maestro, the Jaguar interface, was followed by the complete geometric optimization.

3.2.3 Result and discussion

After the structure optimization and single point energy calculation, the system energies with different imidazole relative orientations and porphyrin redox states are calculated and compared (Table 3.1).

Table 3.1. Calculated system energy comparison between parallel and perpendicular orientations.

Ionization states	Ferrous-porphyrin (neutral)	Ferric-porphyrin (+1)
Parallel (Hartree unit)	-1564.75047	-1564.55647
Perpendicular (Hartree unit)	-1564.75133	-1564.55779
Difference (kcal/mol)	0.5409	0.8323

The energy gaps between parallel and perpendicular complex are less than 1kcal/mol in both ferrous-porphyrin and ferric-porphyrin states with the perpendicular complex energetically favored in the Jaguar calculation. Straatsma's group conducted a study on the same complex with the B3LYP Method and VTZ basis set using the NWChem software. The optimized structure geometries are very close. For example, the Fe-N (porphyrin) distance of 2.03Å and Fe-N (imidazole) of 2.05Å are the same as those

found here. The reported energy gap in the ferrous-porphyrin complex is 0.3kcal/mol, very close to the 0.54kcal/mol reported here, but their calculations favor the parallel complex in the ferric-porphyrin complex by 0.6kcal/mol. (*21, 25*)

3.2.4 Parameter sensitivity of the model

The B3lyp method has proved to be suitable for the simulation of metal center complex. (*16, 24, 25*) Do the other parameters, including basis set, diffusion and polarization of the single point calculation change the conclusions? Table 3.2 describes the energy gap between parallel and perpendicular in ferrous- and ferric-porphyrin systems when the basis set for the single point calculation of the other atoms (see calculation set-up for more details) is changed.

Table 3.2. Energy comparison between parallel and perpendicular imidazole orientation when changing the basis-set for the other atoms of imidazole and porphyrin

Basis-set for "the other atoms"	Ferrous-porphyrin (neutral) (parallel - perpendicular) kcal/mol	Ferric-porphyrin (+1) (parallel - perpendicular) kcal/mol
6-311g**+	0.5409	0.8323
6-311g*+	0.4464	0.6914
6-31g*+	0.3531	0.6631

The energy comparison in Table 3.2 shows the previous conclusions are hold. The energy gaps range between 0.35 to 0.54kcal/mol for ferrous-complex and 0.66 to 0.83 kal/mol for ferric-complex. Perpendicular orientation structure is energetically favored by

less than 1kcal/mol in all scenarios with different basis sets and polarization parameters for the other atoms.

3.2.5 Ruffling

The results and conclusions in table 3.1 and 3.2 are based on the optimized structures with flat heme core. What if the initial heme structure was ruffled? The average value of NA-Fe-NC and NB-Fe-ND angles are defined as the ruffling angle. Jaguar's graphic interface Maestro, which performs a quick refinement before structure optimization yield a ruffling angle of 170˚ for the perpendicular ferrous-Bis-imidazole-porphyrin complex. The average value in the non-redundant heme protein survey is 172˚ and the totally flat porphyrin plane is 180˚ degree. One of the imidazoles in the structure was then rotated by 90° to form the parallel orientation.

After Jaguar structural optimization, both structures become flatter. The ruffling angle for parallel and perpendicular structures are now 174˚ and 178˚ accordingly. Then, single point calculations are conducted with the ruffled complex. The same procedure is carried on for the ferric-complex. After optimization, the ruffling angles are now 174˚ and 176˚ for parallel and perpendicular structures. The ruffling angles and energy differences between parallel and perpendicular complex are presented in table 3.3.

Table3.3 Energy differences between the parallel and perpendicular Bis-imidazole-porphyrin ruffled complex in DFT simulation. The ruffling angles of structures are also presented.

Single point energy / ruffling angle	Ferrous-porphyrin (neutral)	Ferric-porphyrin (+1)
Parallel (Hartree unit) Ruffling angle	-1564.75234 174˚	-1564.560924 174˚
Perpendicular (Hartree unit) Ruffling angle	-1564.75314 178˚	-1564.56102 176˚
Difference of the ruffled porphyrin complex (kcal/mol)	0.5022	0.0605
Difference of the flat porphyrin complex (kcal/mol) (From Table 2.1)	0.5409	0.8323

The perpendicular complexes are always energetically favored by less than 1kcal/mol. Comparing Table3.2 and Table3.3, the preference of orientation is consistent, especially for the ferrous-complex. There is a small energy difference of 0.06kcal/mol between parallel and perpendicular orientation in the ruffled ferric-complex that is 0.8kcal/mol more favorable in the flat ferric-complex. Thus, the perpendicular orientation is destabilized by ruffled heme core.

The ruffling is always reduced during geometry optimization. It was also observed that the structural optimization with ruffled ferric-porphyrin complex could lead to the disassembly of porphyrin core depending on the ruffling angle. The energy comparison between table 1 and 2 also shows that the ruffled structures are energetically unfavorable in the simplified Bis-imidazole-porphyrin model. The vinyl, methyl group and propionic acids in a heme could be the structural factors to stabilize the ruffled heme structure. In addition, the structure of the binding site will have an impact in natural and designed proteins.

In summary, there is no significant energy preference (>1kal/mol) between parallel and perpendicular orientations according to the DFT simulation on the Bis-Imidazole-Porphyrin complex. In a flat porphyrin, the perpendicular orientation is 0.5kcal/mol more favorable in ferrous-Heme complex and 0.8kcal/mol in ferric-Heme complex. The conclusion is consistent with other studies of similar model complexes. (*21*, *25*) The ruffled porphyrin structure is not energetically favored in this simple model. The fact that the ruffled structure of the TMPFE complex favors parallel orientations by 1-3 kcal/mol may be caused by the introduced meso-carbon group. (*3*, *17*, *20*) In the natural heme structure, other groups attached on the porphyrin could be the factor to stabilize the ruffled structure. Thus, the orbital interaction of imidazole planes relative to heme plane are not a key element to determine the energy preference of the flat plane Bis-Imidazole-Porphyrin complex.

3.3 Simulation of the redox potential shift due to Hydrogen bond to a histidine ligand in the porphyrin model complex

3.3.1 Background and objectives

The hydrogen bond is one of the most common non-bonded interactions in a protein environment. It is the attractive interaction between the electropositive hydrogen atom and an electronegative atom, hydrogen bond acceptor. (*26-28*) The hydrogen atom is attached to electron donating atoms such as oxygen or nitrogen. The hydrogen bond interaction is stronger than the van der Waals interaction but much weaker than covalent bonds. (*29*) The typical interaction energy for the O—H-N group is in the range of 1-20Kcal/mol depending on the bond length, bond angle, dielectric constant, temperature and pressure. (*30-36*)

In the statistical survey of the non-redundant heme database, over 80% of the heme histidine ligands form a hydrogen bond with nearby water molecular, backbone or side chain of an amino acid. These hydrogen bonds can shift the redox potential of the histidine ligated heme complex by donating electrons into the histidine and thus into the heme. One question is whether the heme simply feels an electrostatic interaction with the dipole of the hydrogen bond acceptor or if atomic partial charges in electron distribution in the heme ligand complex lead to a large change in heme redox potential. Thus, the electrochemistry of the heme should be studied in addition of the heme-ligand hydrogen bond. Understanding the importance of these features will be helpful to the research field

of protein design (*17, 37-41*), as well as proton and electron transfer process of membrane proteins (*6, 42-44*).

Two model complexes, a Bis-Imidazole-Heme with hydrogen bond partner and a His-HOH-Heme complex are built to study the redox potential shift of heme due to a hydrogen bond to a heme. The interaction energies calculated with DFT and Continuum Electrostatics simulations are compared in the study. The study is helpful to understand and calculate the hydrogen bond energies of the distal histidine ligand of the heme.

3.3.2 The model structures

The statistical survey in Chapter 1 suggested that the heme and ligand type are important factors related to the redox potential of heme, while the relative histidine orientation (in the case of Bis-His-Heme) has less impact on the energy term.

To limit the influence of these factors above, a simplified model complex for the hydrogen bond study is built. As described in section 3.2, the heme plane is perfectly flat without ruffling. The distance between Fe and N atom of the distal ligand is 2.05Å. For the water ligand, the Fe and O of water molecular distance is 2.0Å. The nitrogen atoms form a rectanglular structure within the porphyrin plane. The vinyl and methyl groups are replaced by hydrogen atoms. Thus, the heme plane becomes D_{4h} symmetric with iron in the center. The heme is now a 6-coordinate metal centered complex. The Bis-His and His-HOH porphyrin model are designated as model 1 and model 2.

3.3.3 Simulation of Model 1 (Bis-Imidazole-Porphyrin model)

Porphyrin plane and imidazole rings

The structure of Bis-Imidazole-Porphyrin is the same as described in section 3.2 and presented in Figure 3.1.3. The total charges on ferrous- and ferric-Bis-Imidazole-Porphyrin are 0 and +1.

Hydrogen bond partner

The heme-ligand hydrogen bond survey of the non-redundant PDB database (Figure 3.1.2) shows the distribution of the type of hydrogen bond partner of the histidine ligand in b type Bis-His-Hemes. Out of the 63 representative histidine ligands, 25% do not form hydrogen bonds, while 9.5% have crystallographic water as a hydrogen bond partner and 65% are with amino acids. The oxygen atom of the backbone of the amino acids is the most common hydrogen bond accepter, representing 40% of the total. About a quarter of the hydrogen bond partners are to the side chains of amino acids within the protein. One third of these (9.5% of the total) are aspartic acids. The glutamic acid, serine and other residues are each found only 1-2 times in the total non-redundant dataset. Given their frequency, the backbone, ionized Aspartic acid, neutral Aspartic acid and water are selected as the representative hydrogen bond partners in the model complex study.

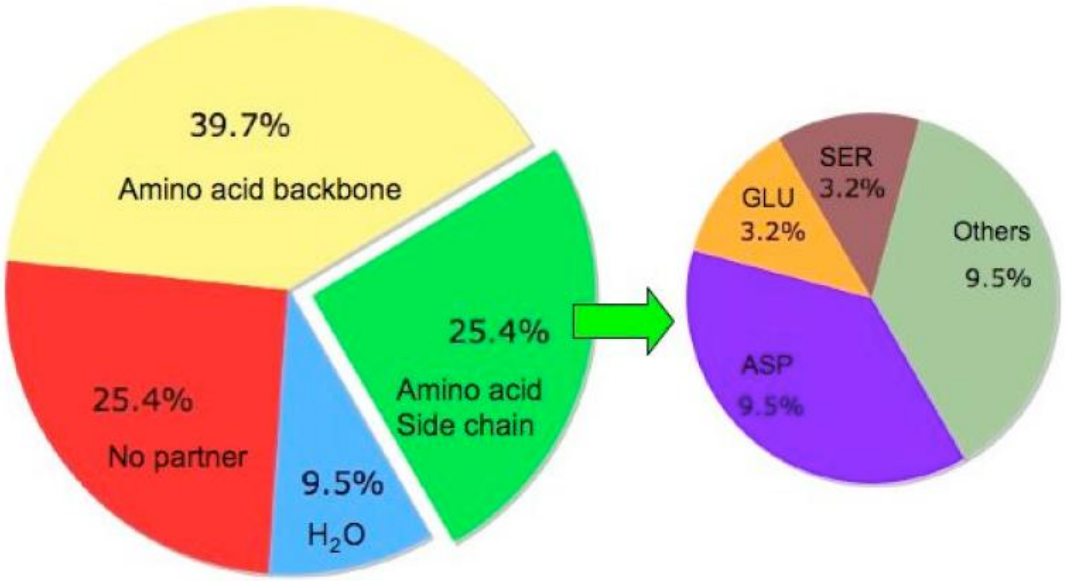

Figure 3.2 The hydrogen bond partners to the histidine ligand in b type Bis-His-Heme in the non-redundant heme database. There are 63 representative histidine ligands of heme in the data set.

The model complex in the DFT and continuum electrostatics calculations

The simplified Bis-imidazole-Porphyrin complex with a representative hydrogen bond partner as R group from the overall complex is shown in Figure 3.1.3. DFT and continuum electrostatics calculations are employed to study the redox potential shift due to the hydrogen bond.

The calculation of the energy components with DFT and CE were carried out with the following procedure. The hydrogen bond distance between R group and imidazole is set as 3.0 Å. In the complex, the dihedral angle between the imidazole plane and hydrogen bond partner is zero degree. Water, glycine and neutral aspartic acids are placed with a range of hydrogen bond angles that vary 15 degree each. The iron is set in the low-spin state.

The overall structure is immersed in a medium with dielectric constant 6 within Jaguar program. The structure is energetically minimized using maestro, the interface of Jaguar. The relaxed structure is then stored for DFT and Continuum electrostatics calculation. As in section 3.2, single point calculations are employed to calculate the system energies for the different structures. The method is B3lyp. There are three basis sets for the complex: LACV3P* for Fe atom, 6-311G** for Fe ligated nitrogen atoms and 6-311G**+ for the other atoms. The selection is consistent with benchmark and literature. (*21, 25, 45-48*)

The output of the atomic partial charge sets from this calculation are mapped into the relaxed structure and used to compute the continuum electrostatics interaction between groups using Coulomb's law. There are four charge sets compared: Hard charge, Mulliken charges, ESP charges and NBO charges. The Hard charge set is the metal center charge set, with the fixed -0.5 on the porphyrin nitrogen atoms and +2 or +3 on the iron atom. It has widely used in the MCCE continuum electrostatics calculations of heme electrochemistry (*49-53*). The Mulliken charge set has electron orbital centered charges. (*54, 55*) The ESP (Electrostatics Potential) charge set has atomic partial charges that reproduce the electrostatics map of the potential over space. (*56*) NBO (Natural Bond Orbital) charge set places the nuclear charges minus the occupied orbital charges onto the atoms. (*57, 58*) Different charge sets are used in the ferric-porphyrin and ferrous-porphyrin states.

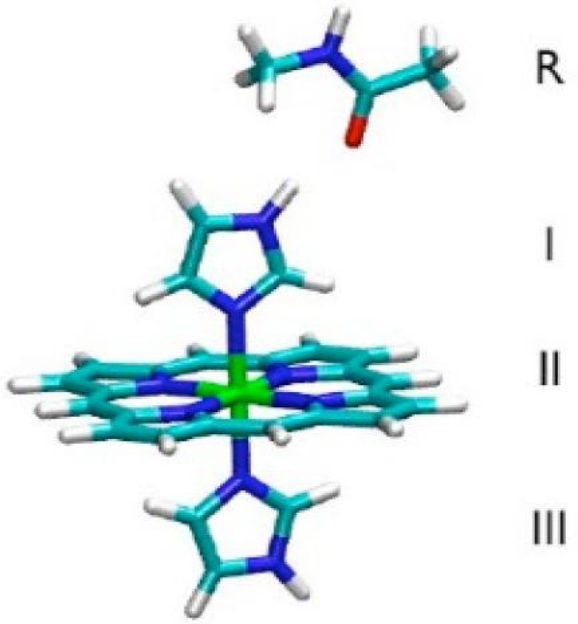

Figure 3.3 Structure of model complex for calculating hydrogen bond interaction energy in DFT and CE calculations. I,II,III present the top imidazole, porphyrin and bottom imidazole. R is the hydrogen bond partner to the histidine ligand of heme.

The basic idea is to calculate the interaction energy between the R group and the Bis-imidazole-Porphyrin complex with ferric- and ferrous-Porphyrin. The energy difference between the two states is equal to the redox potential shift due to the hydrogen bond in the system. Different strategies are used to calculate the interaction energy between R group and Bis-imidazole-Porphyrin complex in the DFT and continuum electrostatics method.

Three DFT calculations are carried out of the system. One is for the overall complex, the second for Bis-imidazole-Porphyrin and lastly for the R group. The interaction energy is the energy difference:

$$\Delta E_{DFT} = E_{total} - E_{heme\text{-}ligands} - E_R \qquad \text{Equation 3.1}$$

ΔE_{DFT} means hydrogen bond interaction calculated by DFT method. E_{total} is the

total system energy of the heme-ligand complex with the R group. $E_{heme\text{-}ligands}$ and E_R are the system energies of the isolated heme-ligand and R groups.

DFT has been proved to be successful in computing bonded compound energies, even for systems with complex electronic orbitals, such as metal centered complexes. (*45*, *59*, *60*) However, it is also computationally costly. For example, the optimization and single point calculation of the porphyrin structure takes more than 150 hours on a machine with Intel Xeon CPU 3.0GHz and 4G memory. Hydrogen bond interaction is much weaker than intramolecular bond such as covalent bond and ionic bond. (*59*) Analysis of hydrogen bonds suggested that they have significant non-bonded electrostatic interaction. (*61-63*) If true, the more efficient continuum electrostatics method can be used to study the redox potential shift of heme complex due to hydrogen bond interaction.

With the continuum electrostatics method, the interaction between the R group and Bis-imidazole-Porphyrin complex are separated into the interaction between the R group and heme porphyrin with the two imidazoles. Coulomb's law is used in the calculation of the interaction:

$$\Delta E_{CE} = \Delta E_{R\&1} + \Delta E_{R\&II} + \Delta E_{R\&III} \qquad \text{Equation 3.2}$$

In the equation, ΔE_{CE} means the hydrogen bond interaction calculated by the Continuum Electrostatics method. $\Delta E_{R\&1}$, $\Delta E_{R\&II}$ and $\Delta E_{R\&III}$ are the pairwise interaction energies between hydrogen bond partner (R group) and top imidazole, porphyrin plane and bottom imidazole respectively.

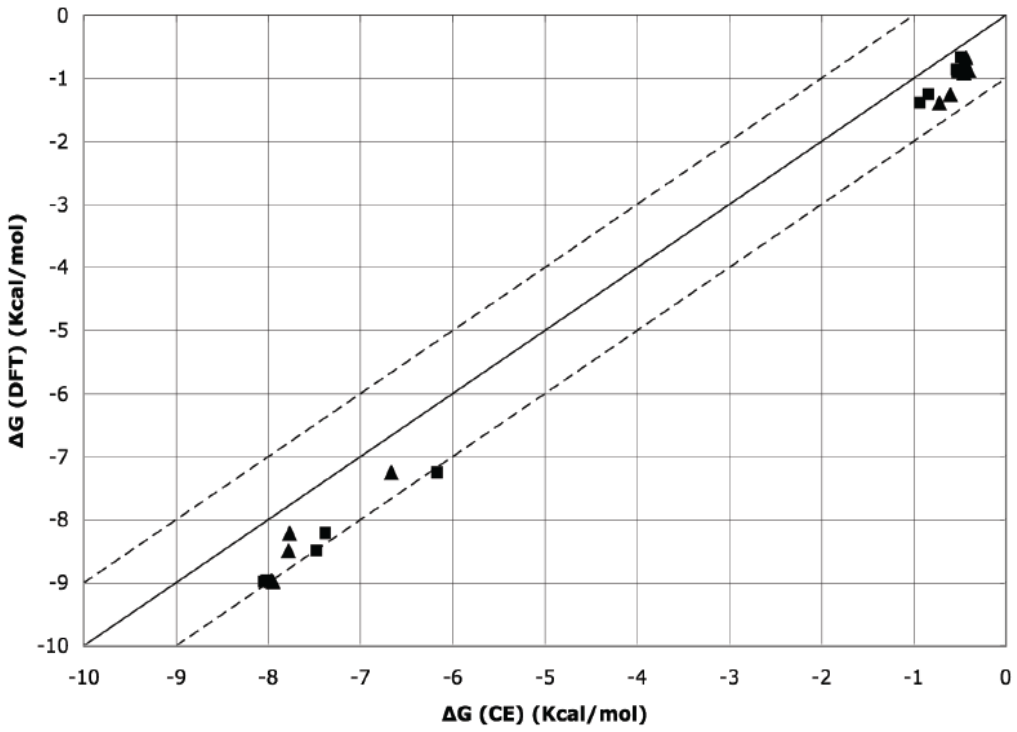

Figure 3.4 Comparison of the calculated redox potential shift calculated using DFT or continuum electrostatics methods for a Bis-Imidazole-Porphyrin model complex in continuum medium with a dielectric constant 6. (■) NBO (▲) Hard charge sets. The hydrogen bond donors are Gly backbone, neutral Asp (near origin) and ionized Asp (ΔG from -6 to -8kcal/mol). The orientation of the ligands was changed to give the distribution energies. The solid line has a slope of 1 passing through the origin. The dashed lines show a difference of ±1kcal/mol.

Results of model 1

The simulation results of the changes in redox potential due to the presence of a hydrogen bond to the imidazole ligand are shown in Figure 3.4. The redox potential shift in DFT and continuum electrostatics calculations are less than 10kcal/mol in the continuum medium of dielectric constant 6. The average energy difference between the two models is 0.6kcal/mol, while the maximum energy difference is 1.2kcal/mol. The RMSD of the two dataset is 0.2 kcal/mol. The RMSD with hard charge is 0.5kcal/mol

compared with 0.7kcal/mol with NBO charge. The results showed the calculated redox potential shift from continuum electrostatics agrees quite well with DFT simulation in the model complex, although oxidation of the complexes is about 1kcal/mol more favorable in the DFT calculation than in the continuum electrostatics calculation. Thus, the hydrogen bond to the ligand affects the heme in a manner that looks like a long-range non-bonded interaction. And in the continuum electrostatics calculations, the difference between hard charge and NBO charge is not significant.

3.3.4 Simulation of Model 2 (Imidazole-HOH-Porphyrin point charge model)

One of the limits of model 1 is the polarization of the R group due to the existence of the hydrogen bond. More electrons are donated from R group to histidine ligand, even shared to iron-porphyrin. As a result, the self-energy of R group, as well as the system energy of the total complex may be shifted. The accuracy of the final results would be affected. (*64*)

A simpler model is employed to focus solely on the changes in energy of the porphyrin and its ligands. Thus the hydrogen bond donor is replaced with a simple positive or negative point charge placed on top of the porphyrin plane. The redox potential shift due to the point charge can be calculated using the method described above. One axial ligand of the porphyrin is now a water molecule allowing more room for point charges in different positions. The positive and negative point charges are distributed 4.5Å away from the porphyrin ring on the side of water ligand. (Figure 3.5)

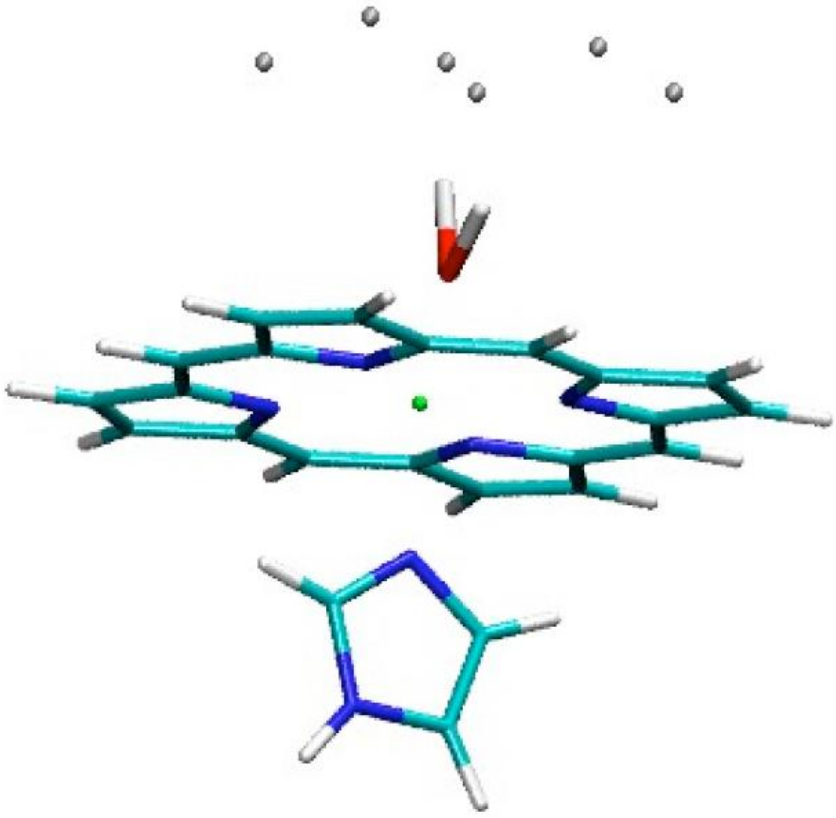

Figure 3.5 Structure of Imidazole-HOH-Porphyrin model complex and point charges.

After structural optimization, the single point energy calculation of DFT (equation 3.1) and Continuum electrostatics calculation (equation 3.2) were carried out for a single point charge. The dielectric constant is 1 (in vacuum) in both DFT and continuum electrostatics models.

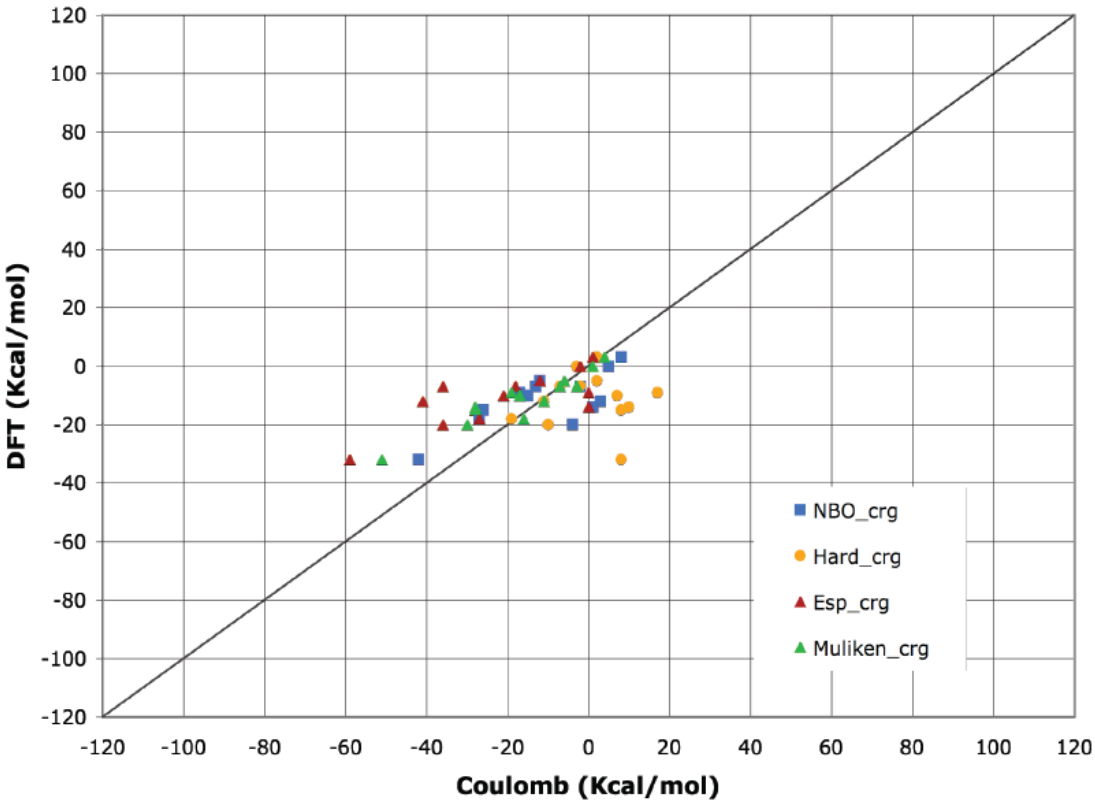
DFT (Kcal/mol)
Coulomb (Kcal/mol)
NBO_crg
Hard_crg
Esp_crg
Muliken_crg
120
100
80
60
40
20
0
-20
-40
-60
-80
-100
-120
-120
-100
-80
-60
-40
-20
0
20
40
60
80
100
120

a)

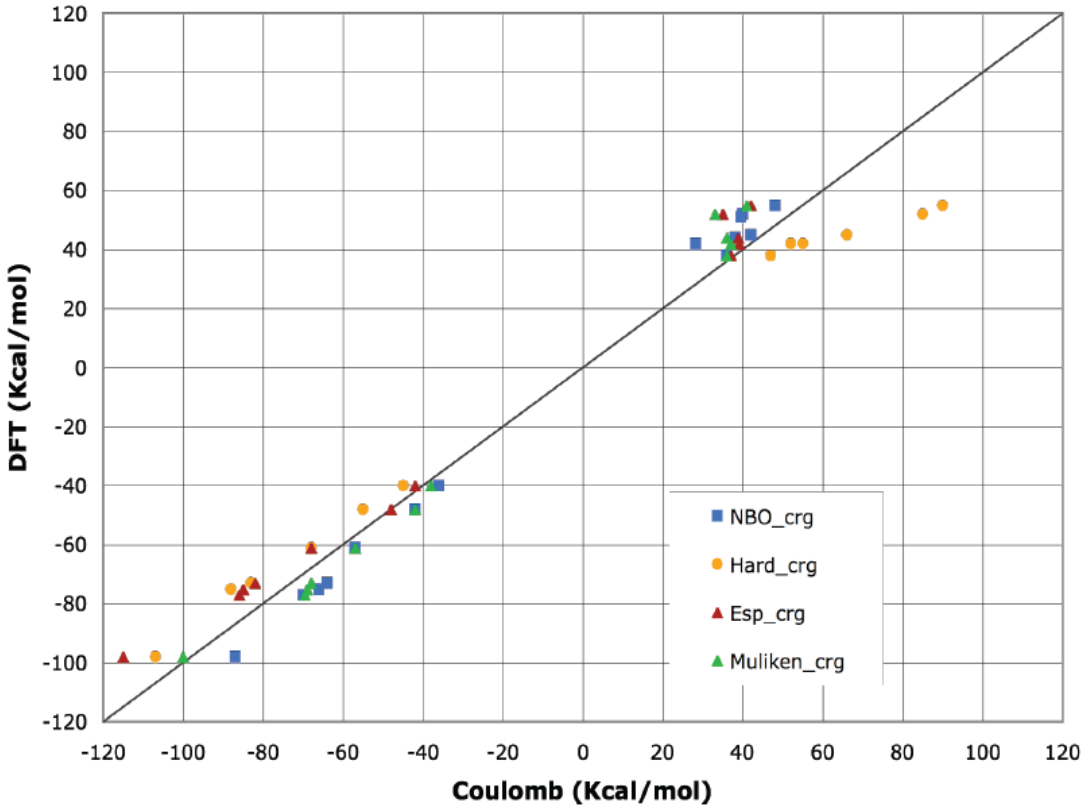
DFT (Kcal/mol)
Coulomb (Kcal/mol)
NBO_crg
Hard_crg
Esp_crg
Muliken_crg

b)

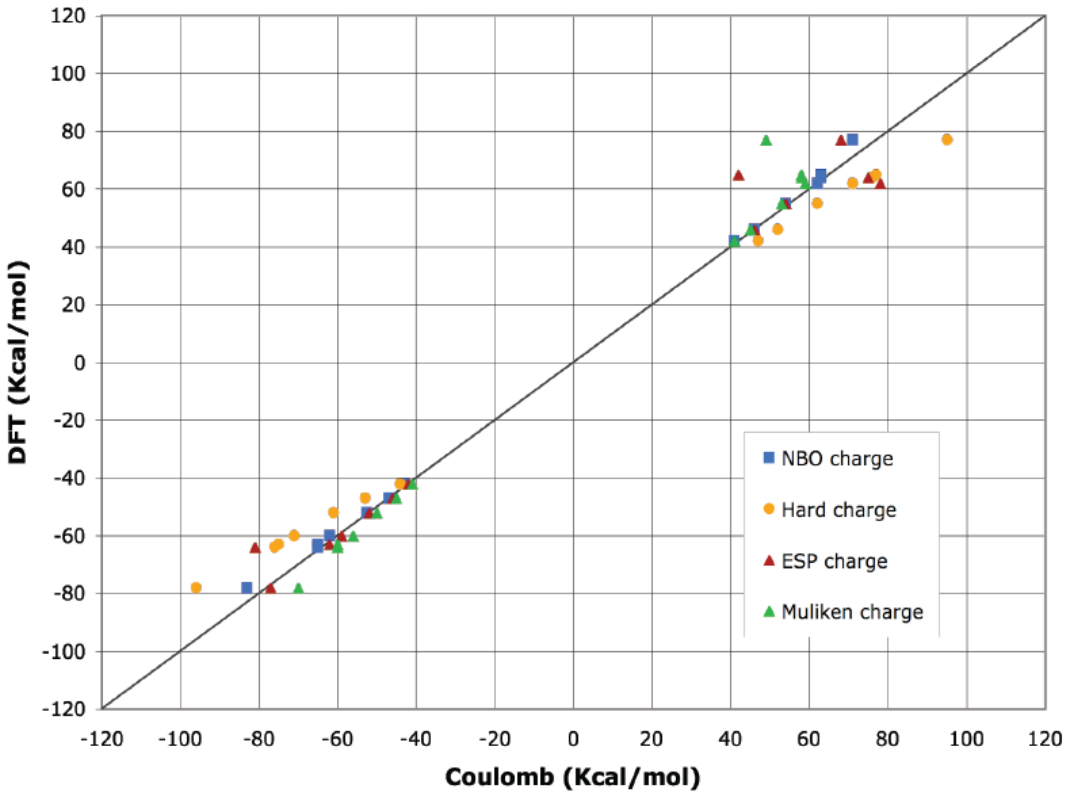

c)

Figure 3.6 Energy Comparison of Imidazole-HOH-Porphyrin due to the point charge calculated using DFT and CE methods. Calculations from four charge sets: NBO, Hard, ESP and Mulliken charges for porphyrin and ligands are compared in the continuum electrostatics calculation. The dielectric constant is 1.
a) Ferrous-Porphyrin; b) Ferric-Porphyrin; c) The difference between ferrous- and ferric porphyrin. It gives the simulated shift of the redox potential.

Results of model 2

The calculated interaction energy between the point charge and the Imidazole-Heme-HOH complex are presented in Figure 3.6 a) and b) for ferrous- and ferric-complex. In Figure 3.6 a), the slope of linear relation between DFT results and CE results is 0.3 in ferrous-complex. The R-square is 0.32. In Figure 3.6 b), the slope and R-square

are 0.82 and 0.89 with the ferric-complex. Thus, the calculated interaction energies from continuum electrostatics and DFT calculations are individually not well correlated for either ferric- or ferrous- complexes.

The redox potential shifts calculated with DFT and Continuum Electrostatics are shown in Figure 3.6 c). The range of the data is now from -100kcal/mol to 100kcal/mol because a dielectric constant of 1 is used. Four different charge sets, including Hard charge, Mulliken charge, ESP charge and NBO charge were compared in the Continuum Electrostatics calculations.

There is clear linear relationship between the redox potential shift calculated with DFT or CE methods. The slope, fitting all the data, is 0.96. R-square is 0.98. The intercept is 1.2Kcal/mol. The R-squares for results with individual charge sets are all better than 0.92. The slope with NBO charge set is 0.99, followed by 0.97 of ESP charge set, 1.10 of Mulliken charge set and 0.85 of hard charges. Thus, the continuum electrostatics calculations with NBO charge sets proved the best match with for the DFT calculation in the model complex. The differences between the energies of ferrous- and ferric-porphyrin complexes due to the point charge are well modeled as a simple electrostatics interaction.

3.3.5 Discussion

The hydrogen bond interaction between histidine ligand of heme and its partner can affect the heme redox potential. With one extra charge transferred into heme center from Fe^{2+} to Fe^{3+}, the total charge of the complex is changed from 0 to +1. During the process,

the hydrogen bond interaction is strengthened due to the stronger charge-charge interaction with an ionized hydrogen bond partner or charge-dipole interaction with a neutral hydrogen bond partner. If the hydrogen bond acceptor is ionized, it can stabilize the oxidized complex by 10kcal/mol in a medium with dielectric constant of 6. This energy is sufficient to charge a heme E_m by 400mV. Thus a single ionized residue near the heme could shift the heme redox potential by about half of the 800mV range found in heme proteins (*49*). The energy stabilization of the oxidized heme can be used to drive conformational changes (*65*) and proton coupling (*66*) in biological systems.

When the redox potential shift is less than 8kcal/mol, the continuum electrostatics and DFT calculation results differ by less than 15%. For the Bis-Imidazole complex with a hydrogen bond, the DFT calculated from the oxidized state is 1.2kcal/mol more than the continuum electrostatics calculations. In the comparison of the His-HOH-Porphyrin complex with point charges, there is no significant shift. This shows the accuracy of continuum electrostatics, which is a much less computational costly method than DFT. The largest absolute difference is less than 1.5kcal/mol in protein environment (dielectric constant 6), which is within the uncertainty of most of the modern computational software in protein. (*67-69*)

Previous calculations have shown that if a charged group is too close to the iron atom in the heme complex, there is significant difference between the calculation results with Continuum Electrostatics and DFT. In binuclear center of cytochrome c oxidase, (*70*) the pair-wise interaction between the Cu_B^{+2} and His-Heme-Hydroxyl are from 50kcal/mol and 150kcal/mol in DFT and in CE calculations. The distance between doubly charged

Cu^{2+} and the Fe is 4.8Å and the heme hydroxyl is sitting between the two atoms. Coulomb's law overestimates the large unfavorable interaction by 20 to 40% compared with DFT results. (*70*) The electronic orbital interaction from heme porphyrin and other groups maybe the reason for the differences.

The calculated redox potential shift from CE matched well with DFT method with a point charge in the His-HOH-Porphyrin or Bis-His-Porphyrin complexes. However, calculations of the interaction of a point charge with the His-HOH-Porphyrin complex by DFT or continuum electrostatics have a slope 0.30 with R-square 0.32 for ferrous and slope 0.82 and R-square 0.89 for ferric complexes (Figure 3.6 b and c). Clearly, there are some important non-electrostatics energy interaction terms in DFT calculations, which are cancelled out during the calculation of the redox potential shift, which is the difference of the calculated hydrogen bond energy on ferric-complex and ferrous-complex state. In contrast, the electrostatics components dominated the redox potential shift in this study. This study does not allow conformational change or strong reorganization energy of the complex during the electron transfer, which could change the conclusion.

Choosing different charge sets for the continuum electrostatics calculations does not significantly change the redox potential shift. NBO and ESP charges fitted the data better with slope close to 1 and higher value of R-square.

References

1. Walker FA, B. H. H., Scheidt WR, Osvath SR. (1986) Models of the cytochromes b. Effect of axial ligand plane orientation on the EPR and Moessbauer spectra of low-spin ferrihemes, *J Am Chem Soc 108*, 5288-5297.

2. Thomas Teschner, L. Y., Volker Schünemann, Hauke Paulsen, Heiner , and Winkler, C. H., W. Robert Scheidt, F. Ann Walker and Alfred X. Trautwein. (2006) Models of the Membrane-Bound Cytochromes: Mössbauer Spectra of Crystalline Low-Spin Ferriheme Complexes Having Axial Ligand Plane Dihedral Angles Ranging from 0° to 90°, *J Am Chem Soc. 128*, 1379-1389.

3. Walker, F. A. (2006) The heme environment of mouse neuroglobin: histidine imidazole plane orientations obtained from solution NMR and EPR spectroscopy as compared with X-ray crystallography, *J Biol Inorg Chem 11*, 391-397.

4. Scheidt W, L. Y. (1987) Recent advances in the stereochemistry of metal-lotetrapyrroles., Springer.

5. Walker, F. A. (2004) Models of the Bis-Histidine-Ligated Electron-Transferring Cytochromes. Comparative Geometric and Electronic Structure of Low-Spin Ferro- and Ferrihemes, *Chemical Reviews 104*, 589-615.

6. Brzezinski, P., and Gennis, R. (2008) Cytochrome c oxidase: exciting progress and remaining mysteries, *J Bioenerg Biomembr 40*, 521-531.

7. Fadda, E., Yu, C., and Pomes, R. (2008) Electrostatic control of proton pumping in cytochrome c oxidase, *Biochimica et Biophysica Acta 1777*, 277-284.

8. Xu, J., and Voth, G. (2008) Redox-coupled proton pumping in cytochrome c oxidase: Further insights from computer simulation, *Biochimica et Biophysica Acta 1777*, 196-201.

9. Smulevich, G., Feis, A., and Howes, B. D. (2005) Fifteen years of Raman spectroscopy of engineered heme containing peroxidases: what have we learned?, *Acc. Chem. Res. 38*, 443-440.

10. Veitch, N. C., and Smith, A. T. (2001) Horseradish peroxidase, *Advances in Inorganic Chemistry, Vol 51 51*, 107-162.

11. Poulos, T. L., Li, H. Y., and Raman, C. S. (1999) Heme-mediated oxygen activation in biology: cytochrome c oxidase and nitric oxide synthase, *Current Opinion in Chemical Biology 3*, 131-137.

12. Meunier, B., and Rich, P. R. (1998) Quantitation and characterization of cytochrome c oxidase in complex systems, *Analytical Biochemistry 260*, 237-243.

13. Antosiewicz, J., and Porschke, D. (1995) Electrostatic of Hemoglobins from Measurements of the Electric Dichroism and Computer Simulations, *Biophys. J. 68*, 655-664.

14. Baere, I. D., Perutz, M. F., Kiger, L., Marden, M. C., and Poyart, C. (1994) Formation of two hydrogen bonds from the globin to the heme-linked oxygen molecule in Ascaris hemoglobin, *Proc. Natl. Acad. Sci. 91*, 1594-1597.

15. Martin K. Safo, W. R. S., *J and Govind P. Gupta. (1990) Axial Ligand Orientation in Iron(11) Porphyrinates. Preparation and Characterization of Low-Spin Bis(imidazole) (tetraphenylporphyrinato)iron(11) Complexes, *Inorg. Chem. 29*, 626-633.

16. Ghosh, A. (2006) Transition metal spin state energetics and noninnocent systems: challenges for DFT in the bioinorganic arena, *J Biol Inorg Chem 11*, 712-724.

17. Berry EA, W. F. (2008) Bis-histidine-coordinated hemes in four-helix bundles: how the geometry of the bundle controls the axial imidazole plane orientations in transmembrane cytochromes of mitochondrial complexes II and III and related proteins., *J Biol Inorg Chem. 13*, 481-498.

18. Zaric, S. D., Popovic, D. M., and Knapp, E. W. (2001) Factors determining the orientation of axially coordinated imidazoles in heme proteins, *Biochemistry 40*, 7914-7928.

19. Fufezan, C., Zhang, J., and Gunner, M. R. (2008) Ligand preference and orientation in b- and c-type heme-binding proteins, *Proteins 73*, 690-704.

20. Munro OQ, S.-G. J., Turowska-Tyrk I, Mohanrao K, Shokhireva TK, Walker FA, Debrunner PG, Scheidt WR. (1999) Two crystalline forms of low-spin [Fe(TMP)(5-MeHIm)2]ClO4. Relative parallel and perpendicular axial ligand orientations, *J Am Chem Soc* 11144-11155.

21. Smith DM, R. K., Dupuis M, Valiev M, Straatsma TP. (2006) Electronic coupling between heme electron-transfer centers and its decay with distance depends strongly on relative orientation, *J Phys Chem B Condens Matter Mater Surf Interfaces Biophys 110*, 15582-15588.

22. Scheidt WR, C. D. (1986) Preferred orientation of imidazole ligands in metalloporphyrins, *J Am Chem Soc 108*, 1163-1167.

23. Jaugar 6.5, J. (2005) Schrodinger, LLC: Porland, OR.

24. Sundholmb, M. P. J. a. D. (2004) Spin and charge distribution in iron porphyrin models: A coupled cluster and density-functional study, *JOURNAL OF CHEMICAL PHYSICS 120*, 3229-3236.

25. Dayle M. A. Smith, M. D., Erich R. Vorpagel, and T. P. Straatsma. (2003) Characterization of Electronic Structure and Properties of a Bis(histidine) Heme Model Complex, *J Am Chem Soc 125*, 2711-2717.

26. Campbell, N. A. B. W. R. J. H. (2006) *Biology: Exploring Life*, Boston, Massachusetts: Pearson Prentice Hall. .

27. Felix H. Beijer, H. K., Anthony L. Spek, Rint P. Sijbesma, E. W. Meijer (1998) Self-Complementarity Achieved through Quadruple Hydrogen Bonding, *Angew. Chem. Int. Ed. 37*, 75-78.

28. Page, G. A. J. (1997) An Introduction to Hydrogen Bonding (Topics in Physical Chemistry) Oxford University Press.

29. Grabowski, S. J. (2006) Hydrogen bonding - new insights (Challenges and Advances in Computational Chemistry and Physics) Springer.

30. Emsley, J. (1980) Very Strong Hydrogen Bonds, *Chemical Society Reviews 9*.

31. Millen, A. C. L. D. J. (1987) Angular geometries and other properties of hydrogen-bonded dimers: a simple electrostatic interpretation of the success of the electron-pair model, *Chem. Soc. Rev. 16*, 467-498.

32. Sinnecker, S., Reijerse, E., Neese, F., and Lubitz, W. (2004) Hydrogen bond geometries from electron paramagnetic resonance and electron-nuclear double resonance parameters: density functional study of quinone radical anion-solvent interactions, *J Am Chem Soc 126*, 3280-3290.

33. Sheu, S.-Y., Yang, D.-Y., Selzle, H. L., and Schlag, E. W. (2003) Energetics of hydrogen bonds in peptides, *Proc. Natl. Acad. Sci. USA 100*, 12683-12687.

34. Kortemme, T., Morozov, A. V., and Baker, D. (2003) An orientation-dependent hydrogen bonding potential improves prediction of specificity and structure for proteins and protein-protein complexes, *J Mol Biol 326*, 1239-1259.

35. Steiner, T. (2002) The Hydrogen Bond in the Solid State, *Angew. Chem. Int. Ed. 41*, 48-76.

36. Weiss MS, B. M., Suhnel J, Pal D, Hilgenfeld R. (2001) More hydrogen bonds for the (structural) biologist., *Trends Biochem Sci 26*, 521-523.

37. Negron C, F. C., Koder RL. (2009) Geometric constraints for porphyrin binding in helical protein binding sites., *Proteins 74*, 400-416.

38. Watanabe. (2002) Construction of heme enzymes: four approaches, *Curr Opin Chem Biol. 6*, 208-216.

39. Hägerhäll C, H. L. (1996) A structural model for the membrane-integral domain of succinate: quinone oxidoreductases, *FEBS Lett. 389*, 25-31.

40. Huttunen KM, M. N., Raunio H, Rautio J. (2008) Cytochrome P450-activated prodrugs: targeted drug delivery, *Curr Med Chem. 15*, 2346-2365.

41. E., O. (2002) Chemical shifts in amino acids, peptides, and proteins: from quantum chemistry to drug design., *Annu Rev Phys Chem. 53*, 349-378.

42. Olsson MH, S. P., Blomberg MR, Warshel A. (2007) Exploring pathways and barriers for coupled ET/PT in cytochrome c oxidase: a general framework for examining energetics and mechanistic alternatives., *Biochim Biophys Acta. 1767*, 244-260.

43. Yu CA, C. X., Ma HW, Yin Y, Yu L, Esser L, Xia D. (2008) Domain conformational switch of the iron-sulfur protein in cytochrome bc1 complex is induced by the electron transfer from cytochrome bL to bH, *Biochim Biophys Acta. 1777*, 1038-1043.

44. Crofts, A. R., Guergova-Kuras, M., Kuras, R., Ugulava, N., Li, J., and Hon, S. (2000) Proton-coupled electron transfer at the Q0 site: what type of mechanism can account for the high activation barrier?, *Biochim. Biophys. Acta 1459*, 456-466.

45. Ghosh, A. (2006) Transition metal spin state energetics and noninnocent systems: challenges for DFT in the bioinorganic arena, *J.Biol.Inorg. Chem. 11*, 712-724.

46. Quenneville, J., Popovic, D. M., and Stuchebrukhov, A. A. (2006) Combined DFT and electrostatics study of the proton pumping mechanism in cytochrome c oxidase, *Biochim Biophys Acta*.

47. Popovic, D. M., Quenneville, J., and Stuchebrukhov, A. A. (2005)

DFT/electrostatic calculations of pK(a) values in cytochrome c oxidase, *Journal of Physical Chemistry B 109*, 3616-3626.

48. Hudaky, P., and Perczel, A. (2004) Conformation dependence of pK_a: Ab initio and DFT investigation of Histidine, *J. Phys. Chem. A. 108*, 6195-6205.

49. Zheng, Z., and Gunner, M. R. (2009) Analysis of the electrochemistry of hemes with E_ms spanning 800 mV, *Proteins 75*, 719-734.

50. Gunner, M. R., and Honig, B. (1992) Calculations of proton uptake in *Rhodobacter sphaeroides* reaction centers, in *The Photosynthetic Bacterial Reaction Center: Structure, Spectroscopy and Dynamics II* (Breton, J., and Vermeglio, A., Eds.), pp 403-410, Plenum, New York.

51. Song, Y., Mao, J., and Gunner, M. R. (2009) MCCE2: Improving Protein pKa Calculations with Extensive Side Chain Rotamer Sampling, *J. Comp. Chem. epub Mar 9*.

52. Song, Y., and Gunner, M. R. (2004) Comparison of bacteriorhodopsin and halorhodopsin by MCCE reveals a possible new chloride binding site in halorhodopsin, *Biophys. J. 86*, 611a-611a.

53. Mao, J. J., Song, Y. F., and Gunner, M. (2004) Multi-Conformation Continuum Electrostatics (MCCE): An efficient, accurate program for calculation of pKas and Ems in proteins, *Biophys. J. 86*, 633a-633a.

54. Mulliken, R. S. (1955) Electronic Population Analysis on LCAO[Single Bond]MO Molecular Wave Functions. I, *J. Chem. Phys. 23*, 1833-1840.

55. Csizmadia, I. G. (1976) Theory and Practice of MO Calculations on Organic Molecules, Elsevier.

56. Wang, J., Cieplak, P., and Kollman, P. A. (2000) How well does a restrained electrostatic potential(resp) model perform in calculating conformational energies of organic and biological molecules?, *J.Comp.Chem. 21*, 1049-1074.

57. Alan E. Reed, L. A. C., Frank Weinhold. (1988) Intermolecular interactions from a natural bond orbital, donor-acceptor viewpoint, *Chem Rev 88*, 899.

58. J. E. Carpenter, F. W. (1988) Analysis of the geometry of the hydroxymethyl radical by the “different hybrids for different spins” natural bond orbital procedure, *Journal of Molecular Structure: THEOCHEM 169*, 41-62.

59. Chermette, H. (1998) Density functional theory: A powerful tool for theoretical

studies in coordination chemistry *Coordination Chemistry Reviews* 699-721.

60. Martin, A. D. B. a. J. M. L. (2003) The role of the basis set: Assessing density functional theory *JOURNAL OF CHEMICAL PHYSICS 119*, 68.

61. Betz, M., Lohr, F., Wienk, H., and Ruterjans, H. (2004) Long-range nature of the interactions between titratable groups in Bacillus agaradhaerens family 11 xylanase: pH titration of B. agaradhaerens xylanase, *Biochemistry 43*, 5820-5831.

62. Gray, M., Cuello, A. O., Cooke, G., and Rotello, V. M. (2003) Hydrogen bonding in redox-modulated molecular recognition. An experimental and theoretical investigation, *J Am Chem Soc 125*, 7882-7888.

63. Gordon, D. B., Marshall, S. A., and Mayo, S. L. (1999) Energy functions for protein design, *Curr Opin Struct Biol 9*, 509-513.

64. Simonson, T. (2008) Dielectric relaxation in proteins: the computational perspective, *Photosynthesis Research This volume*.

65. Song, Y., Mao, J., and Gunner, M. R. (2003) Calculation of proton transfers in bacteriorhodopsin bR and M intermediates, *Biochemistry 42*, 9875-9888.

66. Brzezinski, P., and Larsson, G. (2003) Redox-driven proton pumping by heme-copper oxidases, *Biochim. Biophys. Acta 1605*, 1-13.

67. Paton RS, G. J. (2009) Hydrogen bonding and pi-stacking: how reliable are force fields? A critical evaluation of force field descriptions of nonbonded interactions, *J Chem Inf Model. 49*, 944-955.

68. Olsson, M. H. M., and Warshel, A. (2006) Monte Carlo simulations of proton pumps: On the working principles of the biological valve that controls proton pumping in cytochrome c oxidase, *Proc Natl Acad Sci 103*, 6500-6505.

69. Stephens, P. J., Jollie, D. R., and Warshel, A. (1996) Protein control of redox potentials of iron-sulfur proteins, *Chem. Rev. 96*, 2491-2513.

70. Song, Y., Mao, J., and Gunner, M. R. (2006) Electrostatic environment of hemes in proteins: pK_as of hydroxyl ligands, *Biochemistry 45*, 7949-7958.

CHAPTER IV

Continuum Electrostatics Analysis of Heme a and Asp44 in S44D mutant of Rb. sphaeroides Cytochrome c oxidase

4.1 Introduction

Cytochrome c oxidase is the terminal protein of the aerobic respiratory chain. There are four redox centers within the protein: Cu_A, Heme a, Cu_B and Heme a_3. Electrons are sequentially transferred from cytochrome c to Cu_A, to Heme a and then to the binuclear center composed of Cu_B and Heme a_3, where a oxygen molecule is reduced to water. Synchronized with the 4 electron transfers needed to form water, 8 protons are removed from the cell interior. Four of them are transported to the binuclear center for addition to the substrate oxygen while the other 4 are pumped to the outer side of the membrane, adding to the electrochemical proton gradient across the membrane. (*1-3*)

Cytochrome c oxidase, as with all other intrinsic membrane electron transfer proteins, is designed to bind and release charges at deeply buried sites within the proteins. The movement of electrons and protons are coupled together to reduce the net change in charge with the redox reactions. (*4, 5*) Thus, the introduction of an electron on the redox sites leads to changes in the pK_as of adjacent residues causing them to change their protonation states through the reaction cycle (*6, 7*). It is the coupled reactions that allow

the electron transfer reactions to drive trans-membrane proton transfer. (*7*).

Heme a, the focus of the work reported here, is an a-type low-spin heme ligated to two axial Histidine ligands (*8*). The distal nitrogen of one of the His ligands makes a hydrogen bond with Ser 44 in *Rb. Sphaeroides* while it is a GLY in the Bovine protein. A non-redundant Heme survey of 63 a and b type hemes (*9*), has shown 65% of His ligands to hemes make a distal hydrogen bond to the protein. However, only 1.6% uses the backbone of Gly and 3.2% uses the side chain of Ser. Asp, which will introduced as a hydrogen bind in the work presented here, is found 9.5% of the time. (In preparation, Fufezan & Gunner)

Recent studies have reported the changes in the electron transfer reactions when an Asp has been added into position 44, replacing the Ser that is a hydrogen bond donor to the Heme axial ligand in *Rb. sphaeroides* Cytochrome c oxidase. The observed electron transfer rate from Cu_A to Heme a is $2\times10^4\,s^{-1}$ in the wild type, S44 Rb. Sphaeroides (*10, 11, 12*). With the S44D protein the reaction is now biphasic with a rate of $3\times10^4\,s^{-1}$, similar to that found in the wild-type protein and a much slower rate of 5 to $90\,s^{-1}$. The proportion of the two phases is pH dependent with the fast rate diminishing with increasing pH. The two rates have equal amplitude at pH 5.5. (*13*) In the wild-type protein the Heme a and Cu_a have E_ms within 60 mV of each other so the electron transfer reaction is only slightly downhill. The reaction has little pH dependence. In the mutant the reaction is more pH dependent, becoming less favorable at higher pH. The observed pH dependence suggests that the ionization state of the newly introduced Asp could be controlling the reaction rate.

Cytochohome c oxidase has been the subject of extensive computational studies. These have been carried out with QM/MM (*14*), Empirical Valence Bond molecular dynamics (*15, 16*), Monte Carlo method (*17*) and Continuum Electrostatics techniques(*18*). Previous MCCE (Multi-Conformer Continuum Electrostatics) study of cytochrome c oxidase (*19*) determined the E_m and pK_a of the redox centers and key residues in O, E and R states (*7*) These have all redox centers oxidized (O), two electrons in the Binuclear Center (E) and all four redox cofactors reduced (R).

The newly introduced Asp 44 represents a potentially charged, deeply buried group in a region that has not evolved to stabilize the charge. The experimental studies of the mutant suggest that the Asp may be deprotonated near neutral pH if Heme a is oxidized and that its ionization state is coupled to the redox state of the heme. (*13*). The work presented here aims to understand how the driving force of the electron transfer from Cu_A to Heme a is changed by the introduced Asp. An x-ray structure of the mutant protein (kindly provided by Professor Ferguson-Miller) and the high-resolution protein 2GSM(*20*) from *Rb. sphaeroides* of Cytochrome c oxidase were analyzed with MCCE ver2.4, a new version with updated force field and advanced entropy corrections (*21*). The redox potential of Heme a and pK_a of Asp44, are calculated and compared with the wild type. The study is also used to understand the coupling between electron and proton transfer inside the hydrophobic protein environment. If the introduced Asp is deprotonated, the free energy of electron transfer from Cu_A to Heme a becomes coupled to Asp protonation changes introducing new pH dependence to the reaction. In addition, the addition of a new protonable group tests the ability of a protein to accommodate the

new charge. The response of the protein to move an electron to Heme a is compared to energy of negative charge introduced by deprotonating the nearby Asp.

4.2 Material and Methods

4.2.1 The wild type and derivative structures

Two structures of cytochrome c oxidase from *Rhodobactor sphaeoides* are used as input to the calculations. The wild-type X-ray structure 2GSM (*20*) with the resolution of 2.0 Å is designated WT_S44. The other an S44D mutant X-ray crystal structure provided by Ferguson-Miller group (*13*) is designated Mut_D44. Both wild type and mutant structures were relaxed with Gromacs (*22*) as described below to yield WT*_D44 and Mut*_D44 (with the * indicating it is a product of GROMACS optimization). Ser 44 in the WT_S44 was replaced with Asp and the resultant structure relaxed with Gromacs to yield WT*_D44. In addition Asp44 in WT*_D44 and Mut*_D44 was changed to Ser within MCCE to yield WT*_S44 and Mut*_S44. The Ser was relaxed within MCCE, which imposes a rigid backbone but allows for side chain motions (*21*). In addition to the mutation site of residue 44 in chain A, there are 12 surface residues that are Ala in the mutant crystal structure. MCCE rotamer packing was used to recover the 2GSM wild-type sequence, yielding structures Mut*_S44# and Mut*_D44# (# indicating recovery of the 12 surface residues). Overall, there are 7 structures used in this study, including 4 structures with Ser44 (WT_S44, WT*_S44, Mut*_S44 and Mut*_S44#) and 3 structures with Asp44 (WT*_D44, Mut*_D44 and Mut*_D44#).

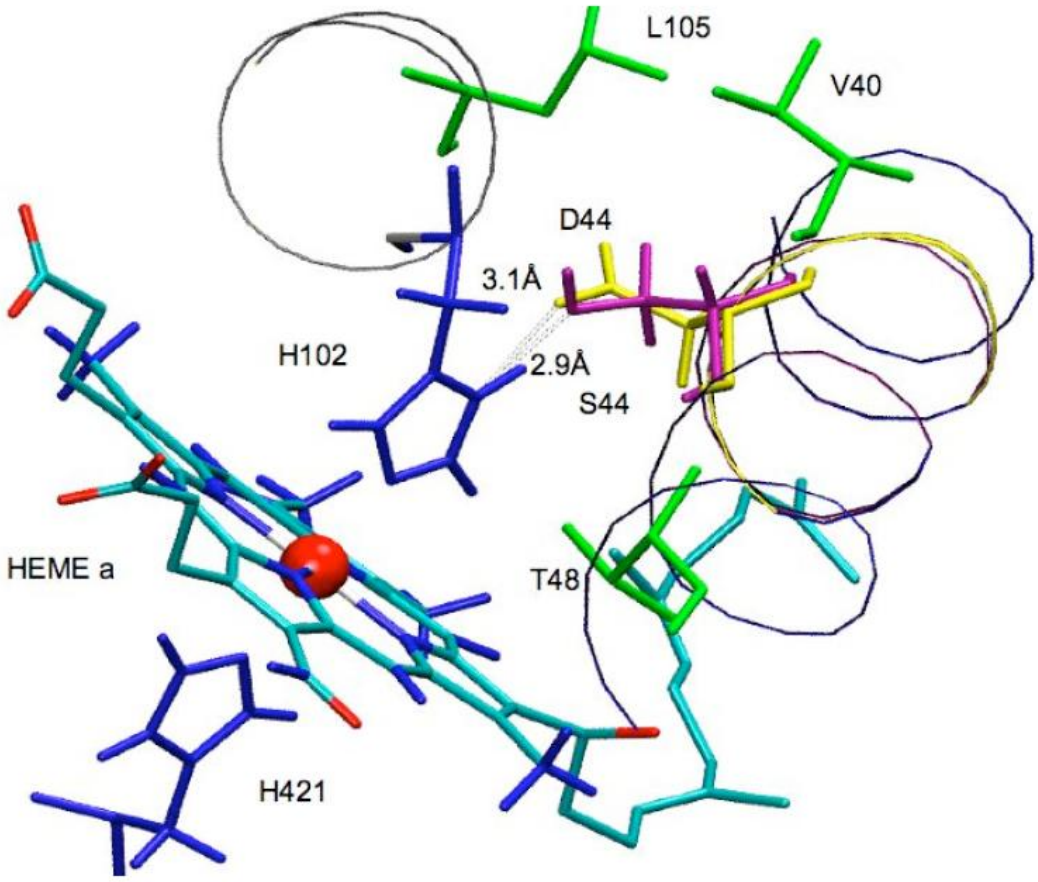

Figure 4.1 The structures of Heme a, residue 44 and nearby residues before and after the Gromacs minimization from 2GSM (WT_S44 and WT*_D44).

Heme a and its two distal ligands are shown. Ser44 and original helical backbone are shown in purple. Asp44 and nearby backbone after GROMACS minimization are shown in yellow. Nearby residues Val40, Leu105 and Thr48 in green are change position during GROMACS minimization. One of the Heme a ligands, His 102, is 2.9Å from S44

in WT_S44, and so can make a hydrogen bond. The H-bond distance is 3.1Å after D44 is introduced and minimized by GROMACS.

4.2.2 In silico mutation of Ser 44 to Asp

Ser is smaller than Asp, so initially the introducing Asp44 clashes with the nearby backbone of Phe 47 and Met 106 in the wild type structure. Gromacs molecular dynamics (version 3.3.2) (*22*) is used to relax the structure, minimizing the total energy. Relaxation is set up using the Gromacs default mode, in vacuum, with no constrained atoms and minimum energy shift of 0.01KJ/mol during the relaxation. The RMSD for the backbone is 0.06Å between WT*_D44 and the original 2GSM wild type structure. However, the hydrogen bond distance between Asp44 and the Heme a ligand His102, shifts from 2.4 to 2.8Å (Figure 4.1). The backbone in the vicinity of Asp 44 shifts by ≈0.3Å to accommodate the larger side chain.

4.2.3 MCCE simulation and analysis

MCCE ver2.4 was used for the simulation of the Heme a and Cu_A redox potential (*21*). MCCE combines continuum electrostatics and molecular mechanics to calculate the pK_a and E_ms for amino acids and cofactors, allowing full rotamer sampling. (*21, 23*) Previous simulation results showed the method provides values that agree with experimental redox potentials in large membrane proteins. (*24-27*) In a survey of redox potential study of 141 different Hemes with experimental E_ms varying by 800meV (*28*) and for benchmark residue pK_as (*21*)

The four key cofactors, Cu_A, Heme a, Heme a_3 and Cu_B, and the amino acids that

serve as ligands are each treated as a complex as described in earlier MCCE calculations. (*19*). A partial charge distribution of Cu_A, with its 2 Cu, side chains of Cys 252 and 256, His 217 and 260 of chain B was calculated using B3LYP method, LANL2DZ basis set and CHELPG algorithm in Gaussian 98. (*29-31*). Metal center charge sets (*28*, *32*) were used for Heme a and Heme a_3. Cu_B is ligated to three His residues (284, 333, 334) and a water/hydroxyl. The charge set was presented in (*19*).

The energy of the hydrogen bond to the His ligand of the heme.

The DFT package, Jaguar (*33*) is employed to determine how well the effect of the hydrogen bond to the His ligand on the Heme E_m is captured by a classical continuum electrostatics program such as MCCE. The single point energy of a Bis-His-Heme model complex (without propionic acids), along with the hydrogen bond partners Asp, Asn or Gly, is calculated together or separately. The difference in the total energy is equivalent to the hydrogen bond energy in the system (see Chapter 3). The electrostatic hydrogen bond energy was obtained by assigning atom partial charges and radii derived from Jaguar and then calculating the interaction using Coulomb's law with a dielectric constant of 6 in MCCE and Jaguar.

Both the DFT and continuum electrostatic analysis shows the energy separating the Bis-His Fe (III) complex to Fe (II) hemes due to a hydrogen bond to the His ligand is stronger in Fe (III) complex. There is good agreement between the two calculations when the total energy of the hydrogen bond is less than 10 kcal/mol in continuum median of dielectric constant 6. The calculated energy difference from the two methods is less than 0.7kcal/mol when the H-bond interaction is less than 8kcal/mol with a dielectric

constant 6. The simple metal centered charge set used here and the Jaguar derived NBO charges for electrostatics calculations were compared, showing only small differences in free energy difference of oxidase (Figure 3.3). Therefore, for MCCE analysis the continuum electrostatics energy is used to obtain the shift in Heme a E_m that occurs when the hydrogen bond to the axial heme ligand is changed. The interaction between Heme a3 and Cub is between groups that are closer together and with larger charges are overestimated in the classical calculations. (*34*)

MCCE analysis of the E_m of heme a

A slab of low dielectric constant material of 35 Å thick is added with IPECE (*26*). DelPhi (*35, 36, 37*) is used to solve the Poisson-Boltzmann equation with an internal dielectric constant for the protein and membrane of 4 and 80 for the solvent. The salt concentration is 150 mM. Reference redox potentials in water are 264mV for the Cu_A complex (*38*), -60meV for Heme a complex (*39*) and -120 for Heme a3. (*8*) PARSE (*40*) charges and radii are used for the amino acids and the AMBER (*41*) force field for torsion and Lennard-Jones parameters. The interaction between Heme a3 and CuB is corrected as described in (*34*). The interaction of the side chain and amide backbone that stabilized the deprotonated Asp is treated by the explicit pairwise electrostatic interaction between these parts of the molecule in MCCE (*42*).

The energy terms that determine the E_m of a redox cofactor can be decomposed as (*43*):

$$nF\,E_m^{mfe} = nFE_{m,sol} + \Delta\Delta G_{rxn} + \Delta G_{bkn} + \Delta G_{res}^{mfe} \qquad \text{(Equation 4.1)}$$

where $E_{m,sol}$ is the E_m in aqueous solution (*44*). $\Delta\Delta G_{rxn}$ is the desolvation energy moving the cofactor from water into protein. $\Delta\Delta G_{bkn}$ is electrostatic and non-electrostatic interaction of the cofactor with the protein backbone. ΔG_{res}^{mfe} is the mean field pair-wise interaction between the cofactor and residues in the protein (See table 4.1). In each case the difference of interaction with the oxidized and the reduced group is given. ΔG_{res}^{mfe} uses a mean-field approximation for the conformer pair-wise interactions, calculated as described in (*19*), while the full microstate energies are used in the Monte Carlo sampling. The reorganization energy due to conformational or protonation changes coupled to the redox reaction creates a difference between the calculated E_m and the E_m^{mfe} (*23*)

The pK_7' calculates is the effective pK_a for the residue when the ionization and conformation of the rest of the protein is fixed in their Boltzmann distribution found at pH 7 (*19*):

$$pK_7' = pK_{sol} + \Delta\Delta G_{rxn} + \Delta G_{pol} + \Delta G_{res}^{mfe} \qquad \text{(Equation 4.2)}$$

The pK_a and pK_7' will be different because of change in the charge of the rest of the protein moving from pH 7 to the pH of the true pK_a. The pK_{sol} used for Asp in MCCE is 4.75, the value for the carboxylate side chain.

4.3 RESULTS and DISCUSSION

The side chain of Ser44 is in a good position to make a hydrogen bond to His102, an axial ligand to Heme a in CcO from *Rhodobactor sphaeroides*, which is 2.9Å away. In

bovine CcO the distal ligand to the His is Gly30 (All residues are in chain A unless noted). Replacing Ser44 with Asp allows the electrochemical behavior of Heme a to be revisited. If the introduced Asp is deprotonated, the free energy of electron transfer from Cu_A to Heme a is expected to become coupled to Asp protonation changes, introducing new pH dependence to the reaction (18). In addition, the addition of a new protonable group tests the ability of a protein to accommodate a new charge (*45*).

4.3.1 Structure comparison

The calculation and analysis were carried out starting with 2 initial crystal structures of *Rb. sphaeroides* CcO. The RMSD of the complete backbone in the two structures is 0.26Å, 0.22Å for chain A, 0.29Å for chain B and 0.12Å for a 15-Å sphere centered at the Heme a iron. There are 3 structures prepared with D44 and 4 with S44. Structures derived from the wild-type structure 2GSM are indicated by WT_ while those derived from a structure of the S44D protein are indicated MUT_. Structures that have undergone Gromacs minimization have a *, while those where the MUT_ structure has 12 surface Ala replaced with the wild-type residues are indicated with #. The WT*_D44 and initial 2GSM structure (WT_S44) have overall backbone RMSD of 0.14Å and 0.06Å in chain A. WT*_S44 and WT*_D44 have the same backbone structure, as do Mut*_S44 and Mut*_D44. These structures are the input for MCCE analysis of the E_m as a function of pH.

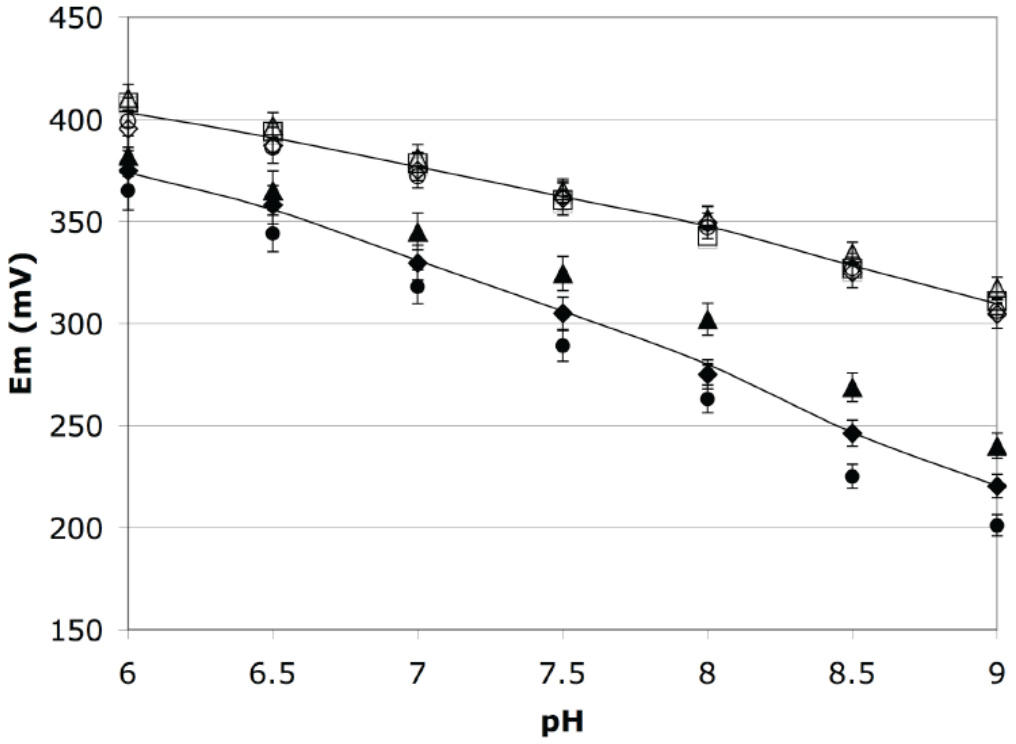

Figure 4.2 Simulated pH dependent of Heme a $E_{m.}$
Structures with Ser44: WT_S44 (□), WT*_S44(△), Mut*_S44(◇) and Mut*_S44#(○).
Structures with Asp44: WT*_D44(▲), Mut*_D44(◆) and Mut*_D44#(●). The lines connect the average E_ms for all structures with S44 or with D44.

Table 4.1: The redox potential (E_m) of Heme a at pH 7 (top) and the pK_a of D44 in the presence of the oxidized or reduced Heme a (bottom).

Structures	$E_{m,sol}$	$\Delta\Delta G_{rxn}$	$\Delta\Delta G_{pol}$	ΔG_{ele}^{mfe}		E_m	Fraction charge of $D44^-$ @pH 7	
				Asp44	Others		Ox	mid
WT_S44	-60	362	177		-101	378		
WT*_S44	-60	363	189		-105	387		
Mut*_S44	-60	374	177		-120	375		
Mut*_S44#	-60	373	180		-119	372		
Av_S44		368±6	181±6		-111±10	378±6		
WT*_D44	-60	363	189	-34	-113	345	0.45	0.18
Mut*_D44	-60	374	180	-85	-87	329	0.85	0.33
Mut*_D44#	-60	373	182	-117	-94	318	0.88	0.37
Av_D44		370±6	184±5	-78±41	-98±13	331±14		
Diff D44-S44		2	3	-78	13	-47		
ASP44	pK_{sol}	$\Delta\Delta G_{rxn}$	$\Delta\Delta G_{pol}$	Heme a	others	pK		
With heme oxidized								
WT*_D44	4.75	600	-97	-392	34	7.2		
Mut*_D44	4.75	630	-65	-482	58	7.3		
Mut*_D44#	4.75	628	-48	-539	53	7.0		
Avg	4.75	619±17	-70±25	-471±74	48±13	7.2±0.1		
With Heme reduced								
WT*_D44	4.75	600	-97	-127	26	15.2		
Mut*_D44	4.75	630	-65	-173	17	17.8		
Mut*_D44#	4.75	628	-49	-199	57	17.9		
Avg	4.75	619±17	-70±24	-166±36	33±21	17.0±1.5		
Diff D44-S44		0	0	-305	15	9.8		

$E_{m,sol}$: the reference E_m of Heme a in aqueous solution (*44*). $pK_{a,sol}$: pK_a of the Asp carboxylate side chain in solution. $\Delta\Delta G_{rxn}$: the difference in desolvation energy of reactant and product. $\Delta\Delta G_{pol}$: the difference of the electrostatic and non-electrostatic interaction with product and reactant with the backbone. ΔG_{ele}^{mfe}: the mean field energy difference of the electrostatic pair-wise and van-der-Waals interactions with the residues in the protein in the reactant and product. The oxidized Heme a and deprotonated Asp are the product states. *the backbone of the structure is minimized using GROMACS. # there are 12 residues in the MUT_ structure reverted to the 2GSM wild-type sequence. See Equation 1 and 2 for more complete description of terms. pK_{sol} and pK_a are in pH units, the E_m is in mV. All energy terms given in meV. 58 meV is the energy need to change a pK_a by 1pH unit.

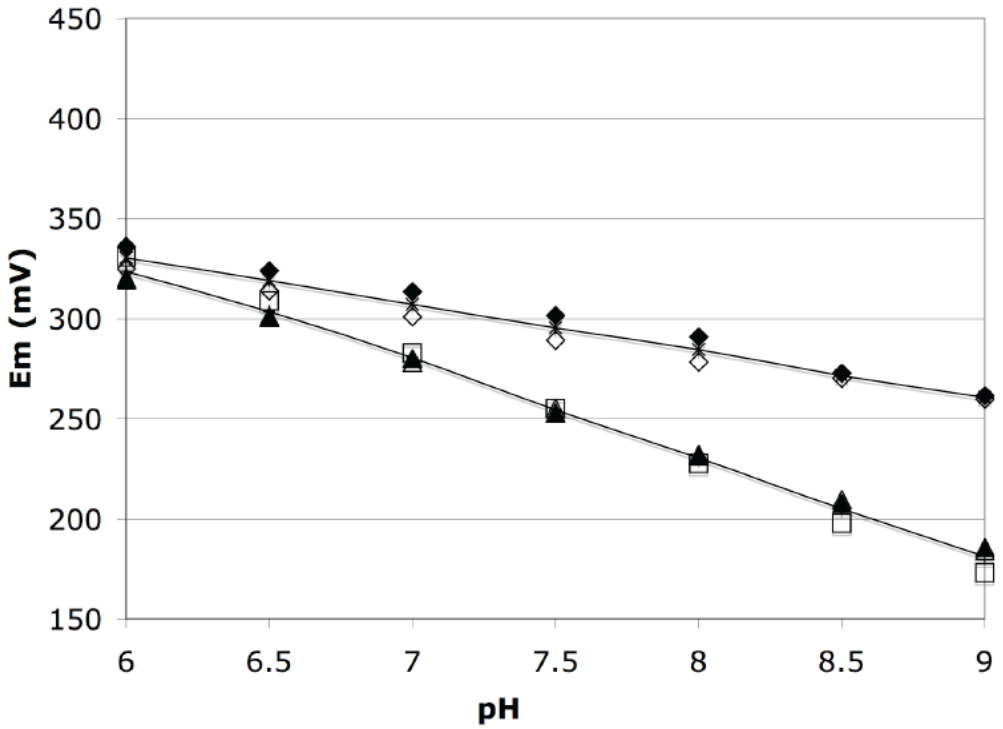

Figure 4.3 Simulated pH dependence of the Cu_a E_m. Structures derived from 2GSM: WT_S44 (□), WT*_S44(△) and WT*_D44(▲). Structures with Asp44: Mut*_S44(◇) and Mut*_D44(◆). The connecting lines are the average. Line through average Ems in structures derived from the Mutant structure (top) and 2GSM (bottom).

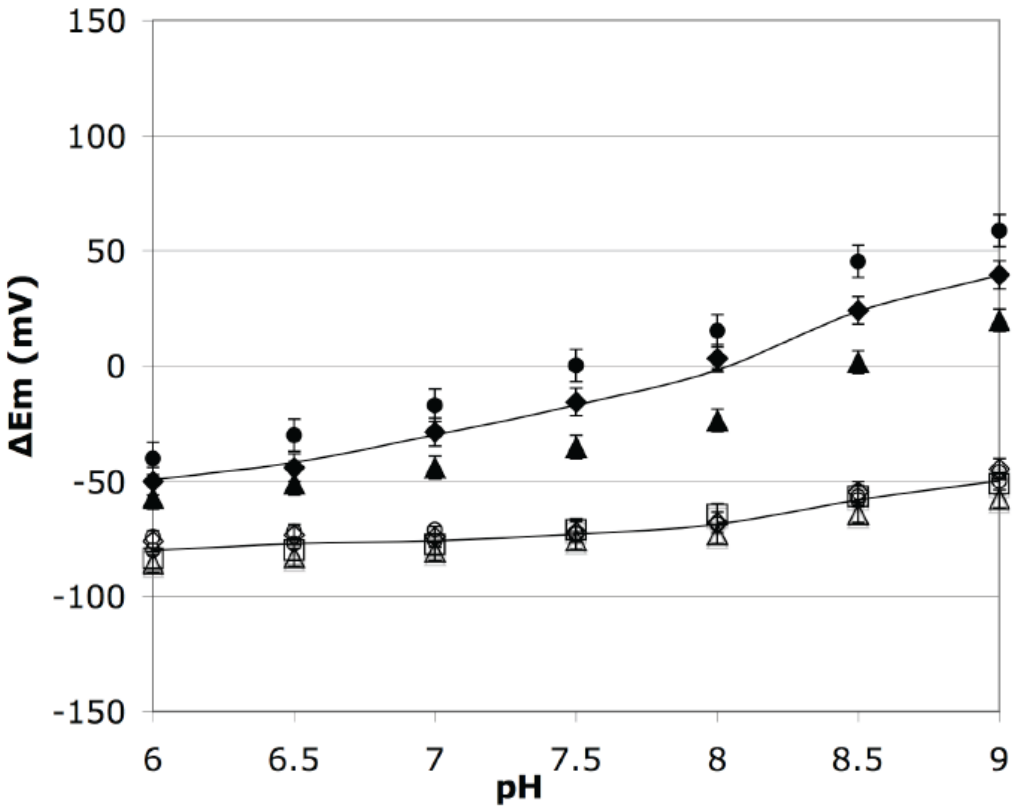

Figure 4.4 The free energy difference between Heme a and Cu_A as a function of pH. Structures with Ser44: WT_S44 (□), WT*_S44(△), Mut*_S44(◇), Mut*_S44#(○). Structures with Asp44: WT*_D44(▲), Mut*_D44(◆) and Mut*_D44#(●). The lines connect the average of the ΔG° for the D44 (top) and S44 (bottom) structures.

Table 4.2. The energy terms contributing to the calculated pK7' of Asp44 (meV). pKa,sol and pK7' in pH units. (Definitions are as Table 4.1)

Asp44	$pK_{a,\,sol}$	$\Delta\Delta G_{rxn}$	$\Delta\Delta G_{pol}$	$\Delta G^{mfe}_{ele,7}$ (OOOO)	$\Delta G^{mfe}_{ele,7}$ (OROO)	pK_7'
WT*_D44	4.75	600	-97	-358		7.2
WT*_D44	4.75	600	-97		-102	11.7
Mut*_D44	4.75	630	-65	-424		7.1
Mut*_D44	4.75	630	-65		-185	11.3

4.3.2 Heme a E_m and D44 pK_a at ph7

The redox potential of Heme a is calculated in the wild-type S44 and D44 mutant structures using MCCE2.4 with the other three redox centers (Cua, Cub and Heme a3) fixed in their oxidized state. The average calculated E_m at pH 7 for Heme a in the S44 structures is 379±7mV (Table.4.1, Figure 4.2). The results show good agreement between the initial WT_S44 structure, the structure derived from the mutant x-ray structure Mut*_S44 and the wild type structure first mutated to D44 and then back to S44, WT*_S44. The Heme a E_m in *Rb. sphaeroides* CcO is estimated to be ≈ 330mV, ≈10 mV lower than that of bovine at 340mV (*46*), if the two structures have the same E_m for Cu_A (*47*). Analysis of the *Rb. sphaeroides* structure1M56 with an earlier version of MCCE gave a Heme A E_m of 360mV. (*19*). Thus, the E_m derived here is in good agreement with experimental estimates and previous MCCE studies.

The E_m of Heme a in the D44 structures is on average 50 mV lower than with S44

at pH 7 (Figure 4.2, Table 4.1). Heme a in all 7 structures has essentially the same desolvation energy ($\Delta\Delta G_{rxn}$) and interactions with the backbone (ΔG_{bkn}). It is the partially ionized Asp, which has a pK_a near 7, which stabilizes the charge on the Heme, shifting the E_m down.

In the 44D structures, the Asp makes a hydrogen bond to the histidine that is a ligand to Heme a. The D44 OD1 to His102 ND1 hydrogen bond distance is 3.16 in WT*_D44 with the in silico mutation and 2.86Å in Mut*_D44, the crystal structure of the mutant. At pH 7, the average interaction of the oxidized Heme a and the partially ionized Asp44 are -34mV in WT*_D44 and - 85mV in the Mut*_D44 structures, which has the shorter hydrogen bond distance. The more favorable interaction also acts to increase the extent of Asp ionization. If the Asp is fixed to be fully ionized in a calculation where all other sites are in equilibrium at pH 7, the E_m is 116mV in WT*_D44 and 61mV in Mut*_D44.

These results rely on the ability of continuum electrostatics to calculate the interaction of the Heme with a group hydrogen bonded to its ligand.(*19*) The interaction of a number of distal His ligands with a Bis-His Heme were calculated by DFT with Jaguar (*36*) and compared with the MCCE result. The classical electrostatics treatment appears to model this interaction quite well (see Chapter 3).

The MCCE calculations show that Asp 44, a newly introduced charge, remains partially ionized at neutral pH in the presence of the oxidized Heme a. The energy breakdown shows the expected, significant desolvation of the residue in the protein, which shifts the pK_a up, while the electrostatics pair-wise interaction between the Asp

and positively charged Heme a shifts the pK_a down (equation 4.2, Table 4.1). With the Heme oxidized the Asp pK_a is 7.1 in the WT*_D44 structure and 7.2 in the Mut*_D44 structure. However, when the Heme is reduced, the Asp pK_a shifts to 15 for WT*_D44 and 18 for Mut*_D44 (Figure 4.5, Table 4.3).

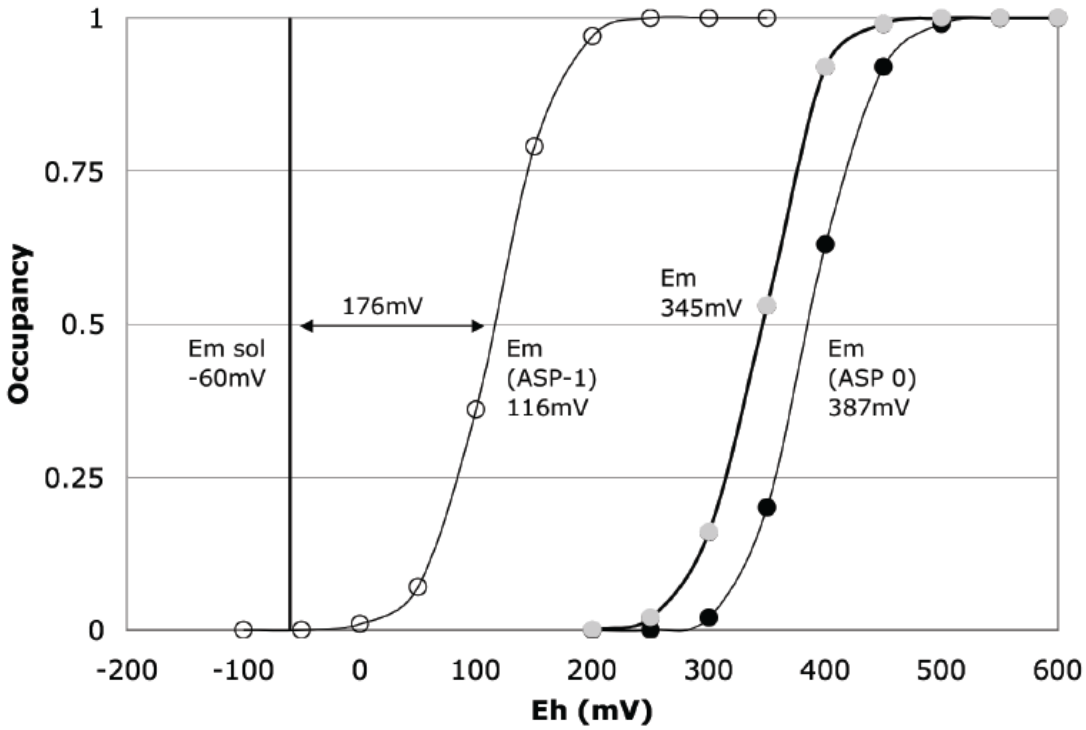

Figure 4.5 a). The Heme a Em titration curve, D44 neutral (●), ionized (○) or at equilibrium with the pH and heme (●).The redox potential of Heme a Em in solution of -60mV is shown.

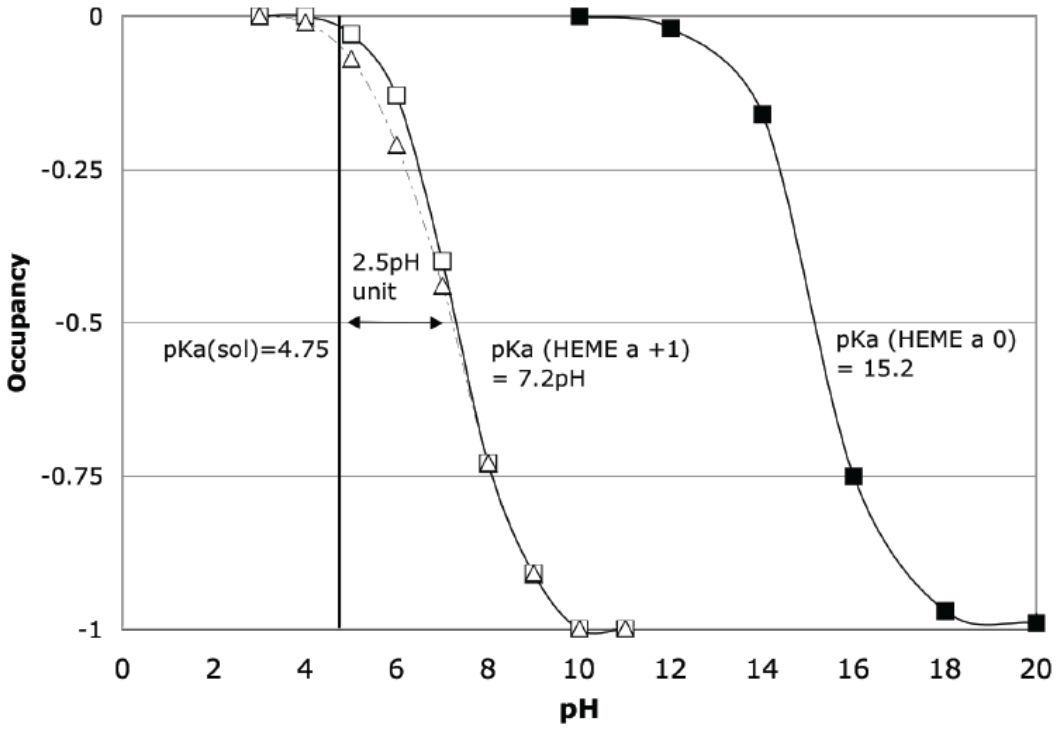

Figure 4.5 b). The D44 pKa titration, Heme neutral (■) or ionized states. (□ for Mut*_44D and △ for WT*_44D). The Asp solution pKa of 4.75pH is shown.

Table 4.3. The calculated ASP44 pK_a at different Heme State

ASP 44 pKa	OOOO	OROO	OXOO
WT*_D44	7.2	15.2	12.4
Mut*_D44	7.3	17.7	11.4
Mut*_D44#	7.0	17.9	11.7

Heme a is fixed in the oxidized state (OOOO), reduced state (OROO) and when it is allowed to remain at equilibrium with Heme a (OXOO).

4.3.3 Coupling of the D44-Heme a titrations

The effect of the introduced Asp on the thermodynamics of Heme a reduction at pH 7 can be analyzed by comparing WT_S44 and WT*_D44 structures (Figure 4.6). The Heme a redox potential in WT*_D44 is 374mV where the Asp is fixed to be neutral at pH7 while it is 378mV in WT*_S44. Thus, the neutral Asp and Ser contribute similarly to the Heme a E_m. When the Asp is fixed in its deprotonated state with charge -1, the Heme a redox potential drops to 116mV, providing the lower limit for the E_m in the mutant.

Fixing the Asp in the ionized state at pH 7 changes the net charge of the protein by only -0.2. Thus, the rest of the protein becomes more positive in response to the newly introduced charge. The gain of 0.8 protons in the ensemble average is distributed to other residues throughout the protein and so this does not change the heme E_m much. The large change in the E_m of Heme A is dominated by the local interactions with the Asp. As the Heme E_m is dependent on the Asp charge, the Asp pK_a is dependent on the Heme ionization state. It is 7.2 with the Heme oxidized and 11.8 with the Heme reduced. Thus, at pH 7 the Asp starts 40% ionized when the Heme is oxidized and is fully protonated when the Heme is reduced. This is in agreement with the EPR measurement showing that in D44 exists in a mixture of protonated and deprotonated states at pH7 (*13*). The resultant E_m of Heme a is 345meV when the titration is free to be coupled to D44 protonation. The pK7' of the Asp44, measures the free energy of protonation at pH7. It is 7.2 pH units in the Heme a oxidized state and 11.7 pH unit in reduced state (equation 4.2).

In simulations with D44 fixed in its deprotonated state in WT*_44D, the Heme a E_m is shifted to be 116mV, 176mV more positive than the -60 mV found for a Heme a in solution (*44*), representing a 176 mV destabilization of the positive charge. A similar analysis shows the newly introduced Asp shifts its pK_a from 4.75 (the pK_a of a carboxylic acid is used) to 7.2 in the protein. This represents a 144meV destabilization of the deprotonated Asp (Figure 4.5b). The Heme is harder to oxidize in the protein than solution by 176meV and the Asp harder to stay deprotonated by 144meV. In MCCE these shifts can be assigned to: desolvation energy ($\Delta\Delta G_{rxn}$), the interaction from backbone ($\Delta\Delta G_{bkb}$) and the electrostatics pairwise interaction (ΔG_{ele}) between Heme a and the rest of the protein (Table 4.2). The Heme, with its bigger radius, has much smaller desolvation energy than the Asp, while the backbone favors Asp ionization. This is due to the overall positive potential within all proteins. The interactions with the other residues is more favorable with the Asp than with Heme a.

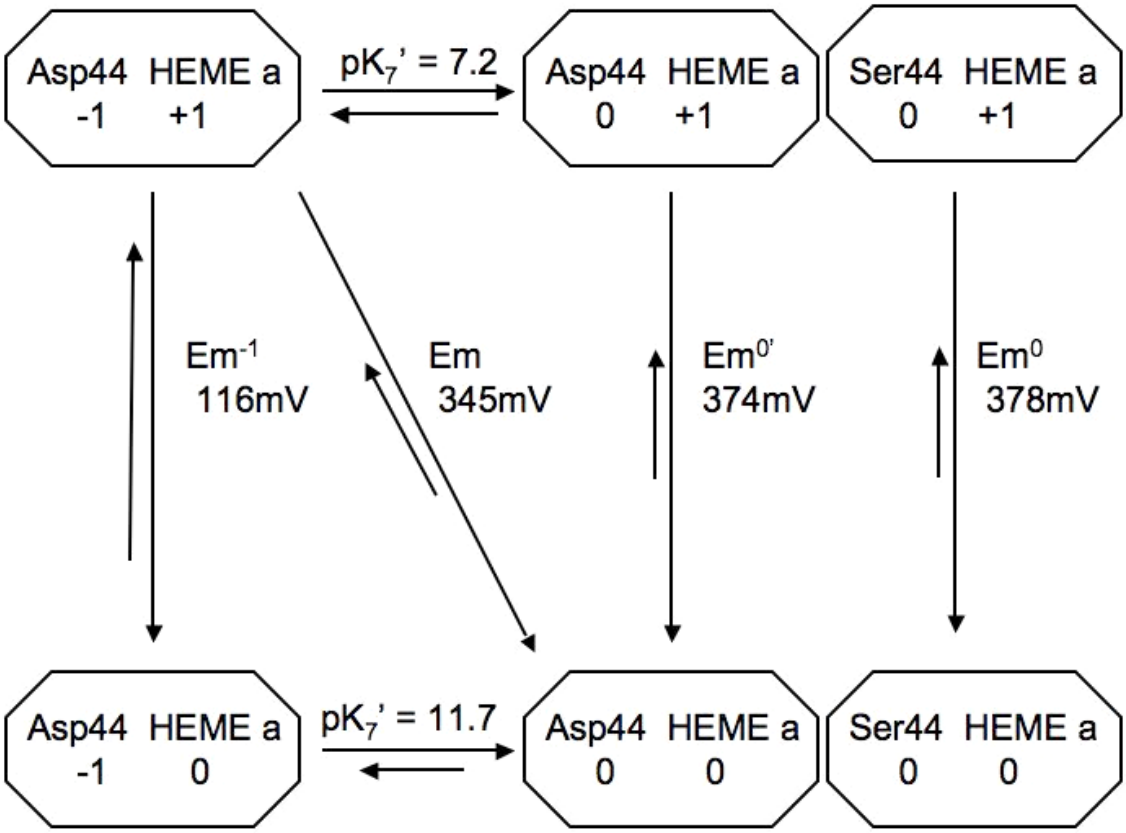

Figure 4.6 Thermodynamic box for Asp44 and Heme a in WT*_D44 and WT_S44 structures. Charges on Ser44, Asp44 and Heme a are labeled inside each box. Em0: the Heme a redox potential in wild type in protein. Em0': the Heme a redox potential of WT*_D44 when ASP is fixed to be neutral. Em-1: the redox potential. Em: the calculated Em in the D44 protein where the Asp ionization is determined within MCCE. At pH 7 the Asp is partially ionized when the Heme is oxidized. Heme ionization is coupled to proton uptake so that the Asp is fully protonated when Heme a is reduced.

4.3.4 pH dependence of Heme a and Cu_A E_ms

The average calculated pH dependence of the Heme a E_m in the S44 structures is 34 mV/pH as derived from the slope of the linear regression line from pH 6 to 9. The earlier calculations also found ≈ 30 mV/pH (*19*). A range of values from ≈10 (*46*) -30 (*48*) mV/pH have been found in bovine CcO. The MCCE value tends to agree with the larger

value. (*19*) The E_ms in the D44 structures are more pH dependent than S44 structures, with a calculated slope of 50 mV/pH. (Figure 4.2)

Previous studies have compared the experimental free energy of electron transfer from Cu_A to Heme a in the wild type and D44 mutant. (*13*) This requires determining the pH dependence of Cu_A as well as Heme a. The calculated redox potential of Cu_A and its pH dependence is independent of the residue at position 44, but differs somewhat with the initial structure. The E_m is ≈30 mV more negative in all 2GSM-derived structure than in the structures derived from the mutant structure. In additions the pH-dependence has a slope of ≈24mV/pH for 2GSM-derived structures and ≈45mV/pH for Mut*_D44 derived structures (Figure 4.3). Experimental data shows a small pH dependence of the Cu_A E_m from pH 7.0 to 8.1, with measured values of less than 10mV/pH in bovine CcO (*46*, *49*). Earlier MCCE calculations, using the 2.3 Å resolution structure of Sphaeroides Cytochrome c oxidase (PDB ID:1M56) found the E_m of Cu_A is dependent on 30 mV/pH (*19*). Analysis with equation 1 reveals the differences between the various structures arises from small changes in relatively distant surface residues of chain B. These residues are further away from the other three redox active centers and do not effect their E_ms significantly. To study the driving force of electron transfer behavior from Cu_A to Heme a, the smaller results in Mut*_S44 with its smaller Cu_A pH dependence was used for all calculations. The ΔG for electron transfer is obtained from $-nF(E_{m,CuA} - E_{m,Heme})$ as a function of pH (Figure 4.4).

At pH 7 the average ΔG^o in the S44 structures is -76meV and while it is -30meV in the D44 mutant. Thus, the driving force for the electron transfer is smaller in the

mutant. This is consistent with the slower measured electron transfer rate from Cu_A to Heme a (*13*). In addition, the reaction is more pH-dependent with D44 than with S44 with an earlier onset of pH dependence and a steeper slope. In the region of pH 7-9 the slope for the reaction ΔG^o is 15 mV/pH in the S44 structures and 35 mV/pH in the D44 structures (Figure 4.2). The electron transfer from Cu_A to Heme a becomes less favorable at high pH as the Asp becomes more charged.

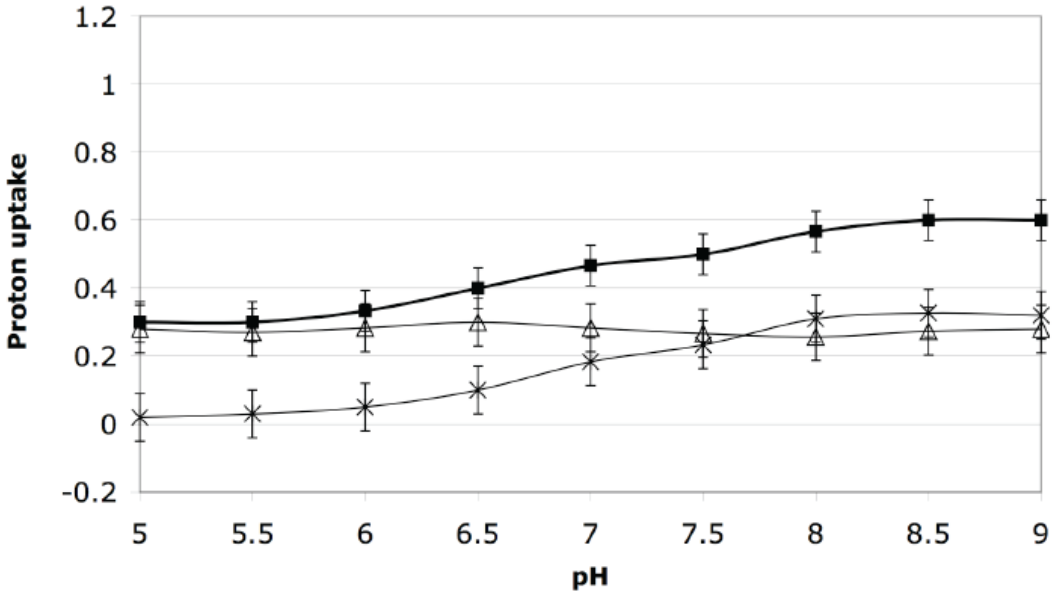

Figure 4.7 a) pH dependent proton uptake number inside the protein when the Heme a is titrated from oxidized to reduced state of the S44 structures. Labels:■ for total number of proton uptake, × for HIS93 and GLU182 pair, ∆ for the rest of proteins.

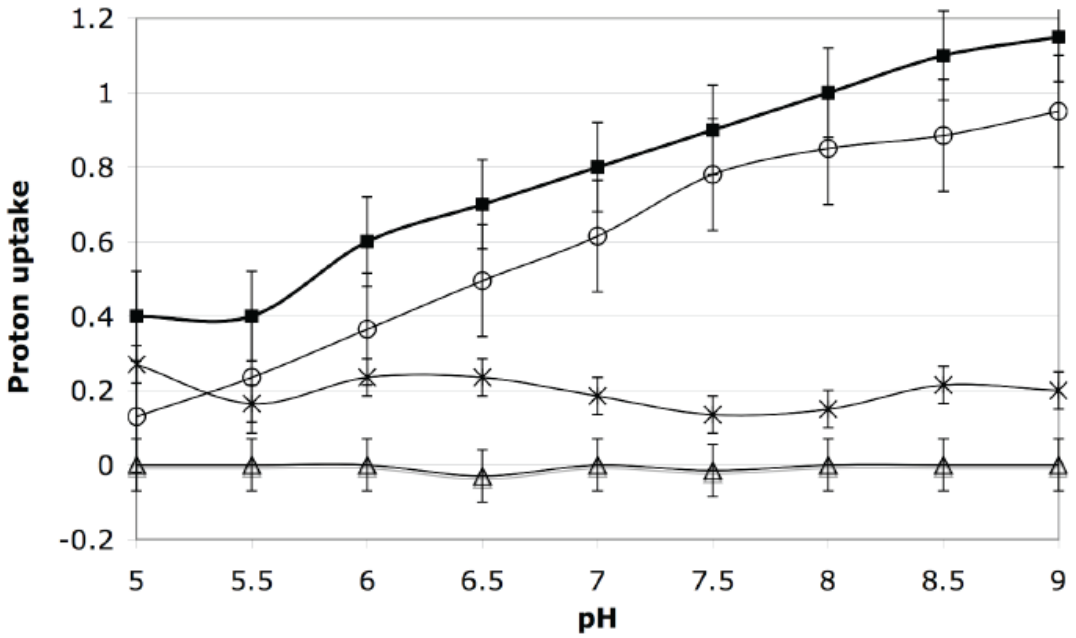

Figure 4.7 b) Average and standard deviation of pH dependent proton uptake
When Heme a is reduced in the Top: 4 S44 structures; Bottom: 3 D44 structures. ■ total proton uptake, × uptake to HIS93 and GLU182 pair; △ to the rest of protein; ○ to ASP44

4.3.5 Proton uptake in the protein

The proton uptake from the protein that accompanies Heme a reduction with the other cofactors held oxidized was determined (Figure 4.7). There are 0.6-0.7 protons taken up when Heme a is reduced in the S44 structures and 1.1-1.2 protons in the D44 mutant (Figure 4.7). As has been seen in earlier MCCE calculations (*19*) His 93 and Glu 182, which are protonated as a coupled group, are the most important proton acceptors in the S44 structures. When Heme a is reduced at pH7, the protein binds 0.4 and 0.5 protons in the WT*_S44 and Mut*_S44 structures. (Figure 4.7 a), with 0.1 to the H93 and E182 cluster. The rest is distributed to groups on the surface of the protein, which individually change their charge by less than 0.05 protons. When the pH increased to 9, the total

proton uptake is 0.6 and 0.7 for WT*_S44 and Mut*_S44 structures, with 0.2 to H93 and E182.

With the WT*_D44 and Mut*_D44 structures, the total proton uptake on Heme a reduction is now 0.7 and 0.8 at pH7 and 1.1 and 1.2 at pH9. The uptake is mostly to D44, while none is to H93 or E182 (Figure 4.7 b). With the exception of D44, no other residue significantly changes proton uptake with pH. The nearest ionizable residues that contribute small (<0.05 H) amounts to proton uptake are Arg 52, 481 and 482, which are 12-13Å away. Other residues that contribute even smaller shifts are > 20Å away.

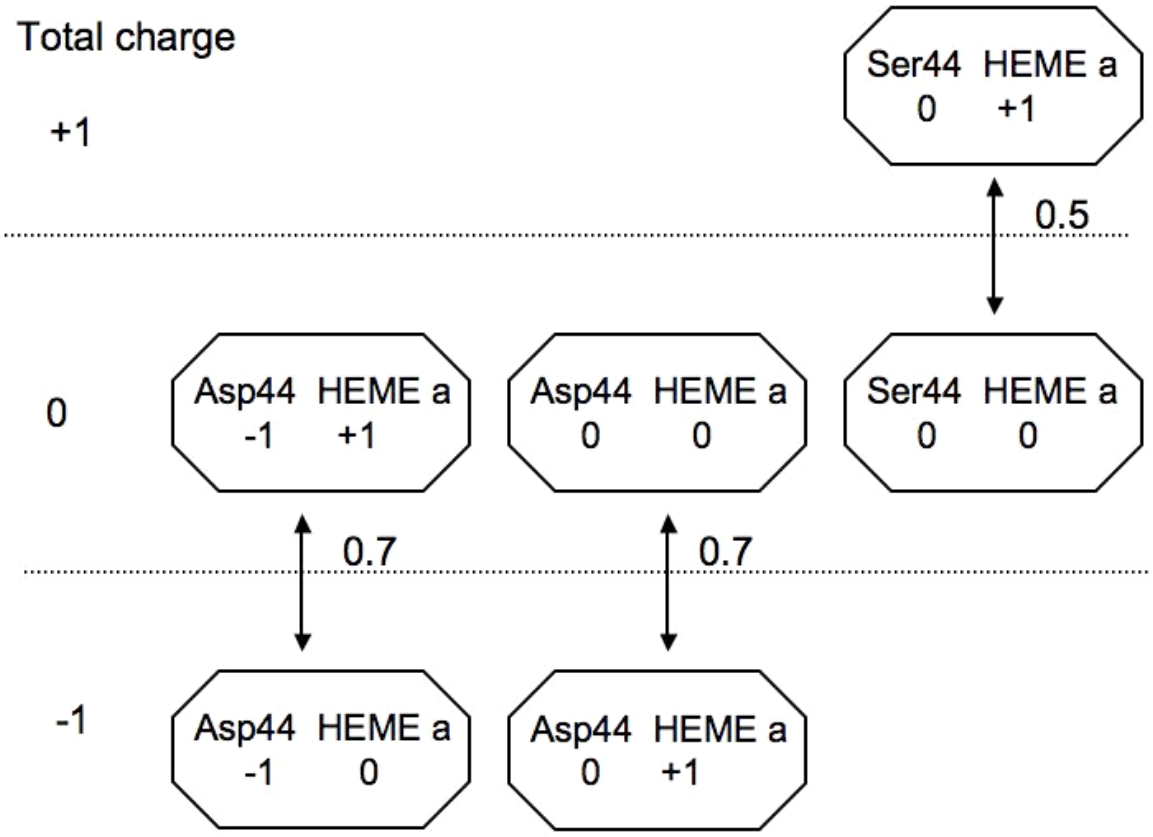

Figure 4.8 The total proton uptake of the protein as a function of the total charge of Asp44 (or Ser44) with Heme a.

Imposition of the negative charge on the introduced Asp generates a similar change in protonation to that found with the addition of an electron to Heme a. Either change leads to the uptake of ≈0.7 protons via small pK_a shifts distributed throughout the protein. The number of protons taken up at pH7 can be classified given the summed charge of Asp or Ser 44 and Heme a (Figure 4.8), while it is +1 when Heme a is oxidized and 44 is either Ser or a protonated Asp, -1 when both Asp44 is ionized and Heme a reduced in WT*_D44 and Mut*_D44 structures, and 0 in other states. At pH 7 when the Heme a/residue 44 charge changes from -1 to 0 the change in net protonation of the proteins changes by ≈0.7±0.13. When the change is due to D44 0.3 protons must be released by the rest of the protein, while the charge change in response to Heme oxidation with fixed Asp- the protein is binding 0.7 protons. The physiological change is from a cluster charge of 0 to 1 when the Heme is oxidized in the presence of Ser 44 (or a neutral Asp 44) leads to a change in charge of 0.4±0.08 indicating release of 0.6 protons. Thus, the protein is behaving as a buffer, reducing the effect of the change in charge in and around Heme a by small, changes distributed throughout the protein.

References

1. Babcock, G. T., and Wikström, M. (1992) Oxygen activation and the conservation of energy in cell respirations, *Nature 356*, 301-308.

2. Ferguson-Miller, S., and Babcock, G. T. (1996) Heme/copper terminal oxidases, *Chem. Rev. 96*, 2889-2907.

3. Wikstrom, M. (2004) Cytochrome c oxidase: 25 years of the elusive proton pump, *Biochim. Biophys. Acta 1655*, 241-247.

4. Rich, P. R. (1995) Towards an understanding of the chemistry of oxygen reduction and proton translocation in the iron-copper respiratory oxidases, *Aust. J. Plant Physiol. 22*, 479-486.

5. Michel, H. (1999) Cytochrome c oxidase: catalytic cycle and mechanisms of proton pumping-a discussion., *Biochemistry 38*, 15129-15140.

6. Verkhovsky, M. I., Belevich, I., Bloch, D. A., and Wikstrom, M. (2006) Elementary steps of proton translocation in the catalytic cycle of cytochrome oxidase, *Biochimica ET Biophysica ACTA 1757*, 401-407.

7. Brzezinski, P., and Larsson, G. (2003) Redox-driven proton pumping by heme-copper oxidases, *Biochim. Biophys. Acta 1605*, 1-13.

8. Reedy, C. J., and Gibney, B. R. (2004) Heme protein assemblies, *Chem. Rev. 104*, 617-649.

9. Fufezan, C., Zhang, J., and Gunner, M. R. (2008) Ligand preference and orientation in b- and c-type heme-binding proteins, *Proteins 73*, 690-704.

10. Winkler, J. R., Malmstrom, B. G., and Gray, H. B. (1995) Rapid electron injection into multisite metalloproteins: intramolecular electron transfer in cytochrome oxidase, *Biophysical Chemistry 54*, 199-209.

11. Ji, H., Yeh, S. R., and Rousseau, D. L. (2004) Modulation of the electron redistribution in mixed valence cytochrome C oxidase by protein conformational changes, *J Biol Chem 279*, 9392-9399.

12. Farver, O., Grell, E., Ludwig, B., Michel, H., and Pecht, I. (2006) Rates and Equilibrium of CuA to heme *a* Electron Transfer in *Paracoccus denitrificans* Cytochrome *c* Oxidase, *Biophysical Journal 90*, 2131-2137.

13. Mills, D. A., Xu, S., Geren, L., Hiser, C., Qin, L., Sharpe, M. A., McCracken, J., Durham, B., Millett, F., and S., F.-M. (2008) Proton-dependent electron transfer from CuA to Heme a and altered EPR spectra in mutants close to heme a of cytochrome oxidase, *Biochemistry 47*, 11499-11509.

14. Ghosh, N., Prat-Resina, X., Gunner, M. R., and Cui, Q. (2009) Microscopic pKa Analysis of Glu286 in Cytochrome c Oxidase (Rhodobacter sphaeroides): Toward a Calibrated Molecular Model, *Biochemistry 48*, 2468-2485.

15. Xu, J., and Voth, G. (2008) Redox-coupled proton pumping in cytochrome c oxidase: Further insights from computer simulation, *Biochimica et Biophysica Acta 1777*, 196-201.

16. Fadda, E., Yu, C., and Pomes, R. (2008) Electrostatic control of proton pumping in cytochrome c oxidase, *Biochimica et Biophysica Acta 1777*, 277-284.

17. Olsson, M. H. M., and Warshel, A. (2006) Monte Carlo simulations of proton pumps: On the working principles of the biological valve that controls proton pumping in cytochrome c oxidase, *Proc Natl Acad Sci 103*, 6500-6505.

18. Quenneville, J., Popovic, D. M., and Stuchebrukhov, A. A. (2006) Combined DFT and electrostatics study of the proton pumping mechanism in cytochrome c oxidase, *Biochim Biophys Acta*.

19. Song, Y., Michonova-Alexova, E., and Gunner, M. R. (2006) Calculated proton uptake on anaerobic reduction of cytochrome c oxidase: Is the reaction electroneutral?, *Biochemistry 45*, 7959-7975.

20. Qin, L., Hiser, C., Mulichak, A., Garavito, R. M., and Ferguson-Miller, S. (2006) Identification of conserved lipid/detergent-binding sites in a high-resolution structure of the membrane protein cytochrome c oxidase, *Proc Natl Acad Sci U S A. 103*, 16117-16122.

21. Song, Y., Mao, J., and Gunner, M. R. (2009) MCCE2: Improving Protein pKa Calculations with Extensive Side Chain Rotamer Sampling, *J. Comp. Chem. epub Mar 9*.

22. D., V. D. S., E., L., B., H., G., G., A.E., M., and H.J., B. (2005) GROMACS: fast, flexible, and free, *J Comput Chem. 26*, 1701-1718.

23. Mao, J., Hauser, K., and Gunner, M. R. (2003) How cytochromes with different folds control heme redox potentials, *Biochemistry 42*, 9829-9840.

24. Lancaster, C. R. D., Michel, H., Honig, B., and Gunner, M. R. (1996) Calculated coupling of electron and proton transfer in the photosynthetic reaction center of *Rhodopseudomonas viridis*, *Biophys. J. 70*, 2469-2492.

25. Alexov, E. G., and Gunner, M. R. (1999) Calculated protein and proton motions coupled to electron transfer: electron transfer from Q_A^- to Q_B in bacterial photosynthetic reaction centers, *Biochemistry 38*, 8253-8270.

26. Song, Y., Mao, J., and Gunner, M. R. (2003) Calculation of proton transfers in bacteriorhodopsin bR and M intermediates, *Biochemistry 42*, 9875-9888.

27. Zhu, Z., and Gunner, M. R. (2005) Energetics of quinone-dependent electron and proton transfers in *Rhodobacter sphaeroides* photosynthetic reaction centers, *Biochemistry 44*, 82-96.

28. Zheng, Z., and Gunner, M. R. (2009) Analysis of the electrochemistry of hemes with E_ms spanning 800 mV, *Proteins 75*, 719-734.

29. Frisch, M. J., Trucks, G. W., Schlegel, H. B., Scuseria, G. E., Robb, M. A., Cheeseman, J. R., Zakrzewski, V. G., J. A. Montgomery, J., Stratmann, R. E., Burant, J. C., Dapprich, S., Millam, J. M., Daniels, A. D., Kudin, K. N., Strain, M. C., Farkas, O., Tomasi, J., Barone, V., Cossi, M., Cammi, R., Mennucci, B., Pomelli, C., Adamo, C., Clifford, S., Ochterski, J., Petersson, G. A., Ayala, P. Y., Cui, Q., Morokuma, K., Malick, D. K., Rabuck, A. D., Raghavachari, K., Foresman, J. B., Cioslowski, J., Ortiz, J. V., Baboul, A. G., Stefanov, B. B., Liu, G., Liashenko, A., Piskorz, P., Komaromi, I., Gomperts, R., Martin, R. L., Fox, D. J., Keith, T., Al-Laham, M. A., Peng, C. Y., Nanayakkara, A., Challacombe, M., Gill, P. M. W., Johnson, B., Chen, W., Wong, M. W., Andres, J. L., Gonzalez, C., Head-Gordon, M., Replogle, E. S., and Pople, J. A. (1998) Gaussian 98, Revision A.9, Gaussian, Inc., Pittsburgh PA.

30. Becke, A. D. (1993) Density-Functional Thermochemistry .3. The role of exact exchange, *J. Chem. Phys. 98*, 5648-5652.

31. Hay, P. J., and Wadt, W. R. (1985) Ab initio effective core potentials for molecular calculations. Potentials for the transition metal atoms Sc to Hg, *J. Chem. Phys. 82*, 270-283.

32. Gunner, M. R., and Honig, B. (1992) Calculations of proton uptake in *Rhodobacter sphaeroides* reaction centers, in *The Photosynthetic Bacterial Reaction Center: Structure, Spectroscopy and Dynamics II* (Breton, J., and

Vermeglio, A., Eds.), pp 403-410, Plenum, New York.

33. 6.5, J. (2005) Schrodinger, LLC: Porland, OR.

34. Song, Y., Mao, J., and Gunner, M. R. (2006) Electrostatic environment of hemes in proteins: pK_as of hydroxyl ligands, *Biochemistry 45*, 7949-7958.

35. Nicholls, A., and Honig, B. (1991) A rapid finite difference algorithm utilizing successive over-relaxation to solve the Poisson-Boltzmann equation., *J. Comp. Chem. 12*, 435-445.

36. Bharadwaj, R., Windemuth, A., Sridharan, S., Honig, B., and Nicholls, A. (1995) The fast multipole boundary element method for molecular electrostatics: An optimal approach for large systems, *J. Comp. Chem. 16*, 898-913.

37. Rocchia, W., Alexov, E., and Honig, B. (2001) Extending the applicability of the nonlinear Poisson-Boltzmann Equation: multiple dielectric constants and multivalent ions, *J. Phys. Chem. B 105*, 6507-6514.

38. Ostermeier, C., Iwata, S., and Michel, H. (1996) Cytochrome *c* oxidase, *Current Opinion in Structural Biology 6*, 460-466.

39. Vanderkooi, G., and Stotz, E. (1965) Reductive alteration of heme a hemochromes, *J. Biol. Chem. 240*, 3418-3424.

40. Sitkoff, D., Sharp, K. A., and Honig, B. (1994) Accurate calculation of hydration free energies using macroscopic solvent models, *J. Phys. Chem. 98*, 1978-1988.

41. Cornell, W. D., Cieplak, P., Bayly, C. I., Gould, I. R., Merz, J., K. M., Ferguson, D. M., Spellman, D. C., Fox, T., Caldwell, J. W., and Kollman, P. A. (1995) A second generation force field for the simulation of proteins, nucleic acids, and organic molecules, *J. Am. Chem. Soc. 117*, 5179-5197.

42. Gunner, M. R., Saleh, M. A., Cross, E., ud-Doula, A., and Wise, M. (2000) Backbone dipoles generate positive potentials in all proteins: origins and implications of the effect, *Biophys. J. 78*, 1126-1144.

43. Gunner, M. R., Mao, J., Song, Y., and Kim, J. (2006) Factors influencing energetics of electron and proton transfers in proteins. What can be learned from calculations, *Biochim. Biophys. Acta 1757*, 942-968.

44. Vanderkooi, G., and Stotz, E. (1966) Oxidation-reduction potentials of heme a hemochromes, *J. Biol. Chem. 241*, 3316-3323.

45. Isom, D. G., Cannon, B. R., Castaneda, C. A., Robinson, A., and Garcia-Moreno, B. (2008) High tolerance for ionizable residues in the hydrophobic interior of proteins, *PNAS 105*, 17784-17788.

46. Moody, A. J., and Rich, P. R. (1990) The effect of pH on redox titrations of Heme a in cyanide liganded cytochrome c oxidase - Experimental and modeling studies, *Biochim. Biophys. Acta 1015*, 205-215.

47. Wang, K., Zhen, Y., Sadoski, R., Grinnell, S., Geren, L., Ferguson-Miller, S., Durham, B., and Millett, F. (1999) Definition of interaction domain for the reaction of cytochrome c with cytochrome c oxidase: II. Rapid kinetics analysis of electron transfer from cytochrome c to Rhodobactor sphaeroides cytochrome oxidase surface mutants., *J. Biol. Chem. 274*, 38042-38050.

48. Artzatbanov, V. Y., Konstantinov, A. A., and Skulachev, V. P. (1978) Involvement of intramitochondrial protons in redox reactions of cytochrome alpha, *FEBS Lett. 87*, 180-185.

49. Erecinska, M., Chance, B., and Wilson, D. F. (1971) The oxidation-reduction potential of the copper signal in pigeon heart mitochondria, *FEBS Lett. 16*, 284-286.